University of Sussex

Hydrodynamics of the Electroweak Phase Transition

Miguel R Sopena

Submitted for the degree of Doctor of Philosophy

University of Sussex

April 2012

Declaration

I hereby declare that this thesis has not been and will not be submitted in whole or in part to another University for the award of any other degree.

Signature:

Miguel R Sopena

To the memory of my mother,

María Pilar Fumanal García

Geography Department, University of Valencia

1940-1998

Un laberinto es una casa labrada para confundir a los hombres; su arquitectura, pródiga en simetrías, está subordinada a ese fin. En el palacio que imperfectamente exploré, la arquitectura carecía de fin.

[A labyrinth is a house built to confuse men; its architecture, rich in symmetries, is subordinated to that end. In the palace which I imperfectly explored architecture had no end.]

Jorge Luis Borges, 'El Inmortal'

And God said, Let there be a firmament in the midst of the waters, and let it divide the waters from the waters.

And God made the firmament, and divided the waters which were under the firmament from the waters which were above the firmament: and it was so.

Genesis 1:6-7

At first there was neither Being nor Nonbeing.
There was not air nor yet sky beyond.
What was its wrapping? Where? In whose protection?
Was water there, unfathomable and deep?

[...] A crosswise line cut Being from Nonbeing.
What was described above it, what below?
Bearers of seed there were and mighty forces [...]

Who really knows? Who can presume to tell it?
Whence was it born? Whence issued this creation?
Even the Gods came after its emergence.
Then who can tell from whence it came to be? [...]

Nasadiya Sukta of the Rigveda

UNIVERSITY OF SUSSEX

Miguel R Sopena

Thesis Submitted for the Degree of Doctor of Philosophy

Hydrodynamics of the Electroweak Phase Transition

Summary

This work investigates the hydrodynamics of the expansion of the bubbles of the broken symmetry phase during the electroweak phase transition in the early universe, in which SU(2) electroweak symmetry is broken and fundamental particles acquire mass through the Higgs mechanism. The electroweak phase transition has received renewed attention as a viable setting for the production of the matter-antimatter asymmetry of the universe. The relevant mechanisms are strongly dependent on key parameters like the expansion velocity of the walls of bubbles of the new phase. In addition, the key dynamical parameters of the phase transition may generate signatures (like gravitational waves) which may become detectable in the near future.

This work builds on existing hydrodynamical studies of the growth of bubbles of the broken symmetry phase and adapts them to novel scenarios, producing predictions of the wall velocity. The early universe at the time of the electroweak phase transition is modelled as a perfect relativistic fluid. A fundamental problem is to account for the interaction between the so-called cosmic 'plasma' and the bubble wall, which may slow down wall propagation and produce a steady state with finite velocity. This 'friction' is accounted for by a separate term in the hydrodynamical equations. This work adapts existing microphysical calculations of the friction to two physical models chosen because of their suitability as regards producing the baryon asymmetry of the universe: 1) An extension of the Standard Model with dimension-6 operators (for which this is the first calculation of the wall velocity ever produced) and 2) The Light Stop Scenario (LSS) of the Minimal Supersymmetric Standard Model (MSSM) (for which this is the first 2-loop calculation). The predicted values of the wall velocity are coherent and consistent with previous studies, confirming, in particular, the prediction of a low wall velocity for the LSS.

Acknowledgements

I would like to thank the following:

My supervisors at Sussex, Dr Stephan Huber and Professor Mark Hindmarsh.

Drs Peter John and José Miguel No for help and clarifications.

My colleagues at the office for their unfailing courtesy, helpfulness, and good cheer.

Friends and relatives for their patience and support and for putting up with my nerves, moods, and occasional blabbering about obscure topics.

My mother and all others who did their best to teach me respect for the truth and the spirit of scientific enquiry.

Contents

List of Tables

List of Figures

Introduction

Ever since the existence of antimatter was predicted by Paul Dirac in 1931 [1], and confirmed experimentally a year later with the detection of the positron, the evidence for a cosmic asymmetry between particles and antiparticles has accummulated. We have found no evidence of the presence of significant amounts of antimatter in our solar system, as confirmed by solar cosmic rays and all available planetary data. Galactic cosmic rays show the same pattern, and the amount of antiprotons present (in a proportion of 10^{-4} compared to protons) is consistent with their having been produced through cosmic ray collisions with the interstellar medium as opposed to indicating the presence of large antimatter regions. On the scale of galactic clusters the presence of intracluster gas could be expected to create a sizeable gamma-ray background from annihilations if matter and antimatter were both significantly present, but in fact the analysis of the cosmic diffuse gamma ray (CDG) spectrum is consistent with no annihilation signals at distance scales as large as the observable universe [2]. On the other hand, if matter and antimatter in symmetric amounts had remained in thermal contact at early times until the time (at T $\sim$ 22 MeV[1]) when their abundances would have naturally 'frozen out', the resulting ratio between the baryon and entropy densities (chosen as a measure of the baryon abundance because it is invariant with the expansion of the universe in the absence of additional entropy release) would be approximately $\frac{n_b}{s} = \frac{n_{\bar{b}}}{s} \approx 7 \times 10^{-20}$, some 9 orders of magnitude smaller than the presently measured nucleon abundance of $\frac{n_b}{s} = (8.9 \pm 0.4) \times 10^{-11}$ [3, 4]. This is the result known as the 'annihilation catastrophe'. To avoid this, if matter and antimatter concentrations were perfectly symmetric, some mechanism would have to have separated matter from antimatter at T $\approx$ 38 MeV to preserve the nucleon abundance we see today, but the causal horizon at that time was far too small to account for the minimal matter/antimatter separation scale required by present observations [5].

[1] We assume the expansion of the universe to be (to a good approximation) adiathermal and adiabatic so that entropy is conserved. Thus, in the radiation-dominated conditions of the early universe, $T \sim a^{-1}$ with a the scale factor in the Friedman-Robertson-Walker metric.

The conclusion is that no such symmetric situation could have existed at very early times (T $\approx$ 1 GeV). Instead, a baryon-antibaryon asymmetry must have been present which resulted, long after baryons and antibaryons fell out of thermal equilibrium and annihilations ceased, in the present maximal asymmetry in which (we believe) we can assume $n_{\bar{b}} \sim 0$.

Our knowledge of the present baryon asymmetry appears to be highly consistent and stems from two independent sources: Firstly, Big Bang nucleosynthesis, since abundances of ^{3}He, ^{4}He, D, ^{6}Li and ^{7}Li are sensitive to $\frac{n_b - n_{\bar{b}}}{s}$. More recently, the relative sizes of the Doppler peaks of the temperature anisotropy of the Cosmic Microwave Background, which are also sensitive to the asymmetry, have confirmed an approximate value of $\eta = \frac{n_b - n_{\bar{b}}}{n_\gamma} \sim (6.14 \pm 0.25) \times 10^{-10}$ [6] (where n_γ is the number density of photons).

The first suggestion that a microphysical mechanism could be devised to explain the baryon asymmetry of the universe (as opposed to accepting it as an initial condition) is due to Andrei Sakharov [7], who laid out his well-known three necessary conditions: Baryon number violation, charge-parity violation, and departure from thermal equilibrium. The need for B-violation is obvious, as is that for an arrow of time to drive the asymmetry away from zero[2]. Slightly more involved is the need for CP violation, to make sure that each reaction that produces a baryon is not exactly matched by an antiparticle-producing reaction. To see this, consider, for example, a particle X which may decay into two left-handed or two right-handed quarks, $X \to q_L q_L$, $X \to q_R q_R$. C violation would imply $\Gamma(X \to q_L q_L) \neq \Gamma(\bar{X} \to \bar{q_L} \bar{q_L})$, but if CP were conserved we would have $\Gamma(X \to q_L q_L) = \Gamma(\bar{X} \to \bar{q_R} \bar{q_R})$ and $\Gamma(X \to q_R q_R) = \Gamma(\bar{X} \to \bar{q_L} \bar{q_L})$ and consequently $\Gamma(X \to q_L q_L) + \Gamma(X \to q_R q_R) = \Gamma(\bar{X} \to \bar{q_R} \bar{q_R}) + \Gamma(\bar{X} \to \bar{q_L} \bar{q_L})$, so starting from an initial symmetry between X and $\bar{X}$ we would arrive at best at an asymmetry between left- and right-handed quarks, not at a baryon asymmetry (see eg [8]).

The question then becomes which physical model not only satisfies these conditions but produces a final value of the baryon asymmetry compatible both with observations and with the ever-tightening experimental constraints on physical parameters. Some of the suggested possibilities are:

- *Planck-scale baryogenesis*: The idea that Planck-scale (T $\approx 10^{32}$ K) baryon-number-violating phenomena (in combination with the arrow of time provided by the Big Bang and CP-violating mechanisms like the ones we already know of in the Standard

[2] In inflationary scenarios any preexisting baryon asymmetry is generally assumed to have been fully diluted by inflationary expansion.

Model) may have produced a net baryon number. As mentioned, and besides the difficulty of investigating such mechanisms in any detail, the huge expansion of the universe provided by inflation at a scale considered to be well below that of quantum gravity would have wiped out any Planck-scale-generated B asymmetry.

- *Baryogenesis in grand unified theories (GUTs)*: These provide a unification of the strong, weak, and electromagnetic interactions in a single gauge group. The new interactions violate baryon number and the decays of the corresponding gauge bosons of masses $m \sim M_{\rm GUT} \sim 10^{16}$ GeV could provide the necessary departure from equilibrium [9]. However, these mechanisms are no longer considered attractive for baryogenesis, fundamentally because they would require the reheating temperature of inflation to be above the GUT energy scale (in order to avoid dilution of the GUT-generated baryon asymmetry); Such a high reheating scale of inflation, however, would in turn fail to dilute cosmologically unwanted concentrations of heavy, long-lived gravitinos (the fermionic superpartners of the graviton, in the context of supersymmetric GUTs), magnetic monopoles etc.

- *Electroweak baryogenesis*: All three Sakharov's conditions can actually be satisfied within the framework of the Standard Model. Baryon number is conserved at low temperature, but in 1976 't Hooft [10] proved that B violation associated with the vacuum structure of SU(N) theories was possible through so-called *sphaleron* processes at high temperature. Sources of CP violation appear in the Kobayashi-Maskawa matrix, and a first-order electroweak phase transition could have provided the necessary departure from equilibrium. In this work we will analyse further the limitations of electroweak baryogenesis within the Standard Model and the possibilities offered by extended settings.

- *Leptogenesis*: This is presently considered one of the most promising scenarios for baryogenesis and it is based on the production of a lepton asymmetry which is later turned into a baryon asymmetry by sphaleron interactions, which preserve the difference between baryon and lepton numbers $B-L$ (even though $B+L$ is not conserved). Because leptogenesis relies on the decays of right-handed heavy Majorana neutrinos it may proceed without compromising the electric charge symmetry of the universe. Right-handed neutrinos are predicted, for example, by $SO(10)$ grand unified theories and are allowed to have a large mass ($\sim M_{\rm GUT}$). Through couplings to left-handed doublets they may decay into a lepton l plus a Higgs or an antilepton $\bar{l}$ plus a Higgs,

processes which are strictly symmetric at tree level but which may produce a net lepton number through quantum corrections thanks to CP-violating phases in the Yukawa couplings [11]. From the moment heavy right-handed neutrinos decay out of equilibrium as the universe expands the lepton asymmetry may become a baryon asymmetry through sphaleron processes. Leptogenesis has gained new relevance as a well-motivated baryogenesis mechanism due to the growing evidence for neutrino masses [12] (a solar neutrino flux in opposition to theoretical predictions, the apparent detection of atmospheric neutrino oscillations, and possible direct detection of neutrino mixing at reactors and accelerators), most easily explained as a consequence of lepton coupling to singlet neutrinos (the 'seesaw mechanism').

- *Affleck-Dine baryogenesis*: This mechanism seeks to avoid the issues posed by the need for the reheating temperature of inflation to be low enough to wipe out the excess of gravitinos and other cosmologically inconvenient entities. In supersymmetry each fermion possesses an associated scalar field with the same quantum numbers. A *coherent field* or condensate (a scalar field with a large vacuum expectation value) can carry a large baryon number, and in the limit in which supersymmetry is unbroken many of these scalar fields have relatively flat potentials and may have been easily excited in the high energy conditions of the early universe. If the baryon number associated with the condensate freezes out as the universe expands, the scalar fields can then decay into fermions resulting in a net baryon asymmetry [13].

Given that the Standard Model (SM) satisfies all three of Sakharov's conditions the first question we may ask is whether the baryon asymmetry of the universe could have been generated without recourse to alternative settings. However, the consensus is that the Standard Model is severely limited in its capacity to produce a large baryon asymmetry and could not have produced the value that we observe today for presently acceptable values of its physical parameters. As mentioned, the mechanism relied upon to provide nonequilibrium conditions in Standard Model electroweak baryogenesis is a first-order electroweak phase transition (the process by which the Higgs field acquires a nonzero vacuum expectation value (VEV), $SU(2)_L \times U(1)_Y$ electroweak symmetry is broken and massive SM particles acquire their masses through their couplings to the Higgs boson). The concept of a first-order transition implies that differentiated regions ('bubbles') of nonzero Higgs VEV nucleate and grow at a given transition temperature, colliding, merging and eventually filling all space, thus completing the transition to the broken symmetry phase [14]. However, seemingly insurmountable complications appear. Lattice analysis of

the electroweak phase transition at nonzero temperature [15] (necessary because of divergences in perturbative calculations, see eg [8, 16]) make clear that the electroweak phase transition in the SM is *not* first-order (but rather a smooth crossover) for Higgs masses $\gtrsim 80$ GeV, well below the recently confirmed experimental value of $m_h \approx 125$ GeV [17,18]. Even assuming that a first-order phase transition is possible there are further problems. In this setting the baryon asymmetry is created by CP-violating interactions in the expanding bubble wall. These reflexion and transmission processes create a particle/antiparticle asymmetry on either side of the wall, with antiparticles becoming more plentiful outside the bubble (even though the separation by itself does *not* create a global B-number asymmetry). The particle/antiparticle imbalance is then turned into a net baryon asymmetry by sphaleron transitions due to the fact that sphaleron rates differ greatly between the unbroken symmetry phase ('false vacuum') outside the bubbles and the broken symmetry phase ('true vacuum') inside. Inside the bubbles sphaleron rates carry an exponential suppression $\sim e^{-E_{sph}/T}$ [19] ($E_{\rm sph}$ being the energy of sphaleron configurations corresponding to half-integer values of the so-called *Chern-Simons number*, N_{CS} [3]), absent from the rate in the symmetric phase ahead of the advancing bubble wall [20]. If B-violating reverse sphalerons are suppressed inside the bubbles they are only active outside, where they act preferentially on the more abundant antiparticles, creating a net global baryon asymmetry in favour of particles. As the bubble wall keeps advancing, the newly created baryon asymmetry is transported into the broken symmetry phase inside the bubble. In the Standard Model there are two obstacles for this mechanism to be effective: The broad consensus is that there are not enough sources of CP violation to reproduce the observed baryon asymmetry [21]; In addition, requiring the exponential suppression of the sphaleron rate in the broken symmetry phase to be large enough (so that reverse sphalerons will not 'wash out' the baryon asymmetry just created) leads to the bound usually expressed as $\frac{v_c}{T_c} \gtrsim 1$ where T_c is the temperature at which the finite-temperature Higgs effective potential develops a second local minimum degenerate with the symmetric one, and v_c is the nonzero VEV at that temperature, see 1.2.1 [22][4]. This in turn provides a bound on the Higgs mass $m_h \lesssim 32$ GeV, again far below present experimental constraints.

Having ruled out the Standard Model as a viable setting for the production of the baryon asymmetry of the universe we must look for alternatives. A common approach has

[3] Integer N_{CS} values correspond to sphaleron configurations with zero energy.

[4] Because it is in the symmetric phase inside the bubble where the washout of the newly created asymmetry must be avoided, it is actually more interesting to study the value of ξ at that temperature (T_b) instead of at T_c. That will be our choice in the course of our calculations.

been to consider some minimal extension of the Standard Model with additional sources of CP violation but which does not contradict experimental results, for instance through the addition of a spin-0 singlet [14] or a second Higgs doublet [23,24]. In this work we focus on two further possibilities: First, an alternative extension of the Standard Model containing dimension-6 nonrenormalisable operators [25], and, second, the light stop scenario (LSS) of the Minimal Supersymmetric Standard Model (MSSM) [26, 27]. The production of the baryon asymmetry of the universe in a first-order electroweak phase transition is a complex issue investigated through many different approaches. In particular, the propagation of the walls of bubbles of the new phase has received special attention [28–33]. This is because the effects of the phase transition are generally dependent on the specifics of the wall propagation and, in particular, on the wall velocity. In addition to the creation of the baryon asymmetry, these effects may include the production of primordial cosmic magnetic fields [34], topological defects [35], density inhomogeneities [36], and gravitational waves [37,38], each one of which has a different dependence on the wall velocity according to the relevant generating mechanisms. This work is based on the application of existing hydrodynamic treatments of the wall propagation to the two models mentioned above. Its main goal is the calculation of the electroweak bubble wall velocity in those models as a function of the model parameters, in the regions in parameter space both relevant to the production of the observed baryon asymmetry and compatible with present experimental bounds. In such hydrodynamic treatments the wall velocity usually increases with the ratio $\frac{v_c}{T_c}$ mentioned above, commonly known as the 'strength' of the phase transition. The other crucial factor in determining the wall velocity is the so-called 'friction term', a slowing term which appears in the hydrodynamical equations and can be seen as analogous to mechanical friction. It is because of friction effects that the walls of the growing bubbles propagate at less than the speed of light, and thus, the determination of friction is central to calculations of the wall velocity.

Our main results are as follows: We apply the results of the microscopic calculation of the wall velocity for the Standard Model carried out in [30] to the extension to the SM with dimension-6 operators. Extrapolating friction effects we produce predictions of the wall velocity ranging from *subsonic* (wall velocities $v_w \approx 0.3$, lower than the speed of sound in the medium) to *supersonic* (higher than the speed of sound in the medium and reaching $v_w \gtrsim 0.8$ in some areas within parameter space). This is the first ever study of the wall velocity in the dimension-6 extension to the SM. In the case of the LSS of the MSSM, we build on the microscopic calculation carried out in [32]. Our study (the first

2-loop calculation ever carries out for this model) results in very subsonic ($\approx$ 0.04-0.05) bubble wall velocities, a value in accordance with previous studies of bubble propagation in supersymmetric settings. As an extension to our calculations we also produce estimations of the wall velocity in other supersymmetric settings of interest.

Chapter 1

The electroweak phase transition

1.1 Phase transitions in the early universe

1.1.1 The early universe and thermal equilibrium

For much of the early history of the cosmos down from the Planck epoch ($T \sim 10^{19}$ GeV), the only cause of departure from thermal equilibrium was the expansion of the universe [5]. The only other significant sources of nonequilibrium were a number of spontaneous symmetry breaking (SSB) transitions, assumed to have taken place in early cosmic history and responsible for the shape of the physics we observe today. The Grand Unification phase transition (at $T \sim 10^{15}$ GeV) separated the strong and the electroweak interactions. Electroweak symmetry breaking then happened at $T \sim 100$ GeV, splitting up the weak and electromagnetic forces. At about $T \sim 200$ MeV, the quark-hadron phase transition gave rise to the formation of mesons and baryons out of strongly-interacting fundamental particles. The epoch of primordial nucleosynthesis took place at $T \sim 1$ MeV. At $T \sim 10$ eV matter density became equal to that of radiation, marking the beginning of the present 'matter-dominated' era and signalling the start of structure formation. Finally, at $T \sim 1$ eV, matter and radiation decoupled as ions and electrons combined to form primordial atoms, bringing to an end the epoch of overall thermal equilibrium which started with the Big Bang. It is useful to remember that, if we take the number of effectively relativistic degrees of freedom[1] $g_* = \sum_{\mathrm{i=bosons}} g_i \left(\frac{T_i}{T}\right)^4 + \frac{7}{8} \sum_{\mathrm{i=fermions}} g_i \left(\frac{T_i}{T}\right)^4$ as *constant* in the context of the radiation-dominated era, the temperature of the universe has the dependence $T \propto a^{-1}$ in this setting (with a the scale factor in the Friedman-Robertson-Walker metric) and the rate of change of T is set by the expansion rate, $\dot{T}/T = -H$, with

[1] Note that unless otherwise specified we assume all particle species to have a common temperature so $g_* = g_{*S}$ with $g_{*S} = \sum_{\mathrm{i=bosons}} g_i \left(\frac{T_i}{T}\right)^3 + \frac{7}{8} \sum_{\mathrm{i=fermions}} g_i \left(\frac{T_i}{T}\right)^3$

H the Hubble parameter $H = \dot{a}/a$.

1.1.2 Symmetry restoration at high temperature. Classes of phase transitions

Spontaneous symmetry breaking is a key concept in modern particle physics and a central pillar of the Standard Model through the Higgs mechanism [39]. It posits that there may be underlying symmetries of Nature which we cannot observe at present but that may be restored at high temperatures, having been 'broken' in the course of the expansion of the universe. Symmetry breaking transitions are also a key cosmological mechanism for the production of 'topological defects' associated with the structure of the vacuum after the phase transition. The production of topological defects is due to the existence of a finite causal horizon at the time of the phase transition (the 'Kibble mechanism'). This implies that the structure of the vacuum after the phase transition cannot possibly be correlated beyond the relevant cosmological horizon. Thus, for example [5], a spontaneously broken scalar theory may result in two uncorrelated regions of space 'picking' nonzero vacuum expectation values equal but of opposite sign, with the regions forcibly separated by a 'domain wall'[2]. Other topological defects include cosmic strings and magnetic monopoles. Cosmological symmetry-breaking transitions (including, as mentioned, the electroweak phase transition) may also have left behind other signatures. These are highly dependent on the specifics of the phase transition and may in some cases be observable or, at the very least, constrained to various degrees by observations.

Cosmological phase transitions are generically classified as first- or second-order. As mentioned, in a first-order phase transition differentiated regions of the new phase nucleate and grow in the medium filled with the old phase until they take up all space and the transition ends. At the boundary between the two phases thermodynamic quantities change discontinuously. Any such quantity may be referred to as an *order parameter* for the phase transition. In a second-order transition the shift happens throughout the medium at all spatial scales, so that no particular scale exists where the medium is clearly divided between the old and the new phases (see eg [8]).

[2]The existence of large-scale cosmological domain walls is no longer considered feasible as their energy density would come to dominate that of the universe, violating the constraints of standard cosmology.

1.2 The electroweak phase transition and the Higgs mechanism

The relevance of the electroweak phase transition (EWPT) lies in the breaking of the $SO(3)_C \times SU(2)_L \times U(1)_Y$ symmetry of the SM Lagrangian via the Higgs field acquiring a nonzero vacuum expectation value. This is the Anderson-Higgs mechanism [39, 40]. The symmetry becomes the $SU(3)_C \times U(1)_{EM}$ that we observe today.

At temperatures close to the electroweak scale the expansion rate of the universe is small next to the rates of all processes involved in the electroweak transition, so the only meaningful deviation from thermal equilibrium stems from the phase transition itself.

1.2.1 The finite-temperature effective potential for the Higgs field

The tool commonly employed [8, 14, 16] to investigate the electroweak phase transition (appropriate to the electroweak scale, $T \approx 100$ GeV) is the *finite-temperature effective potential* for the Higgs field, meant to take into account quantum fluctuations through all relevant interactions, including, through the temperature dependency, the effect of a thermal bath of particles at temperature T. Thermal corrections are no longer relevant at lower energy scales for which the zero-temperature potential is an appropriate description. Since exact analytic calculations of the effective potential are difficult, perturbative methods are usually resorted to. The (temperature-dependent) shape of the effective potential determines the behaviour of the Higgs field and, as we will see, the dynamics of symmetry breaking (Fig 1.1). The minima of the potential determine the feasible ground states of the theory. At high temperature the Higgs potential $V(\phi, T)$ (ϕ being the field's vacuum expectation value) has only one minimum at $\phi = 0$, corresponding to a situation in which electroweak symmetry has been restored. The possibility of a first-order phase transition is indicated by the potential developing a second minimum at $\phi \neq 0$. This minimum is energetically disfavoured at first, but as temperature drops further the second minimum eventually becomes degenerate with the first. The temperature at which this happens is known as the *critical temperature* for the phase transition. From that moment on the system may shift from the symmetric minimum to the new one. Note that if no second minimum appeared with a potential barrier between it and the first, the phase transition would be *second-order* and no bubble nucleation would take place. As temperature keeps descending the barrier eventually disappears, by which time if a first-order first transition has not yet happened it once again becomes impossible.

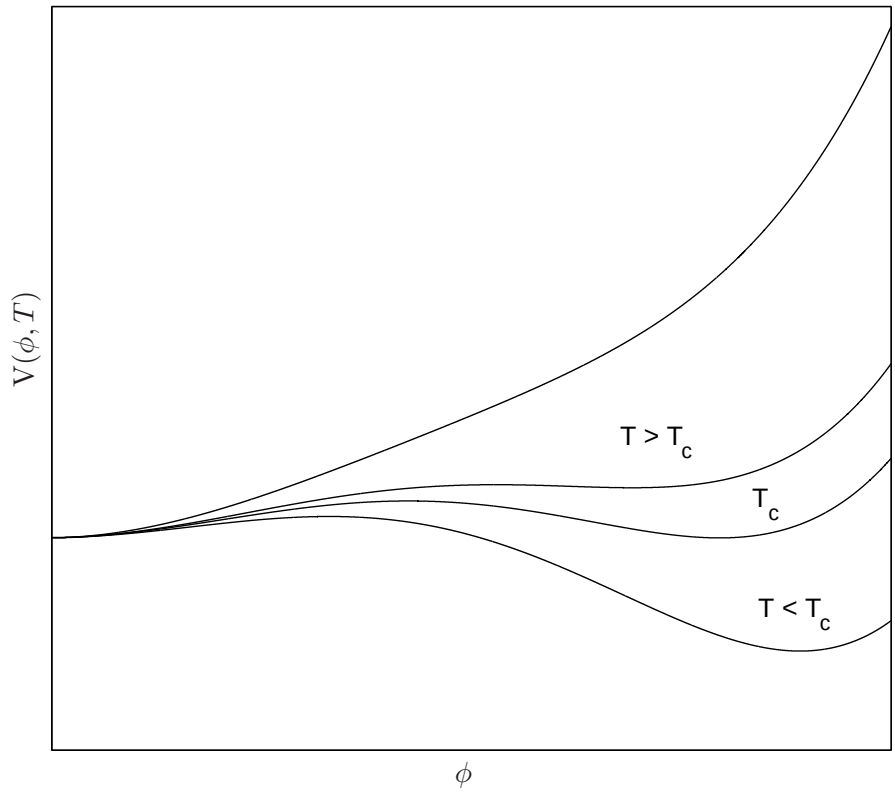

Figure 1.1: Finite-temperature effective potential for a first-order phase transition. If an energy 'bump' failed to develop as temperature descends the transition would be second-order.

1.2.2 Bubble nucleation. Start and end of the phase transition

Given an effective potential, the phase transition may start from the moment the second minimum of the potential becomes degenerate with the first. As temperature keeps descending the second minimum becomes thermodynamically favourable but the system still has to tunnel through the potential barrier in order to shift to the broken symmetry phase. In a first-order phase transition configurations ('bubbles') of the new phase must be able to nucleate and grow, eventually filling up the whole medium [41, 42]. Whether a newly-nucleated bubble will collapse or grow spontaneously depends on its radius. For each temperature there exists a *critical radius*, so that the growth of bubbles nucleated with an equal or larger radius is thermodynamically favourable whereas smaller bubbles will diminish and disappear. In finite-temperature calculations the bubble nucleation rate (of bubbles with at least the critical radius) per unit volume is related to the free energy of the spherically-symmetric 'critical bubble' with the critical radius. The free energy of the critical bubble receives two contributions: One from the variation of the Higgs field across the bubble wall, another from the inner volume of the bubble, filled with the energetically favoured broken symmetry phase. It can be found through the integral

$$F_c \equiv S_3 = \int_V d^3x [\frac{1}{2}\partial_i\phi\partial^i\phi + V(\phi,T)] = 4\pi \int r^2 dr \, [\frac{1}{2}\left(\frac{d\phi}{dr}\right)^2 + V(\phi,T)] \tag{1.1}$$

(with the origin of r located at the centre of the bubble), carried out for the *static* (not time-dependent) configuration of the field ϕ which extremises the action and is therefore a solution to the equation of motion

$$\frac{d^2\phi}{dr^2} + \frac{2}{r}\frac{d\phi}{dr} = \frac{\partial V}{\partial \phi} \tag{1.2}$$

solved with boundary conditions

$$\phi(r \longrightarrow +\infty) = 0$$
$$\left[\frac{d\phi}{dr}\right]_{r=0} = 0.$$

The critical radius (the radius of the critical bubble) is infinite at the critical temperature T_c and decreases with decreasing temperature. Therefore at $T = T_c$ we are left with a planar situation (with one coordinate z) in which the equation of motion reduces to

$$\frac{d^2\phi}{dz^2} = \frac{\partial V}{\partial \phi} \tag{1.3}$$

with boundary conditions

$$\phi(z \longrightarrow -\infty) = 0$$
$$\phi(z \longrightarrow +\infty) = v_c.$$

As a function of the critical free energy, the bubble nucleation rate per unit volume can be written as

$$\Gamma / V = \Lambda^4(T) e^{-F_c/T} \tag{1.4}$$

where Λ in the prefactor is a characteristic scale in the theory, which we will take as $\Lambda^4 \equiv \omega T^4$, with $\omega \approx 1$ being a sufficient approximation as the nucleation rate is dominated by the exponential [14]. It is crucial to determine at which temperature (lower than T_c) the phase transition starts. To find this out we impose the condition that the integrated bubble production rate per horizon volume reach unity. The cosmological horizon in the radiation-dominated era scales as $d_H = 2t = \frac{2\kappa M_{\rm Pl}}{T^2}$ (with the Planck mass $M_{\rm Pl} = 1.22 \times 10^{19}$ GeV and $\kappa \cong 0.3 \times \sqrt{g_*} \approx 1/34$ at the time of the electroweak phase transition) and so $|dt| = \frac{2\kappa M_{\rm Pl}}{T^3} |dT|$. The horizon volume is just $V_H = d_H^3$ so that the number of bubbles nucleated during a time interval dt (corresponding to a decrease in the temperature of the universe of dT) is

$$dP = (\Gamma / V) \cdot V_H \cdot dt = \frac{16\kappa^4 M_{\rm Pl}^4}{T^5} e^{-F_c/T} dT. \tag{1.5}$$

Once $T < T_c$ the phase transition starts at the *nucleation temperature* T_n at which a critical bubble has been nucleated within the horizon volume, that is, when

$$P(T = T_n) = \int_{T_n}^{T_c} dP \equiv 1. \tag{1.6}$$

We must now determine the *finalisation temperature* $T_f < T_n < T_c$ at which the whole medium has been taken over by the expanding bubbles and the phase transition is complete. Assuming that a true-vacuum (broken phase) bubble nucleated at a temperature T' expands within the plasma with a constant terminal velocity β (and ignoring the effects of the expansion of the Universe) the bubble radius will increase in a time dt by $dr = \beta dt$). Therefore its radius at a later temperature T (after a time t has elapsed) will be given by

$$R_B(T,T') = \int_0^{R_B} dR' = \int_0^t \beta dt' = \int_{T'}^{T} \beta \frac{2\kappa M_{\rm Pl}}{T''^3} dT'' = 2\beta\kappa \frac{M_{\rm Pl}}{T}\left(\frac{1}{T} - \frac{1}{T'}\right). \qquad (1.7)$$

Consequently (and taking $\beta \equiv 1$ for simplicity[3]) the fraction f of the causal (horizon) volume in the broken phase at a given temperature $T < T_n$ will be given by

$$f(T) = \frac{1}{V_H}\frac{4\pi}{3}\int_T^{T_c} R_B(T,T')^3 dP(T') =$$
$$= \left(\frac{2\kappa M_{\rm Pl}}{T^2}\right)^{-3}\frac{4\pi}{3}\int_{T_c}^{T}\left(2\beta\kappa\frac{M_{\rm Pl}}{T}\right)^3\left(\frac{1}{T}-\frac{1}{T'}\right)^3\frac{16\kappa^4 M_{\rm Pl}^4}{T^5}e^{-F_c/T}\frac{dT}{T} =$$
$$= \frac{4\pi\beta^3}{3}(2\kappa M_{Pl})^4\int_T^{T_c}\left(1-\frac{T}{T'}\right)^3\frac{1}{T'^5}e^{-F_c/T'}dT'. \qquad (1.8)$$

The phase transition is assumed to end at the temperature T_f for which $f(T_f) = 1$.

The *number of bubbles* present in the horizon volume at any given temperature $T < T_n$ is, in the simplest approximation[4], just the nucleation rate integrated over time:

$$N(T) = \int_{T_c}^{T} dP = \int_T^{T_c} \frac{16\kappa^4 M_{\rm Pl}^4}{T^5} e^{-F_c/T}\frac{dT}{T}. \qquad (1.9)$$

The average radius of the bubbles present at any given temperature T can be approximated simply as the cubic root of the total volume occupied by the bubbles divided by the number of bubbles present, $\langle R\rangle = \left(\frac{V_H(T)}{N(T)}\right)^{1/3}$. Alternatively, the most likely radius can be determined by looking for the maximum in the distribution $R_B(T,T')dP(T')$.

1.3 Modelling the phase transition

1.3.1 Introduction to bubble wall propagation

Different approaches have been extensively explored in order to model the growth of bubbles of the new phase in a first-order electroweak phase transition [28–30, 32, 43–50]. As mentioned, such detailed modelling is key to understanding such parameters of the transition as the bubble wall velocity on which electroweak baryogenesis, as well as other signatures, depends.

[3] In our study of the Light Stop Scenario of the Minimal Supersymmetric Standard Model we will have reason to question this assumption, see 3.3.2.

[4] Note that this expression overcounts the number of bubbles as it doesn't take into account the proportion of the volume already converted to the broken symmetry phase. A more precise expression would require the substitution $dP \longrightarrow f(T)dP$ with an appropriately chosen functional dependence $f(T)$.

It was mentioned in the introduction that a key parameter is the ratio $\frac{v_c}{T_c}$ (the 'strength' of the phase transition), where T_c is the critical temperature and v_c the nonzero Higgs VEV at the second minimum developed by the effective potential as temperature descends and which, at T_c, becomes exactly degenerate with the symmetric minimum (Fig 1.1). Generally speaking, the stronger the phase transition, the higher the difference in free energy per unit volume between the interior of the bubbles of the new phase and the medium outside. This free energy difference ΔF equals the pressure difference between the phases [29] and accelerates the propagation of the bubble wall. Working against the pressure difference are various mechanisms dependent on the microphysics near the bubble wall which slow down wall propagation and are generally referred to as friction. The combination of pressure difference and friction is commonly assumed to produce a steady-state bubble expansion with a fixed bubble wall velocity (at least until bubbles collide or other phenomena, like turbulence, alter the picture). It must be noted, however, that if 'friction' is not strong enough a 'runaway' regime is possible in which the bubble wall accelerates without bound [33, 43].

1.3.2 Basic description of bubble hydrodynamics

Most treatments of the bubble expansion focus on the *hydrodynamics* of the process to study such aspects as the bulk motion of the medium on either side of the bubble wall, the reheating caused by latent heat release, and the variation of thermodynamic variables across the wall (the 'shape of the wall'). The starting point is to model the early universe at the time of the phase transition as a perfect relativistic fluid. Conservation of the fluid's stress-energy tensor makes it possible to relate thermodynamic quantities on either side of a discontinuity such as the advancing bubble wall. Friction is calculated from first principles starting from the microphysics [30, 32], or, alternatively, it is sometimes introduced as a new term in the conservation equations and dealt with through a phenomenological free parameter (eg [29]). This will be our approach in the specific cases we shall deal with in the following chapters.

The basic thermodynamic argument affecting the conservation equations can be easily understood from the form of the energy-momentum tensor for a perfect fluid [28],

$$T^{\mu\nu} = (\rho + P)u^\mu u^\nu - Pg^{\mu\nu} \tag{1.10}$$

with ρ the energy density, P the pressure, u^μ the relativistic 4-velocity,and $g^{\mu\nu}$ the usual Minkowski metric. This is, of course, conserved: $\partial_\mu T^{\mu\nu} = 0$. Assume now a planar

discontinuity moving with a steady velocity in an otherwise homogeneous medium as an initial approximation to the electroweak bubble wall. The conservation equations reduce to

$$\partial_z T^{zz} = \partial_z T^{z0} = 0. \tag{1.11}$$

Now since the enthalpy density is $w = \rho + P = Ts$, from the conservation equations we obtain

$$w_+ \gamma_+^2 v_+ = w_- \gamma_-^2 v_- \tag{1.12}$$

$$w_+ \gamma_+^2 v_+^2 + P_+ = w_- \gamma_-^2 v_-^2 + P_- \tag{1.13}$$

where the subscripts $+, -$ refer to the variables on either side of the discontinuity, v is the bulk velocity of the fluid (in the direction perpendicular to the discontinuity), and γ is the usual relativistic factor $(1 - v^2)^{-1/2}$. Assume now a simple choice of equations of state: Let's say that the $-$ phase represents the broken symmetry phase with an equation of state of pure radiation, $P_- = \frac{\rho_-}{3}$, whereas the $+$ phase is the 'false vacuum', symmetric phase with an added nonzero vacuum energy density (taken to be zero in the broken symmetry phase) ϵ so that $\rho_+ = \rho_{rad,+} + \epsilon$ and $P_+ = \frac{\rho_{rad,+}}{3} - \epsilon$. The equation relating the velocities is then

$$v_+ = \frac{\frac{1}{6v_-} + \frac{v_-}{2} \pm \sqrt{\left(\frac{1}{6v_-} + \frac{v_-}{2}\right)^2 + \alpha^2 + \frac{2}{3}\alpha - \frac{1}{3}}}{1 + \alpha} \tag{1.14}$$

where α is the ratio of vacuum to radiative energy density in the symmetric phase $\alpha = \epsilon/\rho_{rad,+}$ [51]. The solutions with the $+$ sign are known as *detonations* and those with the $-$ sign as *deflagrations*. The allowed velocities for a fixed $\alpha = 0.1$ are reproduced in fig 1.2. From this simple setup we can start to glean the main features of bubble wall propagation. We see that for detonations $v_+ > v_-$ and $v_+ > c_{s,+}$, where $c_{s,+}$ is the speed of sound in the medium, given simply in the case of a relativistic plasma (here, in both phases) by $c_s = \left(\frac{dP}{d\rho}\right)^{1/2} = 1/\sqrt{3}$. For a deflagration $v_+ < v_-$ and $v_+ < c_{s,+}$. Note that so far the treatment has been frame-independent. Consider now the 'frame of the universe' in which the medium far ahead of the bubble wall is at rest, as must be the medium far behind, well inside the bubble, and consider boosting from the 'frame of the universe' to the 'frame of the wall', in which the advancing front is stationary and the fluid moves past it. It is

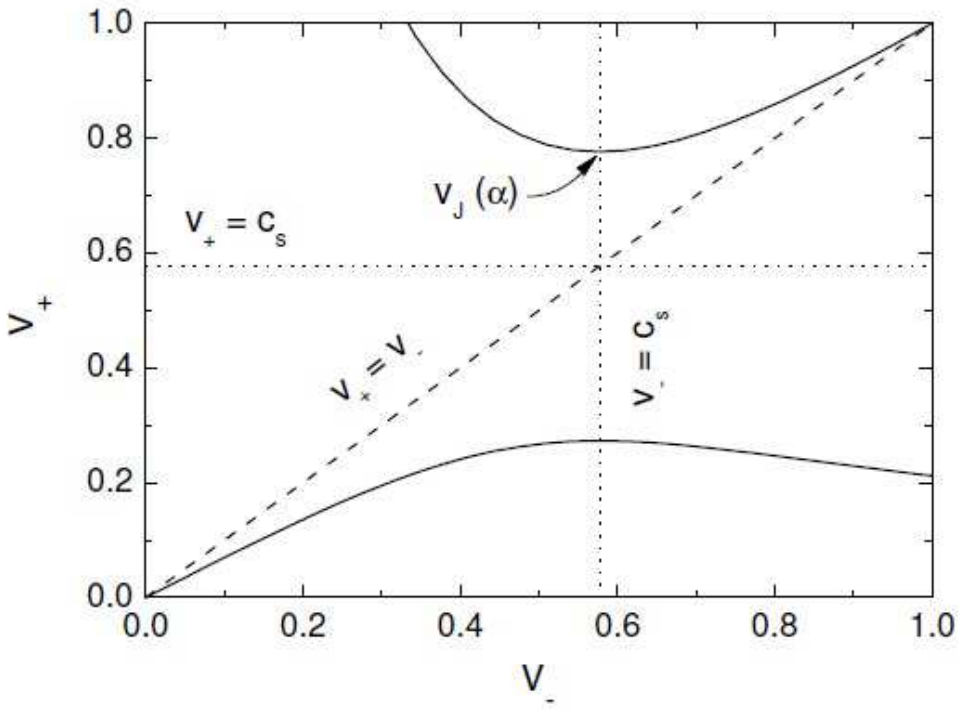

Figure 1.2: v_+ vs v_- from eq 1.14 for $\alpha = 0.1$ (Figure from [28]).

immediately clear that a *single*, infinitely thin front cannot satisfy the boundary conditions set by figure 1.2 unless $v_+ = v_- = 0$ or $v_+ = v_- = 1$, so the structure of the advancing discontinuity must be more complicated. It turns out that a deflagration bubble wall is preceded by a *shock front* which heats up the medium and sets it in motion. The bubble wall itself brings the medium back to rest. On the other hand, a detonation bubble wall hits the medium while at rest, sets it in motion, and is followed by a *rarefaction wave* that brings the medium gradually back to rest. Note that, if we position ourselves in the frame of the wall, the bubble wall velocity is given by $v_w = v_-$ for a deflagration and $v_w = v_+$ for a detonation. From this we see that detonations are necessarily supersonic, while deflagrations may in principle be either subsonic or supersonic. A habitual classification in terms of the velocity of the outflow divides deflagrations into 'strong' ($|v_-| > c_{s,-}$) (strong deflagrations are supersonic), Jouguet ($|v_-| = c_{s,-}$), and 'weak' ($|v_-| < c_{s,-}$) (weak deflagrations are subsonic), while detonations are divided into 'strong' ($|v_-| < c_{s,-}$), Jouguet ($|v_-| = c_{s,-}$(, and 'weak' ($|v_-| > c_{s,-}$).

As a further restriction on this description, it was argued originally that the so-called *Chapman-Jouguet hypothesis*, applicable to a different kind of phase change called *chemical*

combustion[5], was also applicable to cosmological phase transitions. Under this hypothesis detonation fronts are only able to propagate *as Jouguet detonations*. For a time it was assumed that the Chapman-Jouguet hypothesis, which implies that bubble wall propagation was fully determined by the stress-energy conservation equations plus the appropriate boundary conditions, made further hydrodynamic analysis unnecessary, and this approach was employed in investigations of gravitational wave production. However the hypothesis was eventually proven not to be valid for cosmological phase transitions [52].

Within this general picture, therefore, the prediction of a specific wall velocity depends on the specifics of the model and, in particular, on friction. Generally speaking, the larger the supercooling (the drop in temperature from the critical temperature T_c to the nucleation temperature T_n at which the phase transition actually starts), and the smaller the friction, the higher the wall velocity, which might shift from the deflagration into the detonation regime. Another important (and not yet fully elucidated) aspect is the stability of the expanding bubble walls. Some studies (eg [53]) predict that deflagration fronts (the most likely to develop in relatively weak phase transitions, as predicted, for example, for the Standard Model or the MSSM) would develop instabilities as the bubbles grow which would increase the bubble surface, eventually make the bubble wall supersonic, and even affect baryogenesis considerably; According to other studies, however, a more careful analysis reveals the deflagration bubble wall in a relatively weak transition to be hydrodynamically stable [31]. The stability criteria in [31] will be described further and applied to our study in 2.2.2.

1.3.3 The hyperbolic tangent Ansatz

We shall now set down the hydrodynamic equations which will allow us to account for friction and calculate the shape of the expanding bubble wall. Before we begin, however, it is useful to introduce the 2-parameter Ansatz most commonly used to approximate the shape of the wall without explicitly carrying out the hydrodynamic calculation. The variation of the Higgs VEV across the bubble profile (assumed planar) can be approximated by an expression of the form (Fig 1.3)

[5] Chemical combustion requires the temperature of the medium to rise to a specific point for the reaction to begin. If the reaction is exothermic enough it may be sufficient to rise the temperature of the medium at a single point in order for the reaction to extend to the whole of the medium. As opposed to the case of a cosmological phase transition, the combustion front velocity increases with temperature.

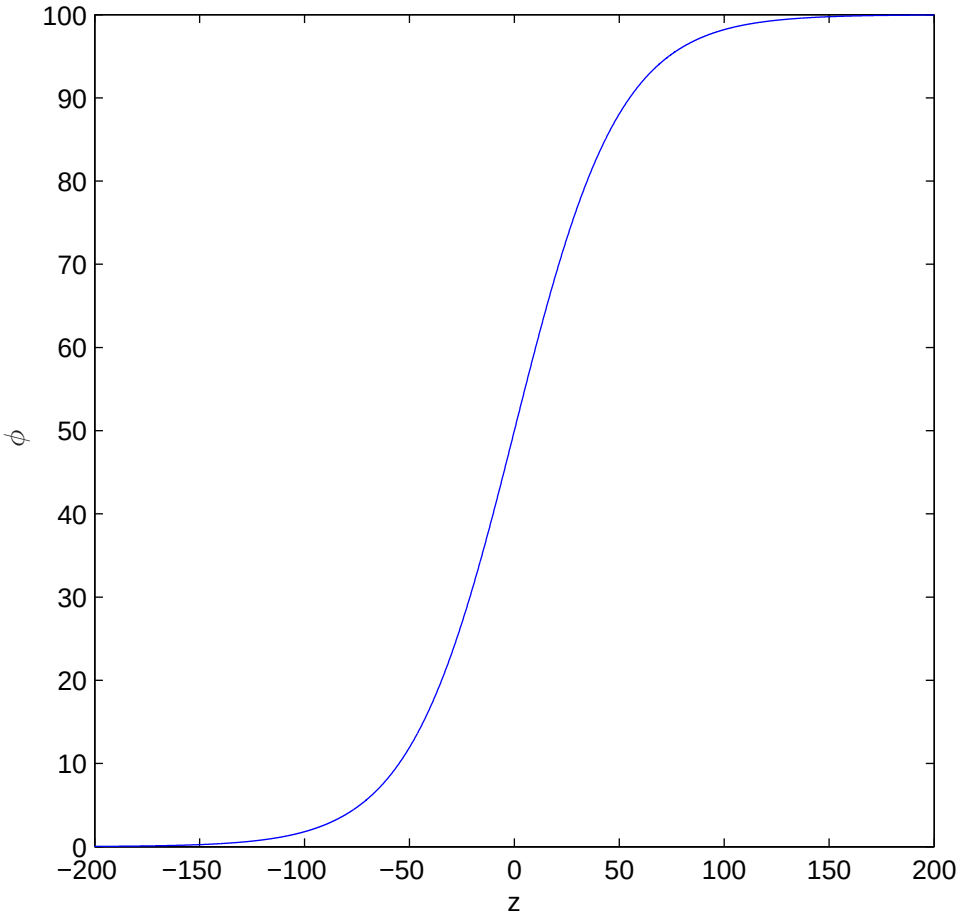

Figure 1.3: Sample hyperbolic tangent Ansatz for the Higgs VEV across the bubble wall. The broken symmetry phase is on the right hand side with an assumed VEV of $\phi_0 = 100$ GeV. We take $L_w = 50$ GeV^{-1}, $\lambda = 1$.

$$\phi(z) = \frac{\phi_0}{2}\left(1 + \tanh\frac{z}{L_w}\right). \tag{1.15}$$

Here L_w is the *wall thickness* which is often expressed in dimensionless form as $L_w \cdot T$ with T a reference temperature. ϕ_0 gives the value of the Higgs VEV in the broken symmetry phase behind the bubble wall as read from the effective potential. Note that this Ansatz is written in the rest frame of the advancing steady-state bubble wall (which will be the preferred reference frame for our calculations) and therefore has no time dependence. A straightforward way to obtain a plausible value for L_w is suggested by the simplified 2-parameter scalar potential $V(\phi) = \frac{\lambda}{4}\phi^2(\phi - \phi_0)^2$ with the equation of motion $\frac{d^2\phi}{dz^2} = \frac{\partial V(\phi)}{\partial \phi}$. Substituting the hyperbolic tangent Ansatz into the equation of motion it is easily shown

that

$$L_w^2 = \frac{8}{\lambda\phi_0^2}. \tag{1.16}$$

Now it is easily checked that the simplified potential has a local maximum half-way (at $\phi = \frac{\phi_0}{2}$) between its two degenerate minima at $\phi = 0$, $\phi = \phi_0$ (fig 1.4) and that the height of that potential barrier is $V_b = V(\phi_0/2) = \frac{\lambda\phi_0^4}{64}$. Therefore

$$L_w^2 = \frac{\phi_0^2}{8V_b} \tag{1.17}$$

which gives us a readily available approximation for the wall thickness for any effective potential with two minima separated by a potential barrier, such as the Higgs finite-T effective potential at the time of the electroweak phase transition (fig 1.1).

1.3.4 Equation of motion for the background Higgs field. The friction term

In our example model in 1.3.2 we merely integrated the energy-momentum conservation equations across the bubble wall without reference to the shape of the relevant variables across the interface and no discussion of friction. In order to carry out a full hydrodynamic analysis (and calculate the wall velocity for a specific model) we need the relevant dynamical equations.

The equation of motion for the background Higgs field can be derived (as in eg [30]) as a function of the phase space population density function $f(p, x)$ for all the particles present in the plasma,

$$\Box\phi + \frac{\partial V(\phi)}{\partial\phi} + \sum \frac{dm^2}{d\phi} \int \frac{d^3p}{(2\pi)^3 2E} f(p, x) = 0 \tag{1.18}$$

with $V(\phi)$ the renormalised vacuum potential. The sum is over massive degrees of freedom so that for the appropriate couplings we may write, in the most general form possible, $m^2 = \frac{y^2\phi^2}{2}$ for fermions, $m^2 = \frac{g^2\phi^2}{4}$ for bosons.

The population density can be expressed *as an equilibrium part plus a deviation*, $f \equiv f_0 + \delta f$ (with the equilibrium distribution for fermions/bosons in the rest frame of the fluid being given by $f_{0,\text{fluid}} = \frac{1}{e^{E/T} \pm 1}$). With this the equation of motion may be written as

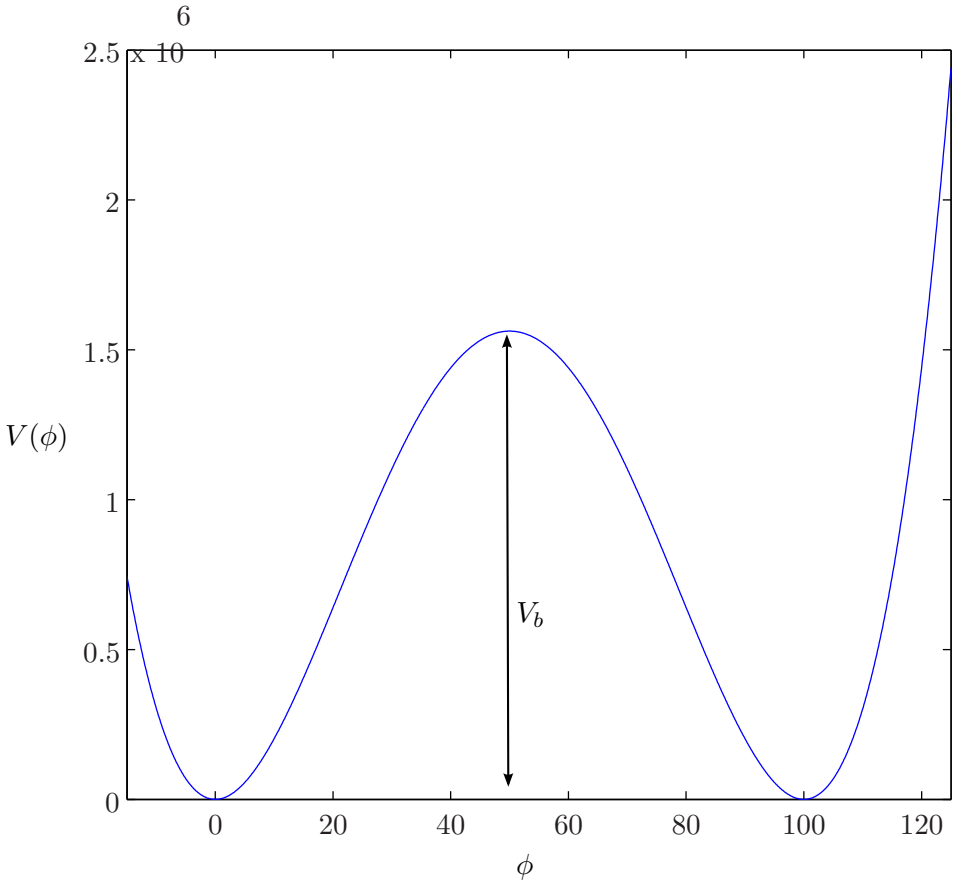

Figure 1.4: Example simplified scalar potential of the form used to provide a readymade expression for the wall thickness L_w from the height of the barrier V_b separating the two local minima of the potential. For a potential of this form the barrier maximum is located exactly half-way between the minima.

$$\Box\phi + \frac{\partial V(\phi,T)}{\partial\phi} + \sum \frac{dm^2}{d\phi}\int \frac{d^3p}{(2\pi)^3 2E}\delta f(p,x) = 0 \tag{1.19}$$

where $V(\phi,T)$ is now the *finite-temperature* effective potential. Note that the derivative of the finite-temperature potential is given by the sum of the derivative of the vacuum potential from (1.18) and the momentum integral for the equilibrium distribution,

$$\frac{\partial V(\phi)}{\partial\phi} + \Sigma\frac{dm^2}{d\phi}\int \frac{d^3p}{(2\pi)^3 2E} f_0(p,x) = \frac{\partial V(\phi,T)}{\partial\phi}. \tag{1.20}$$

The integral term in (1.19) is the friction term. Thus friction effects are fundamentally the result of the deviation of the particle populations in the plasma from equilibrium. Microscopic calculations of friction must proceed by finding a suitable form for δf, and, consequently, for the friction term.

1.3.5 The pressure on the wall

A direct application of eq (1.19) is the calculation of the pressure felt by the wall (see 1.3.1 and eg [30]). Assume a planar wall advancing with a steady velocity in the z direction. (1.19) *in the rest frame of the moving wall* reduces to

$$\frac{d^2\phi}{dz^2} + \frac{\partial V(\phi,T)}{\partial\phi} + \sum \frac{dm^2}{d\phi}\int \frac{d^3p}{(2\pi)^3 2E}\delta f(p,x) = 0. \tag{1.21}$$

We now multiply the whole expression by $\frac{d\phi}{dz} \equiv \phi'$ and integrate over z across the wall. Note that at both ends of the wall we are at either of the zero/nonzero Higgs VEVs so $\frac{d\phi}{dz} \equiv 0$. Consequently $\int \phi''\phi' dz = \left[\frac{\phi'^2}{2}\right]_0^{\phi_0} = 0$. A fundamental point is that the finite-temperature effective potential of the Higgs field equals the free energy density of the whole system F, which is equal to minus the pressure. Thus the z-integration yields

$$\Delta V(\phi,T) + \int \phi' dz \sum \frac{dm^2}{d\phi}\int \frac{d^3p}{(2\pi)^3 2E}\delta f(p,x) = 0 \tag{1.22}$$

which tells us that, in a steady state, the pressure felt by the advancing wall balances out with the integral of the friction term from (1.19) as mentioned in 1.3.1.

1.3.6 Calculating δf. Boltmann equations and relevant limits

The WKB approximation. Boltzmann evolution equations and the collision integral

We now turn our attention to the friction term, and, specifically, the deviation of particle populations from equilibrium which determines friction.

Most friction calculations adopt the so-called WKB or semiclassical approximation, which assumes that the background Higgs field varies slowly enough across the bubble wall that the wall thickness L_w is significantly larger than the particles' de Broglie wavelength, $p \gg \frac{1}{L_w}$. This condition is generally assumed to be satisfied for all except the most infrared particles. A second condition for the semiclassical approximation is that particle scatterings are not too frequent, so that particles can be taken to be on-shell [30].

Within the WKB approximation the evolution of particle distributions is described by a *Boltzmann equation*,

$$\frac{df}{dt} = \partial_t f + \dot{\vec{x}} \cdot \partial_{\vec{x}} f + \dot{\vec{p}} \cdot \partial_{\vec{p}} f = -C[f] \tag{1.23}$$

where $C[f]$ is the *collision integral*. The full form of the integral is given in [30] as

$$C\left[f(x,p)\right] = \sum_i \frac{1}{2E_p} \int \frac{d^3k\; d^3p'\; d^3k'}{(2\pi)^9\; 2E_k\; 2E_{p'}\; 2E_{k'}} \left|M(s,t)\right|^2 \times (2\pi)^2\; \delta^4(p+k-p'-k') P\left[f_i\right] \tag{1.24}$$

where $P[f_i] = f_1 f_2 (1 \pm f_3)(1 \pm f_4) - f_3 f_4 (1 \pm f_1)(1 \pm f_2)$.

Here the sum is over all relevant four leg scattering diagrams. p and k are the incoming, p' and k' the outgoing momenta. M is the scattering amplitude for the process. The f_i are population factors. The first (positive) contribution to P represents a particle with momentum p being removed from the state by a collision, weighted by the populations of colliding particles. The second (negative) contribution represents a particle being scattered into the state. The $(1 \pm f)$ factors stem from particle statistics ($-$ for fermions and $+$ for bosons) [30].

For the following it is useful to generalise the equilibrium distribution for fermions/bosons given in 1.3.4 for the rest frame of the fluid, $f_{0,\text{rest}} = \frac{1}{e^{E/T} \pm 1}$, to that in a *general* frame in which the fluid has a uniform bulk motion with velocity v in, say, the z direction. The equilibrium distribution becomes

$$f_0 = \frac{1}{e^{\beta\gamma(E - v p_z)} \pm 1} \tag{1.25}$$

with $\beta \equiv \frac{1}{T}$ and $\gamma = \frac{1}{\sqrt{1-v^2}}$. Note that by taking $v = 0$ we recover the version for a fluid at rest. The relevant derivatives of the distribution which appear in the Boltzmann equation become in this general frame

$$\frac{df_0}{dp_z} = -\frac{\beta\gamma(\frac{p_z}{E} - v) e^{\beta\gamma(E - v p_z)}}{(e^{\beta\gamma(E - v p_z)} \pm 1)^2} \tag{1.26}$$

and

$$\frac{df_0}{dz} = -\frac{\beta\gamma\frac{(m^2)'}{2E}e^{\beta\gamma(E-vp_z)}}{(e^{\beta\gamma(E-vp_z)}\pm 1)^2}. \tag{1.27}$$

In the rest of this study we shall often choose to work *in the rest frame of the advancing steady-state bubble wall* (always assumed to move in the positive z-direction). A planar wall will 'see' the plasma as moving with a given bulk velocity. Note that, if the plasma itself has a bulk motion induced by the passing of the wall, the plasma velocity 'seen' by the wall at any given position may not coincide with the steady-state velocity of wall propagation. In the rest frame of a steady-state wall $\partial_t \equiv 0$ for all quantities. We now write again $f \equiv f_0 + \delta f$ in the Boltzmann equation. We neglect the momentum derivative of δf, $\partial_{\vec{p}}\delta f \equiv 0$. Note also that $v_z \cdot \partial_z \delta f = \frac{p_z}{E}\cdot\partial_z\delta f$ and $\dot{\vec{p_z}} = -\frac{\partial E}{\partial z}\vec{u_z} = -\frac{1}{2E}\frac{d(m^2)}{dz}\vec{u_z}$. With this the Boltzmann equation finally becomes, in the rest frame of the advancing wall,

$$\begin{aligned}
\partial_t f + \dot{\vec{x}}\cdot\partial_{\vec{x}} f + \dot{\vec{p}}\cdot\partial_{\vec{p}} f = \\
\frac{p_z}{E}\partial_z(f_0+\delta f) - \frac{(m^2)'}{2E}\partial_{p_z} f_0 = \\
\left[\frac{(m^2)'}{2E}(\frac{p_z}{E}-v) - \frac{p_z}{E}\frac{(m^2)'}{2E}\right]\beta\gamma\frac{e^{\beta\gamma(E-vp_z)}}{(e^{\beta\gamma(E-vp_z)}\pm 1)^2} + \frac{p_z}{E}\partial_z\delta f = \\
-\frac{(m^2)'}{2E}v\beta\gamma\frac{e^{\beta\gamma(E-vp_z)}}{(e^{\beta\gamma(E-vp_z)}\pm 1)^2} + \frac{p_z}{E}\delta f' = -C[f].
\end{aligned} \tag{1.28}$$

Simplified forms of the collision integral. The relaxation time approximation

Further simplifications are possible short of employing the full expression for $C[f]$. The *free particle approximation* [44, 45] assumes $C[f] \equiv 0$ and may represent the case in which particle free paths are much larger than the thickness of the wall. In this approximation the Boltzmann equations can be solved exactly (see eg [30]).

A further development, which constitutes the basis for this work, is known as the *relaxation time approximation*. In this approximation we assume $C[f] \equiv \frac{\delta f}{\tau}$, where the relaxation time τ is usually considered independent of momentum [44]. With this the Boltzmann equation for δf becomes

$$-\frac{(m^2)'}{2E}v\beta\gamma\frac{e^{\beta\gamma(E-vp_z)}}{(e^{\beta\gamma(E-vp_z)}\pm 1)^2} + \frac{p_z}{E}\delta f' = -\frac{\delta f}{\tau}. \tag{1.29}$$

Note that it is possible to propose an analytic solution for this equation if we neglect the spatial dependence of the exponentials, that is, if we assume that only δf and m^2

depend on position. With this simplification we can rewrite the Boltzmann equality in the standard form

$$\delta f' + \frac{E\delta f}{P_z \tau} = \frac{\beta\gamma v}{2P_z}(m^2)' \frac{e^{\beta\gamma(E-vp_z)}}{(e^{\beta\gamma(E-vp_z)} \pm 1)^2} \tag{1.30}$$

and integrate it via an integrating factor (again in the usual way) arriving at

$$\delta f(z) = e^{-\frac{E}{p_z\tau}(z-z_{01})} \int_{z_{02}}^{z} e^{-\frac{E}{p_z\tau}(z''-z_{01})} \frac{\beta\gamma v}{2p_z}(m^2)' \frac{e^{\beta\gamma(E-vp_z)}}{(e^{\beta\gamma(E-vp_z)} \pm 1)^2} dz'' \tag{1.31}$$

where z_{01}, z_{02} depend on boundary conditions. Since the integration cannot be solved analytically in a convenient way we shall look for further simplifications.

Relevant limits to the relaxation time approximation. Results for the friction

It is natural to consider under which conditions the δf and $\delta f'$ terms become dominant. The usual approach to the relaxation time approximation (see eg [30]) is to assume $L \gg \tau$ for the wall thickness L, with which $\delta f' \approx \frac{\delta f}{L} \ll \frac{\delta f}{\tau}$. Note that this is a natural limit to take for a relatively *slow* wall since, generally speaking and within any given model, slower walls are thicker and not as sharp (quantities vary more slowly across the bubble profile) and relativistic time dilation is not a factor in increasing the characteristic timescale for particle interaction (the relaxation time) as seen by the wall. Adopting this approximation and dropping the derivative term in (1.28) we have, in a general boosted frame (for one degree of freedom),

$$\delta f_{\text{slow wall}} = \tau \frac{(m^2)'}{2E} v\beta\gamma \frac{e^{\beta\gamma(E-vp_z)}}{(e^{\beta\gamma(E-vp_z)} \pm 1)^2} \tag{1.32}$$

We have arrived at a form for the deviation from equilibrium that we can insert into the equation of motion for the background Higgs field (1.21). Recalling the form of the friction term in that equation (for one degree of freedom) and substituting the expression for δf just derived we obtain

$$\frac{dm^2}{d\phi} \int \frac{d^3p}{(2\pi)^3 2E} \delta f_{\text{sw}}(p,x) = \frac{dm^2}{d\phi} \int \frac{d^3p}{(2\pi)^3 2E} \tau\beta\gamma v \frac{(m^2)'}{2E} \frac{e^{\beta\gamma(E-vp_z)}}{(e^{\beta\gamma(E-vp_z)} \pm 1)^2} \tag{1.33}$$

with which the equation of motion for the Higgs field in the rest frame of the advancing wall, eq (1.21), becomes for a slow wall

$$\frac{d^2\phi}{dz^2} + \frac{\partial V(\phi,T)}{\partial\phi} + \sum \frac{dm^2}{d\phi}\int \frac{d^3p}{(2\pi)^3 2E}\tau\beta\gamma v \frac{(m^2)'}{2E}\frac{e^{\beta\gamma(E-vp_z)}}{(e^{\beta\gamma(E-vp_z)}\pm 1)^2} = 0. \tag{1.34}$$

The pressure difference on the advancing wall as per eq (1.22) for one degree of freedom becomes in this approximation

$$\Delta P_{\rm sw} = \int \phi' dz \frac{dm^2}{d\phi}\int \frac{d^3p}{(2\pi)^3 2E}\tau\beta\gamma v \frac{(m^2)'}{2E}\frac{e^{\beta\gamma(E-vp_z)}}{(e^{\beta\gamma(E-vp_z)}\pm 1)^2}. \tag{1.35}$$

We can extract useful information as to the dependence of the pressure on the relevant mass and temperature scales. Note that if we assume a slow, nonrelativistic wall and make the approximation $E \approx m$, then $\frac{(m^2)'}{(2E)^2} \approx \frac{E^2}{E^2}\frac{1}{L} = \frac{1}{L}$ (and $\frac{1}{L} \sim T$) and with no other spatial dependence outside the exponentials we can take $\int dz\phi' \frac{dm^2}{d\phi} = \int dm^2 = m^2$. Note also that to extract the temperature dependence we can change variables in the momentum integral in the form $p \to p' = \frac{p}{T}$ so that the momentum part of the integrand in spherical coordinates becomes $\beta p^2 dp \to \frac{T^3}{T} p'^2 dp'$ and, finally, we obtain an $\sim m^2T^2$ pressure dependence on mass and temperature in this 'slow wall', $L \gg \tau$ case.

Let us turn now to the opposite limit, that of a *fast*, relativistic wall. This will naturally be a thin, sharp wall and relativistic time dilation will lenghten the characteristic relaxation time for plasma particles so we can assume $L \ll \tau$ and $\delta f' \approx \frac{\delta f}{L} \gg \frac{\delta f}{\tau}$. Thus in this case we can neglect the δf term in the Boltzmann equation (1.29) and are left with

$$\frac{p_z}{E}\delta f' = \frac{(m^2)'}{2E} v\beta\gamma \frac{e^{\beta\gamma(E-vp_z)}}{(e^{\beta\gamma(E-vp_z)}\pm 1)^2} \tag{1.36}$$

which, adopting the relativistic assumption $E \approx p_z$ in the exponentials, can be integrated directly to

$$\delta f_{\rm fast\ wall} = \frac{m^2}{2P_z} v\beta\gamma \frac{e^{\beta\gamma(E-vp_z)}}{(e^{\beta\gamma(E-vp_z)}\pm 1)^2}. \tag{1.37}$$

We can introduce this into the friction term in the Higgs equation of motion,

$$\frac{dm^2}{d\phi}\int \frac{d^3p}{(2\pi)^3 2E}\delta f_{\rm fw}(p,x) = \frac{dm^2}{d\phi}\int \frac{d^3p}{(2\pi)^3 2E}\frac{m^2}{2P_z} v\beta\gamma \frac{e^{\beta\gamma(E-vp_z)}}{(e^{\beta\gamma(E-vp_z)}\pm 1)^2} \tag{1.38}$$

and obtain an equation of motion for the fast wall case

$$\frac{d^2\phi}{dz^2} + \frac{\partial V(\phi,T)}{\partial\phi} + \sum \frac{dm^2}{d\phi}\int \frac{d^3p}{(2\pi)^3 2E}\frac{m^2}{2p_z} v\beta\gamma \frac{e^{\beta\gamma(E-vp_z)}}{(e^{\beta\gamma(E-vp_z)}\pm 1)^2} = 0. \tag{1.39}$$

As we did for the slow wall limit, we can write the pressure on the wall for one degree of freedom as

$$\Delta P_{\text{fw}} = \int \phi' dz \frac{dm^2}{d\phi}\int \frac{d^3p}{(2\pi)^3 2E}\frac{m^2}{2p_z} v\beta\gamma \frac{e^{\beta\gamma(E-vp_z)}}{(e^{\beta\gamma(E-vp_z)}\pm 1)^2}. \tag{1.40}$$

With $E \approx p_z$ the spatial integration can be done directly ($\int dz\phi' \frac{dm^2}{d\phi} m^2 = m^4$) and the change of variable $p \to p' = \frac{p}{T}$ does away with the temperature dependence of the pressure,

$$\Delta P_{\text{fw}} \approx v\gamma m^4 \int \frac{dp'}{(2\pi)^3}\frac{e^{\beta\gamma(E-vp_z)}}{(e^{\beta\gamma(E-vp_z)}\pm 1)^2} \tag{1.41}$$

leaving us with an $\sim m^4$ dependence for the pressure on the wall in the relativistic limit.

Dependence of the pressure on the wall velocity in the relaxation time approximation

We can glean crucial information through studying the pressure difference as a function of the wall velocity. We do this in the slow wall limit of the relaxation time approximation, the form of the friction term that will be most relevant to us in the remainder of this work. In figure 1.5 we plot ΔP_{sw} (for one degree of freedom) from (1.35) vs v_w. We calculate ΔP_{sw} in two ways: 1) By integrating across the wall for each value of v_w (we write $(m^2)' \approx \frac{m_b^2}{L_w}$ with m_b the particle's mass in the broken symmetry phase and perform $\int_0^{m^2} dm^2 \int \frac{d^3p}{(2\pi)^3 2E}\tau\beta\gamma v \frac{m_b^2}{2EL_w}\frac{e^{\beta\gamma(E-vp_z)}}{(e^{\beta\gamma(E-vp_z)}\pm 1)^2}$, recalling that $E = \sqrt{m^2 + |\vec{p}|^2}$)[6], and 2) By assuming a constant particle mass which we set to m_b and integrating over momentum only. We write $\tau \equiv \frac{c}{T}$ and set $c \equiv 1$ for this example case, taking also general example values for all other parameters. We see in the first place that assuming a constant mass across the wall provides a fairly good approximation to ΔP_{sw}, particularly in the fermionic case. More importantly, we see from the plot how the factor $v_w\gamma$ in (1.35) causes the pressure difference to diverge as $v_w \longrightarrow 1$, $\gamma \longrightarrow \infty$. It may be argued that, as we just discussed, the 'slow wall' limit of the relaxation time approximation (the usual assumption in the

[6] In fact the momentum integral has only a very small dependence on velocity and can be solved most easily by assuming $v \equiv 0$ in the exponentials as we show later on in 1.4.3.

literature) is not necessarily an accurate description for high v_w. Note, however, that if we approximate $E \approx p_z$ in what we termed the 'fast wall' approximation (1.40) we end up with the same integral dependence for high wall velocities.

The crucial point to remark is that this divergence of the pressure difference for $v_w \longrightarrow 1$ is, in fact, an artifact of our assumptions. We will see presently (1.3.7) that the pressure difference in fact tends towards a finite limit for $v_w \longrightarrow 1$. It is likely that a properly formulated functional form for the relaxation time τ, which we have so far represented in the simplest possible way (see above), would do away with the γ factor in (1.35), as relativistic time dilation arguments would suggest.

1.3.7 Momentum exchange between the wall and the plasma

The momentum exchange description

We consider now an alternative approximation to the calculation of the pressure on the wall. It consists of calculating the kinetic momentum exchange between the advancing wall and the particles in the plasma (see eg [47]). This approximation will give us essential information as to the behaviour of friction and the pressure on the wall in the ultrarelativistic limit.

To avoid ambiguity it is important to remember that we described the 'pressure' on the advancing wall as the difference in the finite-temperature effective potential for the background Higgs field on either side of the wall, $\Delta V(\phi, T)$. To this we opposed the 'friction' or effect of the deviation from equilibrium of the particle populations in and near the wall. Both contributions cancel out for a steady-state wall. The finite-T effective potential has two parts, the 'vacuum' (independent of temperature) potential and the temperature-dependent additions which arise from the thermal bath. The temperature-dependent part of the potential stems from the *equilibrium* part of the particle distributions.

The momentum-exchange approach aims to account for the effect of the particles in the plasma (the 'thermal bath'), including the influence of the equilibrium *and* non-equilibrium parts of the relevant particle distributions, independently from the effect of the vacuum potential.

This approach is based on the idea that every plasma particle that interacts with the advancing bubble wall experiences a force, and exerts an equal and opposite force on the wall. The force per unit area exerted on/by the wall in this way is the pressure on the wall due to the interaction with the plasma and does *not* include the *vacuum* pressure. The momentum-exchange force per unit area *equals the variation in kinetic momentum*

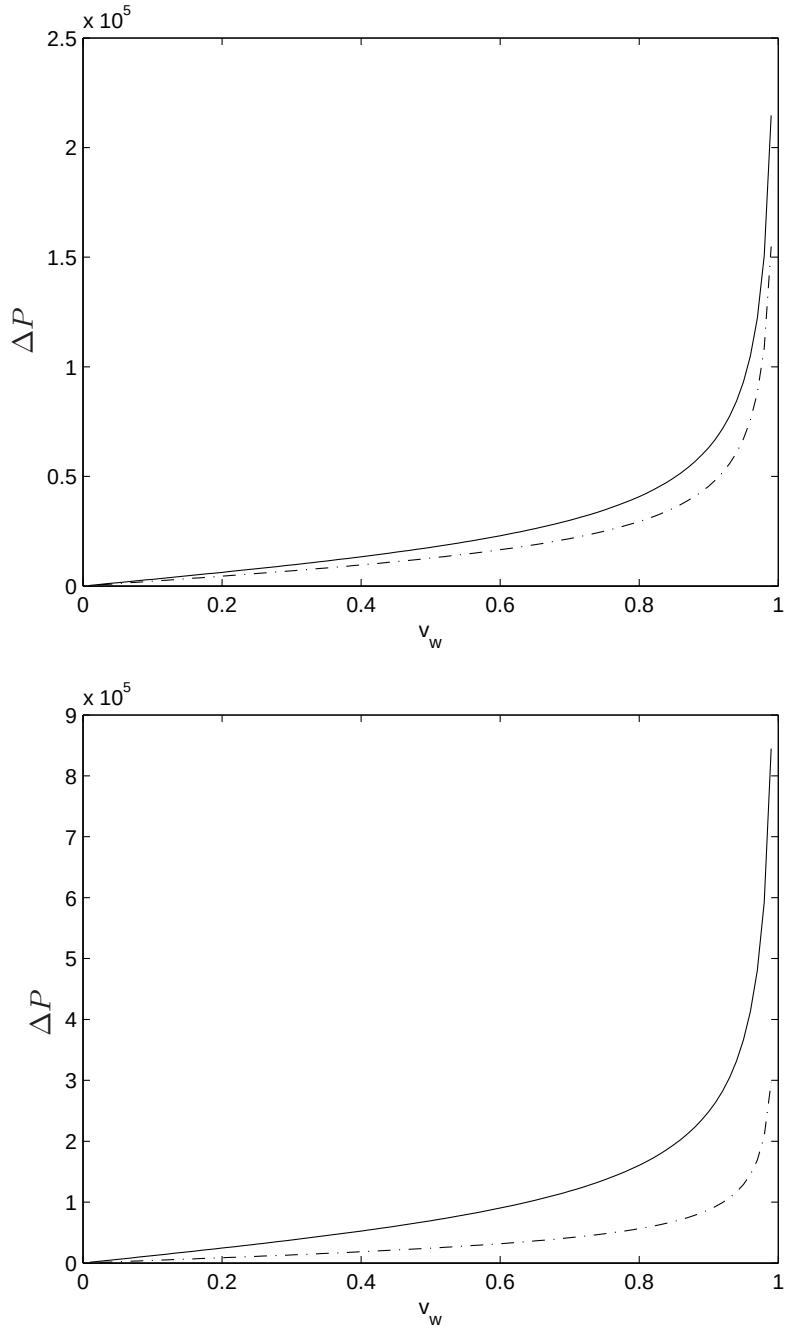

Figure 1.5: Pressure difference (in GeV^4) vs wall velocity in the 'slow wall' limit of the relaxation time approximation for one fermionic (top) and bosonic (bottom) degree of freedom for an assumed $T = 100$ GeV, $L_w = \frac{12}{T}$, $m_b = 100$ GeV, and a Higgs VEV in the broken symmetry phase $\phi_0 = 100$ GeV. The calculation has been done through a double integral over mass and momentum (solid line) and, for comparison, assuming a constant mass across the wall (the particle mass in the broken symmetry phase) (dash-dot line). The relaxation time approximation in the form we have adopted erroneously predicts the pressure difference to diverge as $v_w \longrightarrow 1$.

experienced by the particles that interact with the wall per unit area per unit time.

Let us assume that the interaction between particles and the wall is limited to a plane at the position of the wall, and let us place ourselves in the rest frame of the wall. The wall acts on the particles, inducing a change in momentum, when, and only when, the particles cross the plane of the wall from the symmetric to the broken symmetry phase or viceversa. The advancing wall 'sees' the distribution of kinetic momenta of particles on either side of it. Per unit time and unit area, the amount of particles with kinetic momentum $\vec{p}$ which interact with the wall is given by $f_{\text{incoming}} \cdot v_z$, with v_z the component of velocity directed *towards* the wall. The interaction of a particle with the wall is determined by conservation of energy (which holds in the frame of the wall, see [47]) in the semiclassical picture in which particles are assumed to be on-shell. Particles are assumed to be massive on the broken symmetry side of the interface, massless on the symmetric phase. Consequently for any particle crossing the wall in either direction we have $|\vec{p}|_{\text{symmetric}} = \left(\sqrt{m^2 + |\vec{p}|^2}\right)_{\text{broken}}$. There are two possibilities when the particle reaches the wall: It may cross over or be reflected. Particles crossing from the broken symmetry phase will always cross over, losing their mass and gaining kinetic momentum in the process. However, *(massless) particles hitting the wall from the symmetric phase may be reflected if the component of their kinetic momentum perpendicular to the wall is not sufficient to provide the particle with its mass while keeping some kinetic momentum in that direction*[7]. If particles from the symmetric phase do have enough kinetic momentum in the direction perpendicular to the advancing wall they will cross over to the broken symmetry phase, gaining mass and losing momentum in the process.

Let us assume that the wall propagates in the z direction. As said we operate in the rest frame of the advancing steady-state, planar bubble wall. Looking at either side of the wall, the total pressure due to interactions with the plasma is given by (for one degree of freedom)

$$P_{\text{plasma}} = \int \frac{d^3p}{(2\pi)^3}\, \Delta p_z\, f(\vec{x}, \vec{p})\, v_{\text{z, inbound}} \tag{1.42}$$

for all values of v_z directed *towards* the wall from either phase. This is not a straightforward calculation because in general $f(\vec{x}, \vec{p})$ is not an equilibrium distribution. We can divide this integration into four contributions: 1. Particles reaching the wall from the symmetric phase with total kinetic momentum lower than their mass in the broken symmetry phase,

[7] In the planar approximation the force induced by the wall on the particle is obviously in the direction of wall propagation.

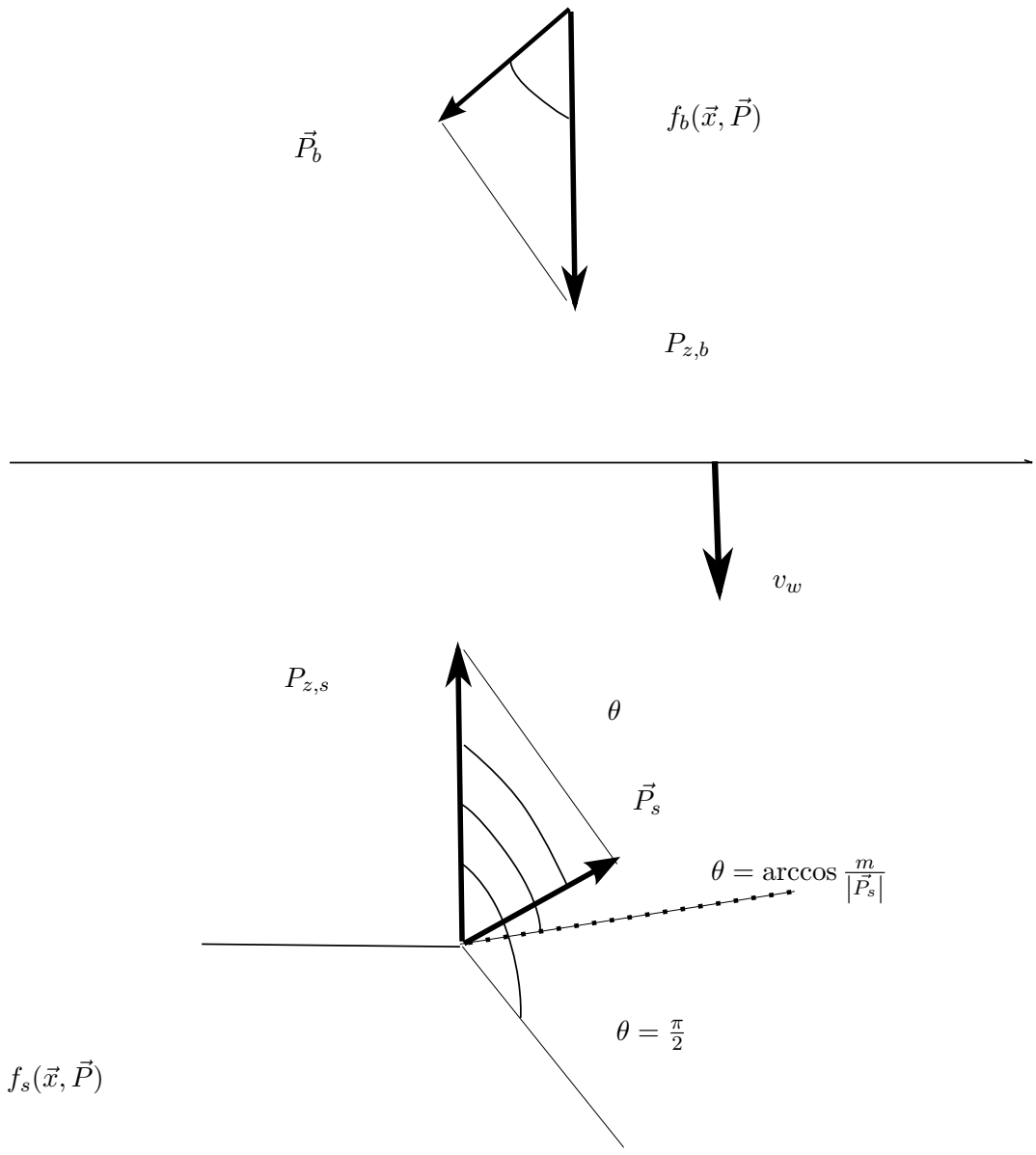

Figure 1.6: Momentum diagram for plasma particles interacting with the planar bubble wall. The broken symmetry phase is at the top, the symmetric phase at the bottom. The wall advances in the negative z direction with velocity v_w. Particles which would acquire a mass m when crossing the wall from the symmetric to the broken symmetry phase will be reflected instead if their momentum points away from the wall with $\theta \geq \arccos \frac{m}{|\vec{P}_s|}$.

and which are therefore reflected ($|\Delta p_z| = 2\,|p_z|$); 2. Particles reaching the wall from the symmetric phase with total kinetic momentum higher than their mass but with p_z *lower* than their mass, also reflected; 3. Particles from the symmetric phase with p_z higher than their mass, and therefore transmitted into the broken symmetry phase ($|\Delta p_z| = p_z - \sqrt{p_z^2 - m^2}$); and 4. Particles reaching the wall from the broken symmetry phase, all of which are transmitted into the symmetric phase. The total pressure due to interactions (for one degree of freedom) becomes $P_{\text{plasma}} = P_1 + P_2 + P_3 + P_4$ with (in spherical coordinates, see fig 1.6)

$$\begin{aligned}
P_1 &= \int_0^m \frac{dp\,p^2}{(2\pi)^2} \int_0^{\frac{\pi}{2}} \sin\theta\, d\theta\, 2p\cos\theta\, v_z\, f_s(\vec{x},\vec{p}) \\
P_2 &= \int_m^\infty \frac{dp\,p^2}{(2\pi)^2} \int_{\arccos\frac{m}{p}}^{\frac{\pi}{2}} \sin\theta\, d\theta\, 2p\cos\theta\, v_z\, f_s(\vec{x},\vec{p}) \\
P_3 &= \int_m^\infty \frac{dp\,p^2}{(2\pi)^2} \int_0^{\arccos\frac{m}{p}} \sin\theta\, d\theta\, \left(p\cos\theta - \sqrt{p^2\cos\theta^2 - m^2}\right) v_z\, f_s(\vec{x},\vec{p}) \\
P_4 &= -\int_m^\infty \frac{dp\,p^2}{(2\pi)^2} \int_{\frac{\pi}{2}}^{\pi} \sin\theta\, d\theta\, \left(\sqrt{p^2\cos\theta^2 + m^2} + p\cos\theta\right) v_z\, f_b(\vec{x},\vec{p})
\end{aligned} \tag{1.43}$$

The subscripts s, b refer respectively to the symmetric and broken symmetry phases. Note that all four contributions have the same sign, that is, all tend to *slow down* the advancing wall. This tells us that the sum of the temperature-dependent part of the effective potential *and* friction effects (given by P_{plasma}, see above) actually contributes 'negative' pressure on the wall, slowing it down in relation to the effect of the vacuum potential.

We may investigate the dependence of P_{plasma} on v_w by making a few simplifications. The calculation is made easier by assuming an *equilibrium* distribution in the symmetric phase and an empty broken symmetry phase, with no particles crossing back into the symmetric phase. For comparison, we calculate, on one hand, the pressure difference (for one degree of freedom, fermionic and bosonic) resulting from *all* particles being reflected irrespectively of their mass; On the other hand we calculate the result of particles being reflected or crossing over to the broken symmetry phase according to their mass and momentum as described above ($P_1 + P_2 + P_3$ in (1.43)). The results are plotted in figure 1.7[8]. We see that assuming total reflection leads to a divergent P_{plasma} as $v_w \longrightarrow 1$.

[8]Note that, since we have assumed an equilibrium distribution in the symmetric phase and, therefore, no particle interactions, the pressure calculated in this way and plotted in figure 1.7 represents an *upper bound* on the real value, as interactions between plasma particles will result in decays and a decrease in

However, considering reflections plus transmissions as above results in $P_{\text{plasma}} = P_1 + P_2 + P_3$ tending towards a finite limit as $v_w \longrightarrow 1$. The explanation for this result, which corrects the apparent conclusions drawn from the relaxation time approximation (1.3.6 and fig 1.5), is as follows: Consider a bubble wall advancing with $v \approx 1$. We can assume in that case that no particles cross over from the broken symmetry phase (behind the wall) to the symmetric phase, and that all particles in the symmetric phase have enough kinetic momentum to acquire mass and cross over to the broken symmetry phase, so that none are reflected. In addition, since in this case (see 1.3.2) the wall hits the medium while at rest, we may consider (with no simplifications applied) the distribution of the incoming particles $f_s(\vec{x}, \vec{p})$ to be an equilibrium distribution. We may also take $p_z \approx p$ so, for small $\frac{m}{p}$, $p - \sqrt{p^2 - m^2} = p\left[1 - \sqrt{1 - \frac{m^2}{p^2}}\right] \approx p\left[1 - (1 - \frac{m^2}{2p^2})\right] = \frac{m^2}{2p}$. The contribution to the pressure due to the plasma left in this case (always for one degree of freedom) can be integrated exactly [33], giving, for bosons,

$$P_{\text{plasma}} = m^2 \int_0^\infty \frac{d^3p}{(2\pi)^3\, 2p}\, f_s(\vec{x}, \vec{p}) = \frac{m^2T^2}{24} \tag{1.44}$$

($\frac{m^2T^2}{48}$ for fermions) (the reason for a finite P_{plasma} in this case can be understood intuitively by taking $E \approx p$ in (1.44); Since $E \sim \gamma$ we are left with the equilibrium particle number density $\int \frac{d^3p}{(2\pi)^3}\, f_s(\vec{x}, \vec{p})$ which goes equally as $\sim \gamma$ [33]). Consequently the pressure on the wall due to plasma interactions in the momentum exchange description (which tend to slow down the wall, as we have seen, in opposition to the vacuum potential contribution) approaches a *finite* limit as $v \to 1$, $\gamma \to \infty$, and therefore arbitrarily high wall velocities are, in principle, possible [33] (put another way, since the vacuum contribution is finite, if the slowing effect of plasma interactions tended to infinity as $v \to 1$, as the relaxation time approximation in the form that we considered suggested, we would already know that there is an upper bound to the bubble wall propagation velocity)[9].

The 'mean field' criterion for runaway walls

Eq (1.44) from [33] provides a natural criterion to determine whether the wall may 'run away' with constant acceleration in a given setting, never reaching a steady state. Recall

friction.

[9] Note again that the pressure difference as calculated from the relaxation time approximation in 1.3.6 does *not* include the effect of the equilibrium part of the particle distributions. That contribution is, however, finite, so it is still true that for that result to agree with the result from this subsection the integral of the friction term in (1.35) would have to tend to a finite limit as $v_w \to 1$.

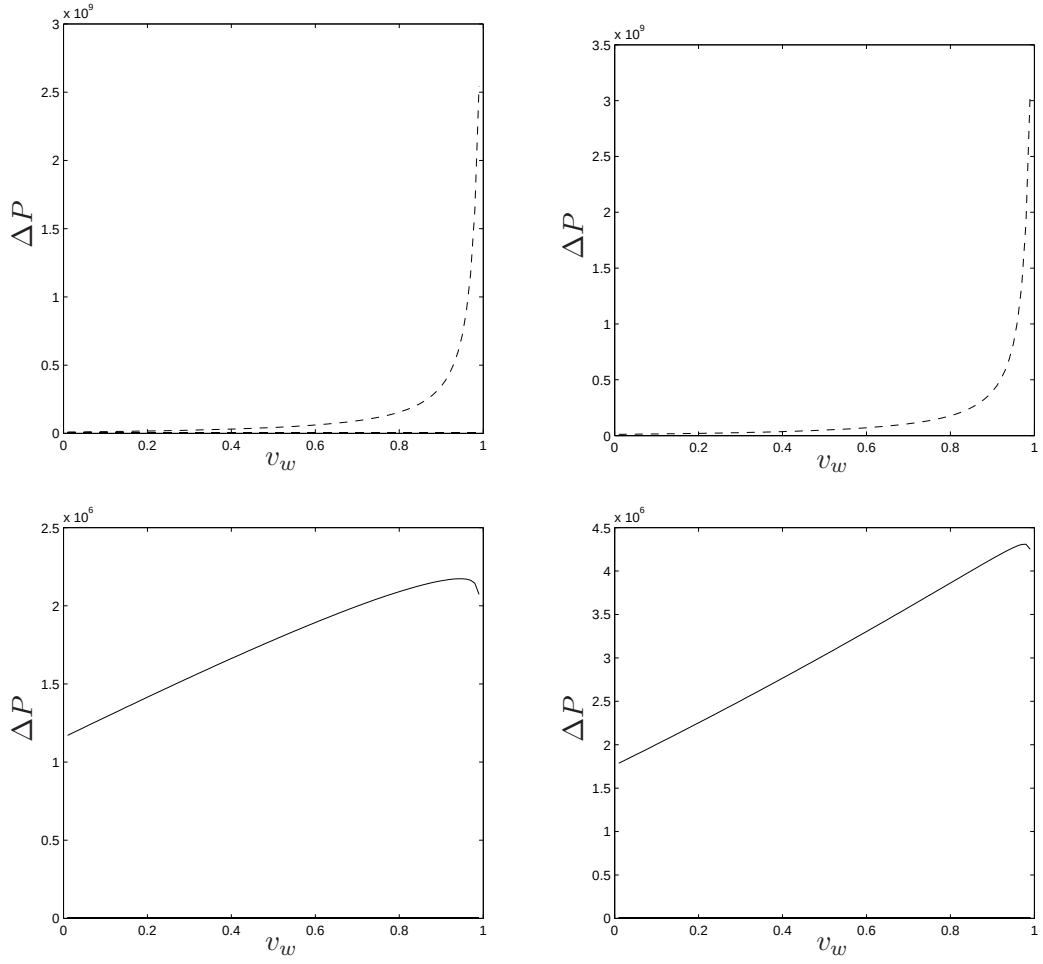

Figure 1.7: Pressure difference (in GeV^4) vs wall velocity in the momentum exchange approximation, assuming an equilibrium distribution in the symmetric phase and no particles crossing back from the broken symmetry phase. Assuming total reflection for all particles results in a diverging ΔP as $v_w \longrightarrow 1$ (top left for fermions, top right for bosons). Taking into account reflections plus transmissions, depending on the particle's mass and momentum, results in a finite limit to ΔP as $v_w \longrightarrow 1$, in accordance with the theoretical limit set in [33] (bottom left for fermions, bottom right for bosons). The downward falloff in the reflection + transmission case as $v_w \longrightarrow 1$ stems from integrating numerically with finite p. We assume $T = 100$ GeV, $m = 100$ GeV.

that the total pressure on the wall is the vacuum pressure (that is, minus the value of the vacuum potential at its second minimum with nonzero VEV, taking its value at the symmetric minimum to be zero) plus the sum of the P_{plasma} from all relevant particles in the 'thermal bath' through which the wall propagates. The total pressure thus defined (which includes friction effects) must be zero for a steady-state wall. Consider now the case of a wall moving with velocity $v_w = 1$, for which P_{plasma} (for one degree of freedom) is given by eq (1.44)[10]. If the total pressure is actually *negative*, or, as stated in [33], if the 'mean-field pseudopotential' formed by the vacuum potential plus the total P_{plasma} from eq (1.44) has a second minimum at nonzero VEV *higher* than the 0-VEV one, then that case may not arise and the wall cannot run away. However, if the pseudopotential has a second minimum *lower* than the 0-VEV one the opposite is the case and the wall *will* run away with constant acceleration.

We will come back to this criterion in our study of the dimension-6 extension to the Standard Model (see 2.2.3).

1.4 Project formalism

1.4.1 General hydrodynamic treatment

Thermodynamic relations and the energy-momentum tensor of the fluid-field system

We are now ready to lay out the formalism that we shall use in this project. We follow essentially the approach in [29] in which friction is described by a phenomenological parameter, included in a friction term introduced by hand in the stress-energy conservation equations for the combined system formed by the background Higgs field and the cosmic plasma. We will suggest an alternative choice of friction term to that found in [29] based on our results in 1.3.

We start by writing the energy-momentum tensor of the system, which receives contributions from both the Higgs scalar field (see eg [54]) and the 'cosmic plasma' of the early universe modelled as a perfect relativistic fluid. As mentioned, the finite-temperature effective potential of the Higgs field equals the free energy density of the whole system F, which is equal to minus the pressure. The thermodynamic relations we shall use are (with s the entropy density)

[10] With *negative* sign as discussed after eq (1.43). P_{plasma} tends to slow down the wall.

$$P = -F \tag{1.45}$$

$$\rho = Ts - P = T\frac{\partial P}{\partial T} - P = -T\frac{\partial F}{\partial T} + F. \tag{1.46}$$

As in our initial example in 1.3.2 it is convenient to divide the pressure and the energy density (both derived through the thermodynamic relations from the Higgs effective potential) into a *radiative* (temperature- but not field-dependent) and a *field-dependent* part. The 'radiative', exclusively temperature-dependent contributions appear in the relevant expansions of the potential and correspond to a pure radiation equation of state $P_r = \rho_r/3$. Note that from now on when we write $V(\phi, T)$ or refer to the effective potential of the Higgs field we will refer to the *field-dependent* part of the potential, chosen to satisfy $V(0, T) \equiv 0$. The contributions to the energy-momentum tensor are therefore

$$T^{\mu\nu}_{\text{field}} = \partial^\mu\phi\partial^\nu\phi - g^{\mu\nu}\left(\frac{1}{2}\partial_\alpha\phi\partial^\alpha\phi\right) \tag{1.47}$$

$$T^{\mu\nu}_{\text{plasma}} = (\rho + P)_{\text{plasma}}u^\mu u^\nu - g^{\mu\nu}\left(P_r - V(\phi, T)\right) \tag{1.48}$$

where u^μ is the 4-velocity of the fluid. Note that we have assigned all contributions from the effective potential to the plasma part and that, as mentioned, P_r is temperature- but not field-dependent. We can now equally split $(\rho + P)_{\text{plasma}}$ into a radiative- and field-dependent part, so that, as per the thermodynamic relations, $(\rho + P)_{\text{plasma}} \equiv (\rho + P)_r - T\frac{\partial V(\phi,T)}{\partial T} = \omega_r - T\frac{\partial V(\phi,T)}{\partial T}$, where the *radiative enthalpy* is $\omega_r = \rho_r + P_r$. With this we have

$$T^{\mu\nu} = \partial^\mu\phi\partial^\nu\phi - g^{\mu\nu}\left(\frac{1}{2}\partial_\alpha\phi\partial^\alpha\phi + P_r - V(\phi, T)\right) + \left(\omega_r - T\frac{\partial V(\phi, T)}{\partial T}\right)u^\mu u^\nu \tag{1.49}$$

We now parametrise the radiation pressure as its form for pure radiation, $P_r = aT^4 = \frac{\pi^2}{90}g^*T^4$, g^* being the number of effective degrees of freedom at the temperature T. Again from the thermodynamic relations and with this parametrisation the radiative entropy is $s_r = \left(\frac{\partial P}{\partial T}\right)_r = 4aT^3$ and $w_r = 4P_r = 4aT^4$.

Energy-momentum conservation equation. The friction term

We are now ready to work with the conservation equation for this energy-momentum tensor, $\partial_\mu T^{\mu\nu} = 0$. We shall follow [29] in splitting the conservation equation into two and

equating each part to plus or minus a suitable friction term with the proper Lorentz structure. Noting that $\partial_\mu \left\{ g^{\mu\nu} V(\phi, T) \right\} = \frac{\partial V(\phi,T)}{\partial \phi} \partial^\nu \phi + \frac{\partial V(\phi,T)}{\partial T} \partial^\nu T$ we write the conservation equation as

$$\partial_\mu \left\{ \partial^\mu \phi \partial^\nu \phi - g^{\mu\nu} \left(\frac{1}{2} \partial_\alpha \phi \partial^\alpha \phi \right) + \left(\omega_r - T \frac{\partial V(\phi,T)}{\partial T} \right) u^\mu u^\nu - g^{\mu\nu} P_r \right\} + \frac{\partial V(\phi,T)}{\partial \phi} \partial^\nu \phi + \frac{\partial V(\phi,T)}{\partial T} \partial^\nu T = 0. \quad (1.50)$$

We must now choose an appropriate form for the friction term. Different forms have been proposed in previous studies, usually dependent on the covariant combination $\partial_\mu \phi u^\mu$ and an adimensional free parameter which describes the effect of microphysics near the bubble wall. An often-suggested form for the term is $T \eta u^\mu \partial_\phi$ with T a characteristic temperature and η a friction parameter [28,43]. To justify our choice of a different friction term recall the form of the term we derived in the relaxation time approximation for a 'slow wall' (see 1.3.6 and eq (1.32)),

$$\frac{dm^2}{d\phi} \tau \beta \gamma v (m^2)' \int \frac{d^3p}{(2\pi)^3 (2E)^2} \frac{e^{\beta\gamma(E - v p_z)}}{(e^{\beta\gamma(E - v p_z)} \pm 1)^2} \approx \phi^2 \phi' \tau \beta \gamma v \int \frac{d^3p}{(2\pi)^3 (2E)^2} \frac{e^{\beta\gamma(E - v p_z)}}{(e^{\beta\gamma(E - v p_z)} \pm 1)^2}$$

(with $\beta = \frac{1}{T}$). The 'slow wall' description is the choice usually made in the literature (see eg [30]), and we expect it to hold (see Fig 1.5) for wall velocities up to $v_w \approx 0.8$. As mentioned in 1.3.6 the integral in this form of the friction term can be made adimensional through the change $p \to p' = \frac{p}{T}$ which contributes a further T factor outside the integral. With a characteristic dependence of the relaxation time $\tau \sim \frac{1}{T}$, we are left with a prefactor to the (adimensional) integral $\sim \frac{1}{T} \phi^2 \phi' \gamma v$. For this reason we propose a friction term of the form $\eta \frac{\phi^2}{T} u^\mu \partial_\mu \phi$, with η our adimensional friction parameter.

Having made this choice we proceed formally by splitting the energy-momentum conservation equation:

$$\partial_\mu \left\{ \partial^\mu \phi \partial^\nu \phi - g^{\mu\nu} \left(\frac{1}{2} \partial_\alpha \phi \partial^\alpha \phi \right) \right\} + \frac{\partial V(\phi,T)}{\partial \phi} \partial^\nu \phi = -\eta \frac{\phi^2}{T_{s1}} u^\mu \partial_\mu \phi \partial^\nu \phi \quad (1.51)$$

$$\partial_\mu \left\{ \left(\omega_r - T \frac{\partial V(\phi,T)}{\partial T} \right) u^\mu u^\nu - g^{\mu\nu} P_r \right\} + \frac{\partial V(\phi,T)}{\partial T} \partial^\nu T = +\eta \frac{\phi^2}{T_{s1}} u^\mu \partial_\mu \phi \partial^\nu \phi \quad (1.52)$$

where we have picked a fixed reference temperature for the denominator of the friction term (instead of the time and space-dependent variable T) so as to simplify our calculations later. As a reference temperature we pick T_{s1} which is the temperature in the symmetric

phase immediately ahead of the bubble wall (fig 1.8) [11].

We proceed in parallel to [29]. Manipulating the equations (for now in a frame-independent fashion) it is easily shown that

$$\partial_\mu \partial^\mu \phi + \frac{\partial V(\phi, T)}{\partial \phi} = -\eta \frac{\phi^2}{T_{s1}} u^\mu \partial_\mu \phi \tag{1.53}$$

$$\partial_\mu \left\{ \left(\omega_r - T \frac{\partial V(\phi, T)}{\partial T} \right) u^\mu u^\nu - g^{\mu\nu} \left(P_r - V(\phi, T) \right) \right\} = \\ = \left(\frac{\partial V(\phi, T)}{\partial \phi} + \eta \frac{\phi^2}{T_{s1}} u^\mu \partial_\mu \phi \right) \partial^\nu \phi. \tag{1.54}$$

As a note, from (1.54) it is possible to derive the entropy production equation for the system (due to the presence of friction) by contracting both sides of the equation with the fluid 4-velocity u_ν. We obtain

$$T \partial_\mu \left\{ \left(s_r - \frac{\partial V(\phi, T)}{\partial T} \right) u^\mu \right\} = \eta \frac{\phi^2}{T_{s1}} (u^\mu \partial_\mu \phi)^2. \tag{1.55}$$

1.4.2 Application to the expanding bubble profile

Up until now our formalism has been fully covariant. We shall now develop it further and apply it to the study of the steady-state hydrodynamics of the expanding bubble.

As we saw in 1.3.2, a single planelike front is not enough to satisfy the boundary conditions of the advancing bubble wall. We shall assume that a deflagration bubble front is preceded by a shock front, and a detonation wall followed by a rarefaction wave.

We shall start by studying the shape of the variables across the bubble wall proper, be it for a deflagration or a detonation bubble. By doing this we connect the values of thermodynamic and hydrodynamic variables (as well as the Higgs VEV) in the symmetric phase immediately ahead of the wall to the values in the broken symmetry phase immediately behind it. This calculation, given our initial choice of values at one end of the wall, gives us the wall velocity. For a deflagration bubble we then determine the variation of the relevant quantities in the region between the bubble wall and the shock front (fig 1.8) [12]. Lastly, we shall study how variables 'leap' across the shock front and shall find their values in the undisturbed universe ahead of the front. In this way we may relate

[11] We could make an alternative choice for this characteristic temperature, like the critical (T_c) or the nucleation (T_n) temperature (see 1.2.1 and 1.2.2). However, as we shall see in the following chapters, temperature variations across the bubble profile are in practice small ($\Delta T \ll T_n$) unless the phase transition is extremely strong and the choice of characteristic temperature for the friction term produces only a small effect.

[12] The deflagration bubble wall and shock front move in general at different velocities. If both are assumed to be planar the hydrodynamic variables do not change in the region between them, but they do if the

conditions inside the bubble, in the broken symmetry phase, to those in the undisturbed medium ahead of the shock front. In particular, we may link the wall velocity to the temperature of the undisturbed universe, which, as a first approximation, we may identify with the nucleation temperature T_n (see 1.2.2). Note that for a detonation wall (which hits the medium while at rest) with no shock front the temperature of the undisturbed universe is the temperature directly ahead of the bubble wall.

The bubble wall

We wish to apply the hydrodynamic equations (1.53)-(1.54) to the advancing bubble front. Once the growing bubble reaches steady-state expansion we may neglect the curvature of the wall, so we adopt the usual 1+1 dimensional approximation, with the spatial dimension taken as perpendicular to the wall, along the direction of bubble expansion (here the x-direction for simplicity). We place ourselves in the rest frame of the advancing wall, in which a steady-state solution with constant wall velocity becomes time-independent. Note that in this frame $u^0 = \gamma$, $u^1 = \gamma v$ and $u^2 = u^3 = 0$. Note also that in a steady state ∂_x is the only nonzero derivative. Eq (1.53) directly becomes

$$\frac{d^2\phi(x)}{dx^2} = \frac{\partial V(\phi,T)}{\partial\phi} + \eta\frac{\phi^2}{T_{s1}}v\gamma\frac{d\phi(x)}{dx} \tag{1.56}$$

Eq (1.54) is a vector equality. In the wall rest frame only the components $\nu = 0{,}1$ are nontrivial. They become

$$\partial_x\left\{\left(\omega_r - T\frac{\partial V(\phi,T)}{\partial T}\right)\gamma^2 v\right\} = 0$$
$$\partial_x\left\{\left(\omega_r - T\frac{\partial V(\phi,T)}{\partial T}\right)\gamma^2 v^2 + P_r - V(\phi,T) + \frac{1}{2}\phi'(x)^2\right\} = 0.$$

From these we write

$$(4aT^4 - T\frac{\partial V(\phi,T)}{\partial T})\gamma^2 v = C_1 \tag{1.57}$$
$$(4aT^4 - T\frac{\partial V(\phi,T)}{\partial T})\gamma^2 v^2 + P_r - V(\phi,T) + \frac{1}{2}(\frac{d\phi}{dx})^2 = C_2 \tag{1.58}$$

where, to sum up, v and T in addition to ϕ are functions only of the spatial coordinate perpendicular to the wall, γ is the usual relativistic factor $(1-v^2)^{-1/2}$, η is our phenomenological friction parameter characterising the resistance of the plasma to the wall's

calculation is refined by taking into account the sphericity of the bubble, as we shall do in this study. For a previous calculation in which the sphericity of the bubble was taken into account see [43].

movement, and T_{s1} is the temperature of the plasma in the symmetric phase just ahead of the wall. The value of the two arbitrary constants C_1 and C_2 is easiest to calculate in the symmetric phase, where $V(\phi, T)$ as well as ϕ and both their spatial derivatives vanish.

For the purposes of solving the coupled system of equations formed by (1.56), (1.57) and (1.58) we define the wall as the region where the Higgs VEV ϕ varies from zero in the symmetric phase to its value in the broken symmetry phase, as given by the effective potential. The boundary conditions applicable to the field are

$$\phi'(x) = 0 \ \text{ (at both ends of the integration interval)} \tag{1.59}$$

$$\phi = 0 \ \text{ (at the symmetric end of the integration interval)} \tag{1.60}$$

We solve the coupled system numerically after calculating C_1, C_2 in the symmetric phase. In order to do this we redefine the temperature and velocity in (1.56)-(1.58) as a reference temperature and velocity plus a deviation, $T \equiv T_0 + \Delta T$, $v \equiv v_0 + \Delta v$ with T_0, v_0 chosen appropriately [13]. Introducing this into (1.57)-(1.58) allows us to solve for ΔT and Δv as a function of the Higgs VEV ϕ (and its first spatial derivative). We can then introduce those expressions into eq (1.56), which becomes a 2nd-degree ordinary differential equation for ϕ that can be solved by numerical methods. As regards interpreting the solution note that for a deflagration bubble wall that brings the fluid back to rest the wall velocity is given by $v_w = |v_b|$ (the fluid velocity of the 'outflow' at the broken symmetry end of the integration interval, just behind the wall, fig 1.8), whereas for a detonation bubble the wall velocity is given by $v_w = |v_{s1}|$, the velocity of the 'inflow' at the intact symmetry end of the integration interval. Since for a detonation solution the 'temperature of the universe' is just the temperature at the restored symmetry end of the integration interval just ahead of the wall ($T_u = T_{s1}$), and since this already gives us the information we are looking for, we shall not concern ourselves with the dynamics of the rarefaction wave which follows the detonation front and brings the fluid back to rest.

Transforming between frames

It is useful to reflect now on the transformation laws between the different frames of reference relevant to our calculation. We have already described the rest frame of the bubble wall and the 'rest frame of the universe', in which the fluid far ahead of and behind

[13] As noted, temperature and velocity deviations across the bubble profile are relatively small ($\Delta T \ll T_n$, $\Delta v \ll v_w$) unless the phase transition is extremely strong, a case we will seldom encounter in our calculations.

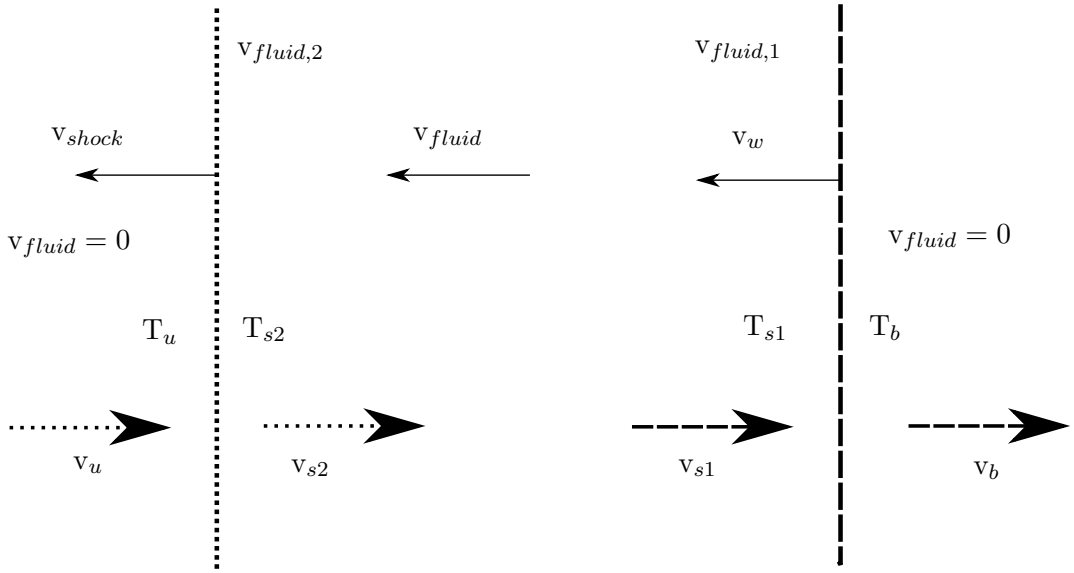

Figure 1.8: Schematic of a deflagration bubble. The vertical dashed line on the right is the bubble wall, the dotted line on the left the shock front. Both propagate from right to left. The relevant fluid velocities are expressed in the rest frames of reference of the bubble wall (v_{s1}, v_b, dashed arrows), the shock front (v_{s2}, v_u, dotted arrows), and the 'universe' (v_{fluid}, v_{shock}, v_w, solid arrows). $v_{\text{fluid},1}$ and $v_{\text{fluid},2}$ are the fluid velocities in the frame of the universe immediately ahead of the bubble wall and immediately behind the shock front, respectively (as, if the sphericity of the bubble is taken into account, the fluid velocity varies in the region between the two). By comparison, v_{s1} is the fluid velocity immediately ahead of the bubble wall in the frame of the wall, and v_{s2} the fluid velocity immediately behind the shock front in the rest frame of the front. T_{s1} is the temperature immediately ahead of the bubble wall, T_{s2} the temperature immediately behind the shock front. Because the rate of propagation of the bubble wall and the shock front are in general different velocities must be transformed covariantly between these three frames as necessary.

the wall is at rest. We have just seen that, for a detonation bubble, $v_w = |v_{s1}|$ (the velocities of the fluid ahead of the wall in the wall frame and that of the wall in the frame of the fluid are equal in module). For a deflagration bubble $v_w = |v_b|$. The third frame of reference of relevance in a deflagration bubble is that of the shock front, which does not in general move with the same velocity as the bubble wall. We call the velocity of the fluid immediately ahead of the shock front *in the shock front's frame* v_u (in the frame of the fluid this velocity is evidently zero). This is obviously the same as the velocity of the shock front in the frame of the universe, $v_{\rm shock} = |v_u|$. We already mentioned that the shock front hits the medium while at rest, heats it up and sets it in motion (in the same direction as the propagation of the bubble). The medium is therefore not at rest in the frame of the universe in the region between the bubble wall and the shock front in a deflagration bubble. We call the velocity of the medium in the frame of the Universe $v_{\rm fluid}$. Because, as mentioned, we shall take the sphericity of the bubble into account, $v_{\rm fluid}$ is *not* constant in the bubble's radial direction. We label as $v_{\rm fluid,1}$ the fluid velocity in the frame of the universe immediately ahead of the bubble wall, and as $v_{\rm fluid,2}$ the fluid velocity in the frame of the universe immediately behind the shock front. The relevant relativistic transformations are then

$$v_{\rm fluid,1} = \frac{v_b - v_{s1}}{1 - v_b v_{s1}} \,|_{\rm bubble\,wall} \tag{1.61}$$

$$v_{\rm fluid,2} = \frac{v_u - v_{s2}}{1 - v_u v_{s2}} \,|_{\rm shock\,front} \tag{1.62}$$

where v_{s2} is the velocity of the fluid in the rest frame of the shock front (not of the bubble wall) immediately behind the front. Figure 1.8 shows the fluid velocities in each of the three frames of reference relevant for a deflagration bubble, as well as the fluid temperatures.

From the bubble wall to the shock front (deflagration bubble)

We return now to the details of our hydrodynamical calculation. By solving the system (1.56)-(1.58) we have found the values of T_{s1}, v_{s1} in front of the bubble wall. As mentioned, we shall improve on previous calculations (eg [29]) by taking the sphericity of the region between the bubble wall and the shock front (in a subsonic bubble) into account, as in [43]. This requires integrating the conservation equations up to the shock front. We do this in the 'frame of the universe', after transforming v_{s1} as shown above. In the frame of the fluid the system is clearly not in a steady state. However, spherically symmetric solutions

to the fluid equations are *similarity solutions* dependent only on the ratio $\zeta = r/t$. The stress-energy conservation equations $\partial_\mu T^{\mu\nu} = 0$ become [43]

$$\frac{\zeta - v}{w}\frac{\partial \rho}{\partial \zeta} = 2\frac{v}{\zeta} + \frac{\partial v}{\partial \zeta}\left(1 - \gamma^2(\zeta - v)\right)$$
$$\frac{1 - v\zeta}{w}\frac{\partial P}{\partial \zeta} = \gamma^2(\zeta - v)\frac{\partial v}{\partial \zeta}.$$

Applying our equations of state and isolating derivatives we obtain

$$\frac{dT}{d\zeta} = \frac{2vT}{3\zeta(1 - v\zeta)}\left[\frac{\zeta - v}{1 - v\zeta} - \frac{1 - v\zeta}{3(\zeta - v)}\right]^{-1} \tag{1.63}$$
$$\frac{dv}{d\zeta} = \frac{2v(1 - v^2)}{3\zeta(\zeta - v)}\left[\frac{\zeta - v}{1 - v\zeta} - \frac{1 - v\zeta}{3(\zeta - v)}\right]^{-1}. \tag{1.64}$$

We integrate numerically along the radial direction, starting at the bubble wall and making an initial guess for the value of ζ at the shock front. At the shock front, ζ *is* the shock front velocity so we transform the final value of the fluid velocity $v_{\text{fluid},2}$ given by the integration (immediately behind the front) to its value in the frame of the front v_{s2}, then calculate the leap in variables (see below) to find the fluid velocity v_u ahead of the front. We keep taking guesses until v_u matches our guessed ζ at the position of the front and the solution becomes self-consistent. With the right $\zeta_{\text{shock front}}$, the calculation of the leap across the front gives us the temperature of the undisturbed universe T_u.

The shock front in a deflagration

The stress-energy conservation equations have a simple expression in the rest frame of the steady-state shock front where (as for the case of the rest frame of the bubble wall) all variables are time-independent. As we are in the restored symmetry phase the Higgs VEV and the effective potential vanish. The two nontrivial stress-energy conservation equations simplify to

$$\partial_x[(P + \rho)\gamma^2 v] = 0$$
$$\partial_x[(P + \rho)\gamma^2 v^2 + P] = 0$$

which integrate to

$$v_u = \frac{1}{\sqrt{3}}\sqrt{\frac{3T_{s2}^4 + T_u^4}{3T_u^4 + T_{s2}^4}} \tag{1.65}$$
$$v_{s2} = \frac{1}{3v_u}. \tag{1.66}$$

By finding T_u we have completed the calculation that we started by solving the energy-momentum conservation equations across the bubble wall.

We have now outlined the basic formalism of our calculation and are ready to tackle specific physical examples.

1.4.3 Validity of the modelling of friction through the friction parameter

Having described our treatment in detail it is worth pausing to consider whether it is fully justified to model friction effects through a single numerical parameter. Following [29] we have introduced our choice of friction term into the hydrodynamical equations written in covariant form. This implies that the friction parameter η is a Lorentz scalar and thus independent of the velocity of our rest frame relative to the cosmic fluid, that is, of the wall velocity. Evidently the friction term as a whole ($\eta\frac{1}{T}\gamma v\phi^2\phi'$) has an explicit velocity dependence, as well as an indirect dependence as the wall velocity is likely to have an effect on the shape of the wall which is given by the factors $\phi(z)^2\phi'(z)$. However, in our formalism, the relevant physics (the particle content of the model as well as the interactions between the particles and the wall) is parametrised by a fixed dimensionless number η for a set of the relevant model parameters. We now attempt to verify that this is a reasonable assumption by examining again the physical model for the friction that we set down in 1.3.

We must address two separate issues: First, is the physics of the interactions between the wall and the plasma, as expressed by the friction parameter, independent of velocity (notwithstanding the dependence on velocity of the friction term that we have just discussed)? Second, since we are studying the hydrodynamics of the expanding bubble by integrating the equation of motion for the Higgs across the bubble wall, is parametrising the friction by a single numerical parameter *constant across the wall* a good enough approximation? If the answer to either question is no our formalism may be in danger.

Does the friction parameter depend on velocity?

Recall the model for the friction term suggested by the slow wall limit of the relaxation time approximation (1.33),

$$\frac{dm^2}{d\phi}\int\frac{d^3p}{(2\pi)^3 2E}\tau\beta\gamma v\frac{(m^2)'}{2E}\frac{e^{\beta\gamma(E-vp_z)}}{(e^{\beta\gamma(E-vp_z)}\pm 1)^2}\sim\phi^2\phi'\tau\beta\gamma v\int\frac{d^3p}{(2\pi)^3(2E)^2}\frac{e^{\beta\gamma(E-vp_z)}}{(e^{\beta\gamma(E-vp_z)}\pm 1)^2}$$

where we have assumed a general mass dependence $m\sim y\phi$ with y the relevant coupling constant. Comparing with the friction term we have chosen for our formalism, $\eta\frac{1}{T}\gamma v\phi^2\phi'$,

we see that the friction parameter η would, in this limit, be given by a combination of constants times the momentum integrals for the relevant particle species. We may therefore study the velocity dependence of the friction parameter by focusing on the behaviour of the momentum integrals. Noting that $E = \sqrt{m^2 + \vec{p}^2}$ and $p_z = p\cos\theta$ we may write[14]

$$\int \frac{d^3p}{(2\pi)^3(2E)^2} \frac{e^{\beta\gamma(E-vp_z)}}{(e^{\beta\gamma(E-vp_z)} \pm 1)^2} = \int_0^\pi \int_0^\infty \frac{(2\pi)p^2 \sin\theta d\theta dp}{(2\pi)^3 4(m^2+p^2)} \frac{e^{\beta\gamma(E-vp_z)}}{(e^{\beta\gamma(E-vp_z)} \pm 1)^2} =$$
$$= T \int_0^\pi \int_0^\infty \frac{1}{4(2\pi)^2} \frac{p'^2 \sin\theta d\theta dp'}{\left((\frac{m}{T})^2 + p'^2\right)} \frac{e^{\gamma\left(\sqrt{\left((\frac{m}{T})^2+p'^2\right)} - vp'\cos\theta\right)}}{(e^{\gamma\left(\sqrt{\left((\frac{m}{T})^2+p'^2\right)} - vp'\cos\theta\right)} \pm 1)^2} \quad (1.67)$$

where in the last equality we have made the change $p \to p' = \frac{p}{T}$. With this change, as noted, the temperature dependence suggested by the relaxation time approximation matches that of our chosen friction term from 1.4.1. Eq (1.67) can be solved numerically as a function of $(\frac{m}{T})$ for a given v. Comparing the results (Fig 1.9) we see that the momentum integrals that determine the friction coefficient in our description show only *a very slow variation with* v. Consequently (and particularly since in our calculations we shall seldom encounter ultrarelativistic wall velocities) we may consider the friction coefficient, for our purposes, as independent of the wall velocity.

The friction parameter across the bubble wall

Let us study the behaviour of the friction term across the bubble wall. We can do this without referring to a specific hydrodynamic calculation using the hyperbolic tangent Ansatz for the wall profile (1.3.3). As mentioned, our formal choice for the friction term was suggested by the slow wall limit of the relaxation time approximation (1.4.1),

$$\phi^2\phi' \frac{\tau}{T}\gamma v \int \frac{d^3p}{(2\pi)^3(2E)^2} \frac{e^{\beta\gamma(E-v_w p_z)}}{(e^{\beta\gamma(E-v_w p_z)} \pm 1)^2} \longrightarrow \eta \frac{1}{T}\phi^2\phi'\gamma v$$

(here we place ourselves, as always, in the rest frame of the advancing planar bubble wall and are thus left with a dependence on a single spatial dimension). Let us compare both forms of the term for a simple example case, taking $v_w \equiv 0$ in the exponentials in accordance with our previous result. We adopt a VEV of 100 GeV in the broken symmetry phase, a temperature $T = 100$ GeV, a wall thickness given by $L_w \cdot T = 15$ (a realistic value)

[14] Note that this integral is essentially the *integrand* of the pressure difference in the 'slow wall' limit of the relaxation time approximation. We shall see presently that it depends very slightly on v_w, which confirms our comments in 1.3.6 to the effect that the dependence of $\Delta P_{\rm sw}$ on v_w is essentially given by the overall γv_w factor.

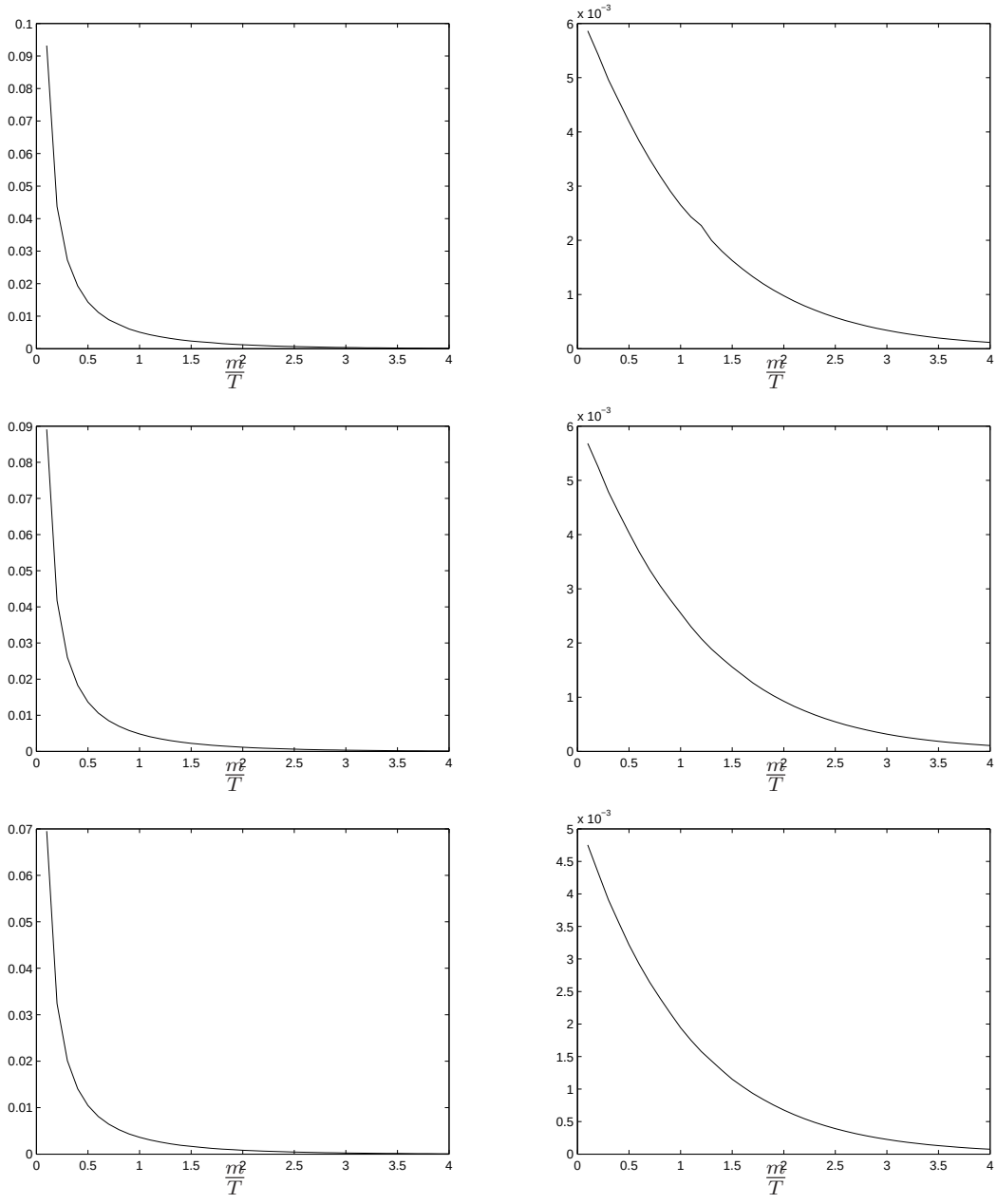

Figure 1.9: Momentum integrals in (1.67) for bosons (left) and fermions (right) vs $\left(\frac{m}{T}\right)$ for $v = 0.05$ (top row), 0.4 (middle) and 0.8 (bottom).

and a mass coupling $m \equiv \frac{1}{\sqrt{2}}\phi$. In the relaxation time approximation for a slow wall the spatial dependence of the friction (that is, of the effect of the deviation of plasma particle populations from equilibrium) is given by the momentum integral through the expression for the energy $E = \sqrt{m(z)^2 + \vec{p}^2}$. We may therefore plot $\int \frac{d^3p}{(2\pi)^3(2E)^2} \frac{e^{\beta E}}{(e^{\beta E} \pm 1)^2} \phi^2\phi'$ vs $C\ \phi^2\phi'$, with C an appropriately chosen (fermionic or bosonic) fitting constant. The result is shown in figure 1.10.

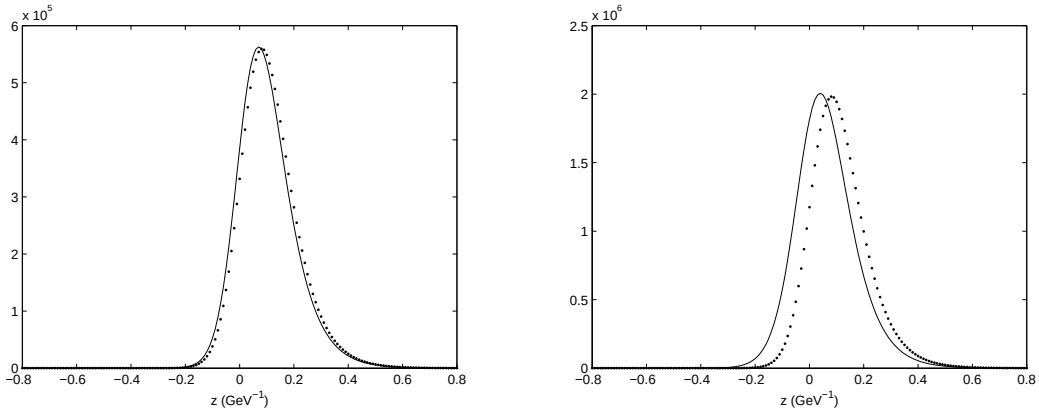

Figure 1.10: Spatially varying part of the friction term according to the relaxation time approximation (slow wall), $\phi^2\phi' \int \frac{d^3p}{(2\pi)^3(2E)^2} \frac{e^{\beta\gamma(E - v_w p_z)}}{(e^{\beta\gamma(E - v_w p_z)} \pm 1)^2}$ (solid line), and the same term with the momentum integral replaced by a fitted constant (dotted line), $C\ \phi^2\phi'$, for fermions (left) and bosons (right) in an example case. We use the hyperbolic tangent Ansatz to approximate the bubble profile and assume $\phi_0 = 100$ GeV in the broken symmetry phase, $T = 100$ GeV, $L_w \cdot T = 15$, and a mass dependence $m \equiv \frac{1}{\sqrt{2}}\phi$.

Note that the fitting constant has been chosen to equalise the peaks of the two profiles. As we can see it is possible to fit the momentum integral by a constant which, to a high degree of precision, gives an identical behaviour for the friction term across the wall, for any given wall velocity. In particular, it is clear that the constant fit would produce the same result for the pressure integral, eq (1.35). We may conclude, therefore, that any given result we may arrive at by explicitly accounting for the variation of friction effects across the bubble wall may be reproduced by a properly chosen, invariant friction coefficient.

Having convinced ourselves that it is valid to account for friction in our treatment through a single numerical parameter we are prepared to tackle specific physical cases.

Chapter 2

The wall velocity in the Standard Model with dimension-6 interactions

2.1 The dimension-6 model

2.1.1 Motivation

We have already noted (see Introduction) the limitations of the Standard Model as regards replicating the observed baryon asymmetry of the universe in the context of a first-order electroweak phase transition, and have mentioned some of the proposed alternatives. Several authors have investigated the possibility that new physics, showing up as higher-dimensional, nonrenormalisable operators in the scalar potential, may get around the constraints posed by present experimental bounds on the Higgs mass and provide additional sources of CP violation [55–57]. Studies in recent years have suggested adding dimension-6 operators to the Higgs potential [25, 58, 59] while noting that, as shown by numerical calculations, further higher-order terms suppressed by the same low cut-off scale give corrections of only a few percent to the strength of the phase transition $\frac{v_c}{T_c}$ [58]. In such a setting the dynamics of the electroweak phase transition are fully parametrised by the Higgs boson mass m_H and the cut-off scale M. It is interesting to note that in such a situation the quartic coupling of the Higgs potential may assume negative values. As to the origin of the dimension-6 operators, they could stem from integrating out a massive degree of freedom like a scalar singlet [58]. More exotic alternatives include strongly coupled gravity [25]. A further motivation to investigate these models is that new physics

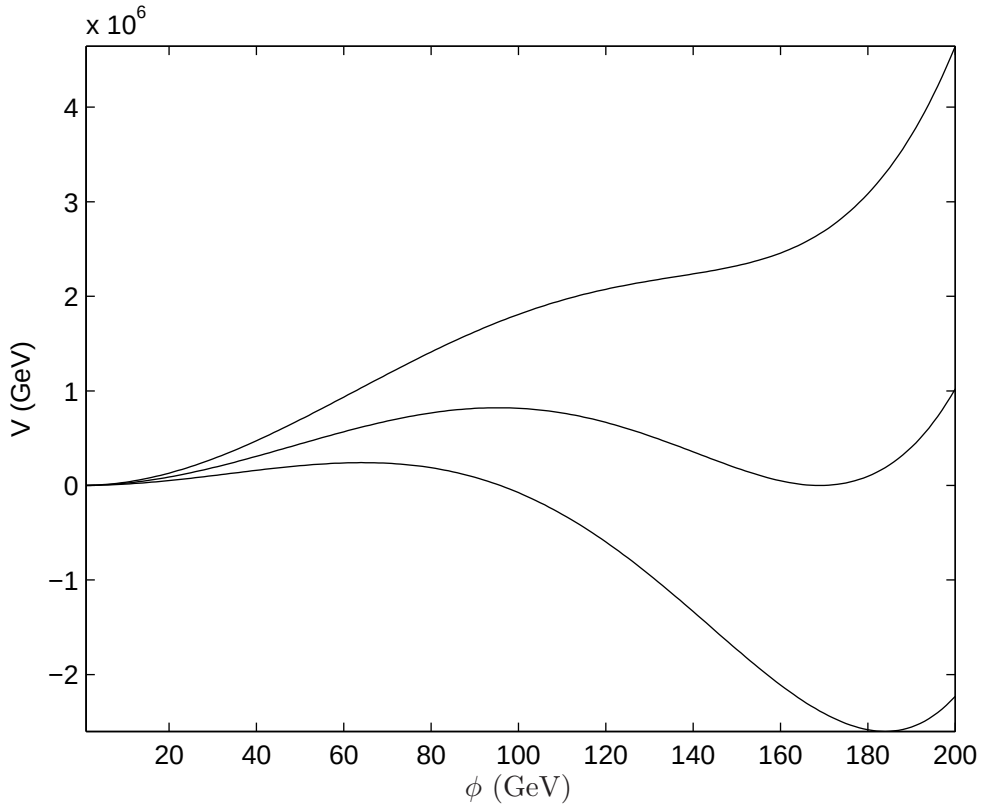

Figure 2.1: High-temperature expansion of the finite-T Higgs effective potential in the dimension-6 model for model parameters $M = 800$ GeV, $m_h = 115$ GeV. The three successive curves (from top to bottom) mark the potential at $T = 111$ GeV $> T_c$, at the critical temperature $T_c \approx 108.14$ GeV, and at the nucleation temperature $T_n \approx 105.49$ GeV.

with a comparatively low cut-off may lead to non-standard signals which could be picked up in the near future, such as modified Higgs self-couplings [25, 58].

The behaviour of the effective potential $V(\phi, T)$ near the critical temperature T_c for $M = 800$ GeV, $m_h = 115$ GeV can be seen in figure 2.1. The form of the potential is given in detail in Appendix A.

2.1.2 Interest for baryogenesis

As mentioned, the Standard Model Higgs potential augmented by a dimension-6 contribution allows for a 1st-order electroweak phase transition with sufficient sources of CP-violation for presently acceptable values of the Higgs boson mass. In addition, figure 2.2 shows the strength of the phase transition as calculated at 1-loop in [25] as a function of the Higgs mass and the cut-off scale for the dimension-6 term M.

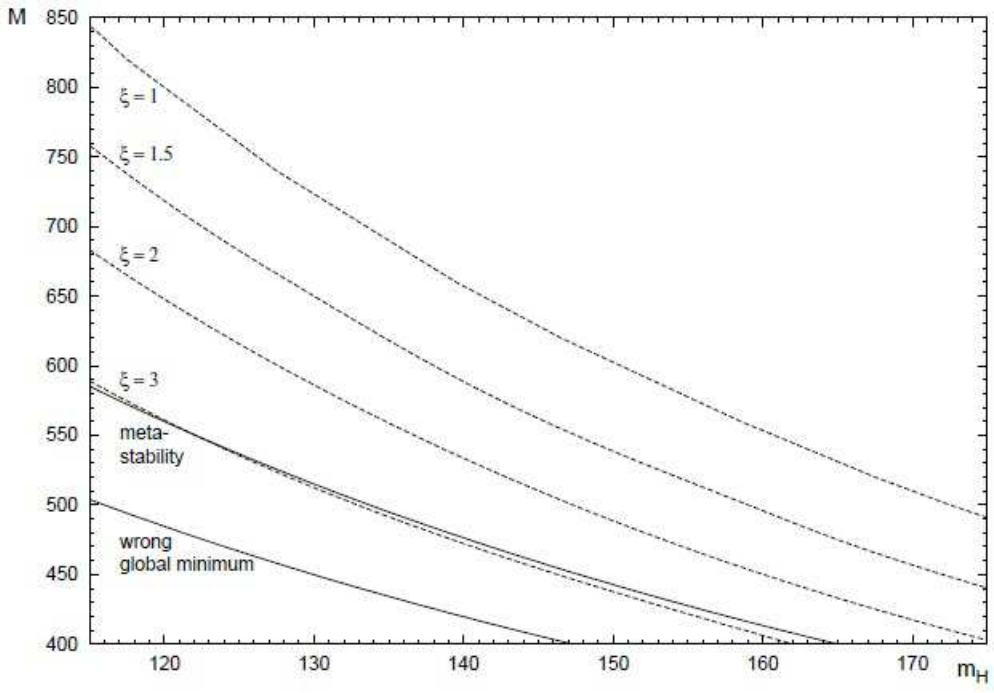

Figure 2.2: Strength of the phase transition $\xi_c = \frac{v_c}{T_c}$ as a function of the Higgs mass m_H and the cut-off scale M (both in GeV) for the dimension-6 model (Figure from [25]). Below the higher solid 'metastability' line the tunneling probability becomes too small for the phase transition to take place as outlined in 1.2. Below the lower solid line the second minimum of the Higgs potential (with VEV $\neq 0$) at zero temperature is *higher* than the VEV $= 0$ one.

2.2 Calculation of the wall velocity

2.2.1 Strategy

We now present the results of carrying out the full hydrodynamic calculation for this model as outlined in Chapter 1. We focus on the region in parameter space in which a sufficiently strong ($\xi \gtrsim 1$) phase transition can occur. For each relevant set of model parameters (M, m_H) we compute the nucleation temperature. Provided we know the value of the friction parameter η we may then calculate the steady-state bubble wall velocity.

We start our exploration of the dimension-6 model by studying the general behaviour of the wall velocity for deflagration (subsonic) and detonation (supersonic) solutions as a function of temperature and friction. We then turn to physically meaningful cases by employing the microscopic calculation of the wall velocity carried out at 2-loop in [30] for the Standard Model (without extensions). We do this by, firstly, calculating the values of the friction parameter that reproduce the 2-loop results from that reference. We then employ the relaxation time approximation (see 1.3.6) to the Boltzmann evolution equations to extrapolate our findings to our dimension-6 extension to the SM, thus obtaining a prediction for the friction[1]. We employ that prediction to investigate the steady-state wall velocity within our model's parameter space.

2.2.2 General behaviour of the wall velocity as a function of the model parameters and friction

Calculation of the nucleation temperature

Figure 2.3 shows an example critical bubble profile (a solution to (1.2)) for the dimension-6 model, in this case the solution at the nucleation temperature T_n for the model parameters $M = 800$ GeV, $m_h = 115$ GeV. After solving the equation of motion for a sufficient number of critical bubbles and finding their free energies (as per 1.1) we may integrate numerically to find the nucleation temperature as per (1.5)-(1.6). It can be seen from the plots in figure 2.4 that a good approximation to T_n is given by the temperature at which the free energy of the critical bubble F_c satisfies $\frac{F_c}{T} = 140$.

Shape of the hydrodynamical solutions

As laid out in 1.4, we now calculate the variation of the relevant quantities across the bubble profile for a choice of model parameters. Let us start with a deflagration bubble.

[1] The limitations of such a prediction and its reliability will be commented on later.

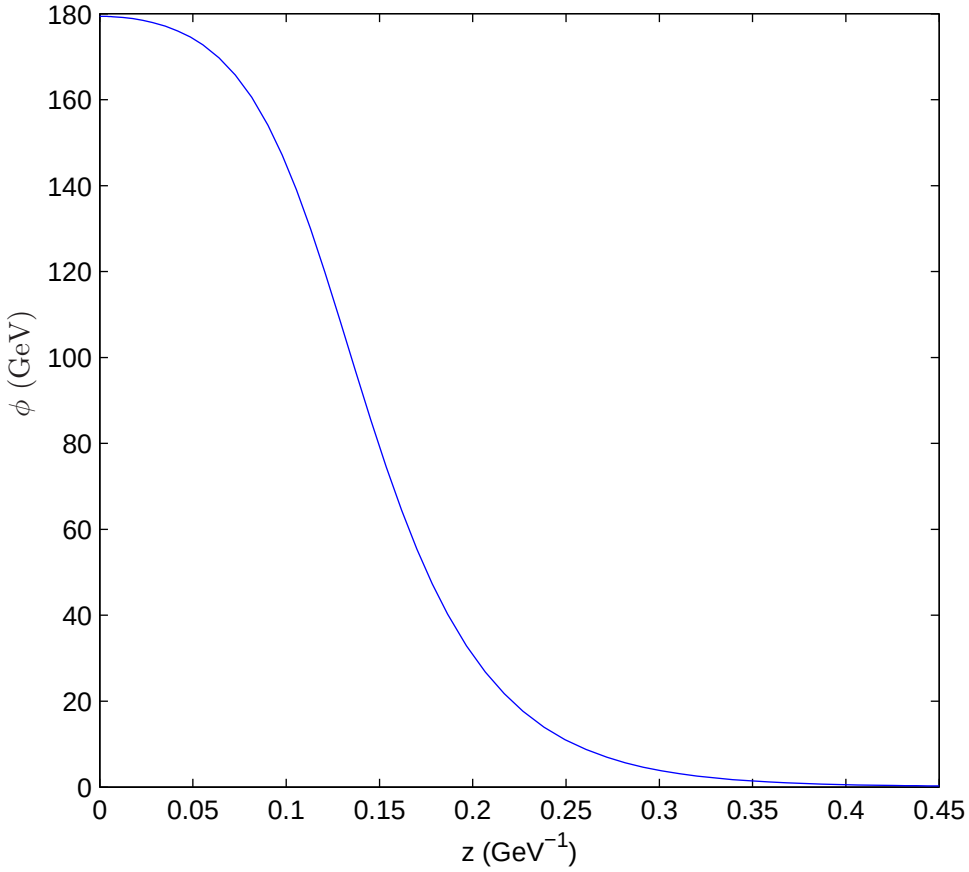

Figure 2.3: Critical bubble solution for the ϕ^6 model with $M = 800$, $m_h = 115$ GeV at $T = 105.49$ GeV.

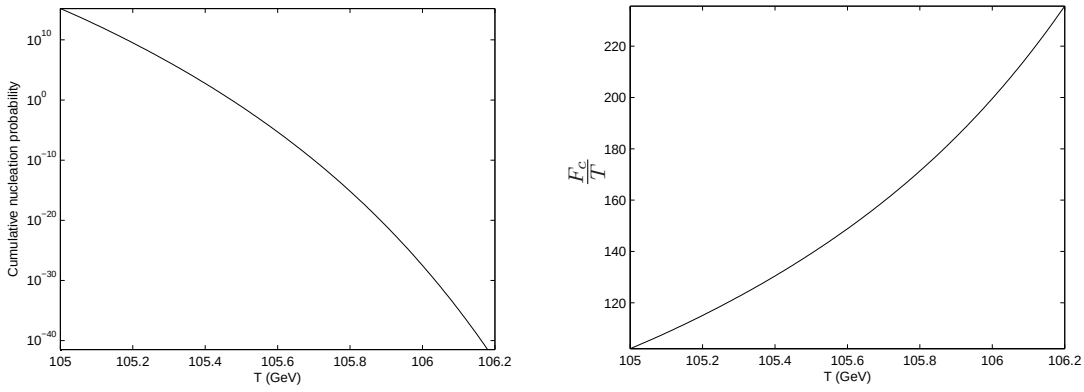

Figure 2.4: Integrated nucleation probability (left) and free energy of the critical bubble divided by temperature ($\frac{F_c}{T}$) (right) vs temperature (in GeV) for the dimension-6 model with $M = 800$ GeV, $m_h = 115$ GeV. From this we adopt $T_n \equiv 105.49$ GeV for this case. The plots illustrate the result that the condition $\frac{F_c}{T} = 140$ gives a good approximation to $\int dP \equiv 1$ at T_n.

Figure 2.5 shows the result of integrating the system (1.56)-(1.58) numerically as a boundary value problem assuming an initial value for either T_{s1} or T_b and a value of the friction coefficient η, and imposing the boundary conditions (1.59)-(1.60). We can see how the Higgs VEV, acting as the order parameter for the phase transition, evolves from zero to its nonzero value at the second minimum of the effective potential in the broken symmetry phase. The medium, heated up and set in motion in the direction of wall propagation by the shock front, is cooled down and brought back to rest by the passing bubble wall so that v_b gives us the wall velocity (see 1.4.2). After solving the hydrodynamic equations across the wall profile, we transform the relevant quantities to the rest frame of the fluid and calculate the variation of the temperature and fluid velocity across the region between the bubble wall and the shock front. The boundary condition for this calculation consists of the velocity of the fluid ahead of the shock front (in the shock front frame, found by computing the 'leap' across the front via (1.65)-(1.66)) equalling $\zeta = \frac{r}{t}$ for the shock front. The results of this integration are shown in figure 2.6. Finally, with (1.65)-(1.66) we find the value of the variables in the undisturbed medium ahead of the shock front, including the temperature of the undisturbed universe T_u.

Our calculation is easier for a detonation bubble (Fig 2.7). In this case there is no shock front and the advancing bubble wall hits the medium while as yet undisturbed. Therefore T_{s1} as given by (1.56)-(1.58) is already T_u (1.4.2) and v_{s1} gives us the wall velocity. Since this is the information we are after we do not investigate in detail the rarefaction wave which follows the bubble wall proper and brings the medium back to rest.

The wall velocity as a function of temperature. Stable solutions.

Before tackling the problem of calculating the friction parameter for a realistic physical situation we explore the general behaviour of the steady-state wall velocity as a function of temperature and friction for a given choice of M, m_h. Figure 2.8 shows the result of such a study for the model parameters $M = 800$ GeV, $m_h = 120$ GeV and a choice of $\eta = 0.3$, 0.4, 0.5. Our result shows the same general characteristics as previous studies (see eg [60]). Deflagration (subsonic) steady-state solutions for a given value of the friction become faster (approaching the speed of sound in the medium) with decreasing temperature. If the temperature is low enough additional solutions appear in the form of two branches of supersonic solutions (detonations). The consensus [60] is that the lower of these branches is unphysical, as it would imply that the wall velocity *decreases* while both the pressure difference $\Delta V(\phi, T)$ and the temperature difference between the symmetric and the broken

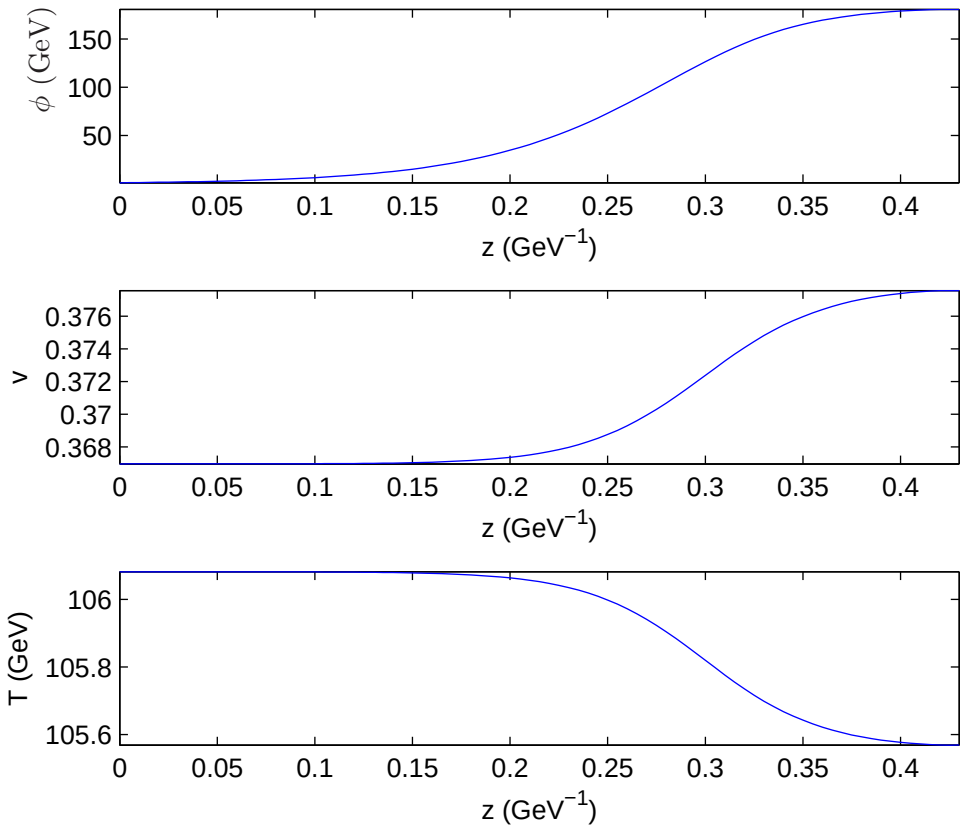

Figure 2.5: Higgs VEV ϕ, velocity and temperature profiles across the (deflagration) bubble wall for the ϕ^6 model with $M = 800$ GeV, $m_h = 115$ GeV at the temperature of the universe (ahead of the shock front) $T_u = 105.49$ GeV and a value of the friction coefficient $\eta = 0.398$. The broken symmetry phase is on the right and the bubble wall propagates from right to left.

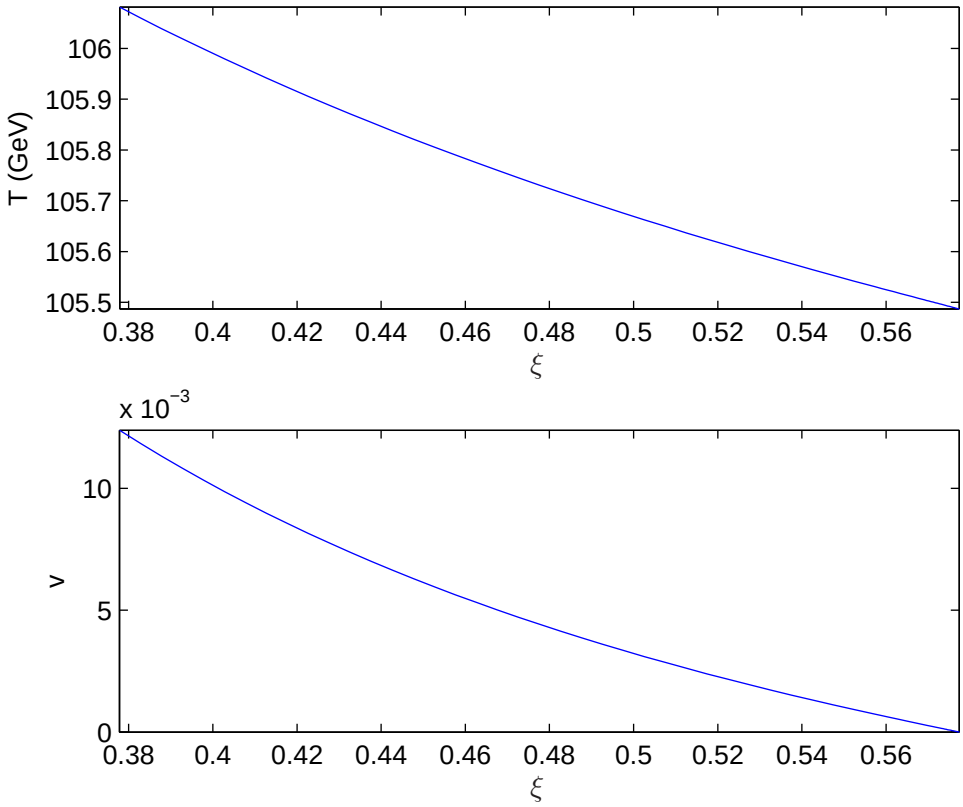

Figure 2.6: Velocity and temperature profiles across the intermediate region between the bubble wall and the shock front for the same deflagration bubble as in figure 2.5 with $M = 800$ GeV, $m_h = 115$ GeV at $T_u = 105.49$ GeV. Here the position of the bubble wall is on the left end of the integration interval and that of the shock front on the right. If the sphericity of the bubble is neglected (and a less realistic planar approximation adopted instead) v and T do not vary across this region.

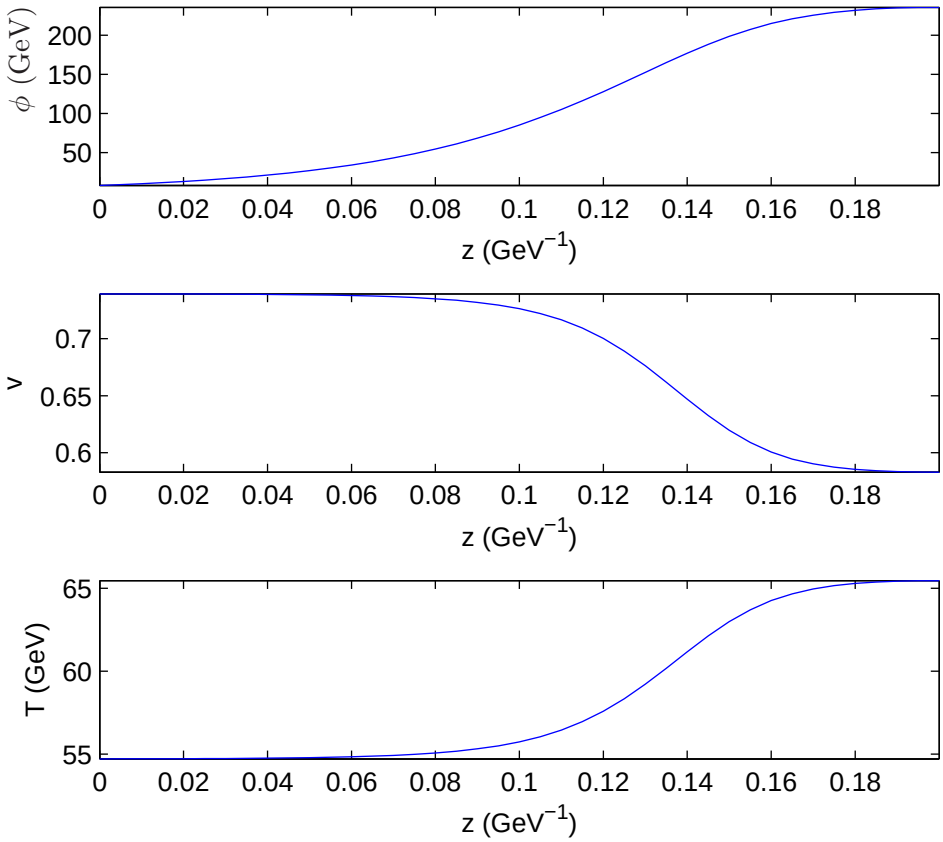

Figure 2.7: Higgs VEV ϕ, velocity and temperature profiles across the (supersonic) bubble wall for the ϕ^6 model with $M = 610$ GeV, $m_h = 115$ GeV at the temperature of the universe (immediately ahead of the bubble wall for a detonation) $T_u = 54.70$ GeV and a value of the friction coefficient $\eta = 0.153$. The broken symmetry phase is on the right and the bubble wall propagates from right to left.

symmetry phases become *larger* (with decreasing temperature). In general, and as we would expect, lower values of η produce higher velocities except for the lower supersonic branch (another reason for deeming it unphysical). As we can see, the values of the nucleation and finalisation temperatures for a set of the model parameters tell us whether supersonic solutions may exist for a given value of η. Because some treatments of the bubble wall hydrodynamics (eg [29]) fail to take into account the sphericity of the bubble when calculating the evolution of variables across the bubble profile (1.4.2), we plot by comparison the deflagration bubble wall velocities found by adopting that simplification as dotted curves in the subsonic part of the diagram. We see that the planar approximation gives *higher* (by $\lesssim 10\%$) wall velocities for a given η than does our full treatment. Lastly, we refer briefly to the stability criterion for small wall velocities described in [31] and mentioned in 1.3.2. That reference essentially establishes that the growing deflagration bubble may be unstable to perturbations to the bubble wall *larger than a critical scale* λ_c whenever the wall velocity decreases with decreasing T_{s1} (more precisely, but in practice nearly always equivalently given the strong dependence of v_b on T_{s1}, whenever $\frac{dv_b}{dT_{s1}} > 1$). Figure 2.9 shows the dependence of T_{s1} with T_u for the setting in figure 2.8. As we have seen, the wall velocity for a deflagration increases monotonically with decreasing temperature of the universe, so the stability criterion is fulfilled for high temperatures down to the point when T_{s1} starts rising with decreasing T_u. The point at which this criterion would indicate possible instability to perturbations of the bubble wall is marked (for each η) with a cross and an error bar in figure 2.8, the possible instability region lying to the left of the mark. We can see that the appearance of instability as T_u descends, according to this criterion, coincides roughly with that of supersonic solutions for that value of η [2].

Figures 2.10 and 2.11 represent the case $M = 900$ GeV, $m_h = 120$ GeV. As we can see, the value of the nucleation temperature depends sensitively on the choice of model parameters.

2.2.3 Calculation of the friction parameter based in existing results for the Standard Model. The wall velocity in the dimension-6 model.

As mentioned, we now employ the microscopic, 2-loop calculation of the wall velocity in [30] to obtain a realistic value for the friction coefficient in the parameter space of our

[2] It must be noted, however, that in some areas in parameter space a range of T_us appears to exist in which deflagration bubbles are no longer stable but detonation solutions have not yet appeared for some ηs. We did not probe this any further since our goal was to focus on physically meaningful cases, see 2.2.3.

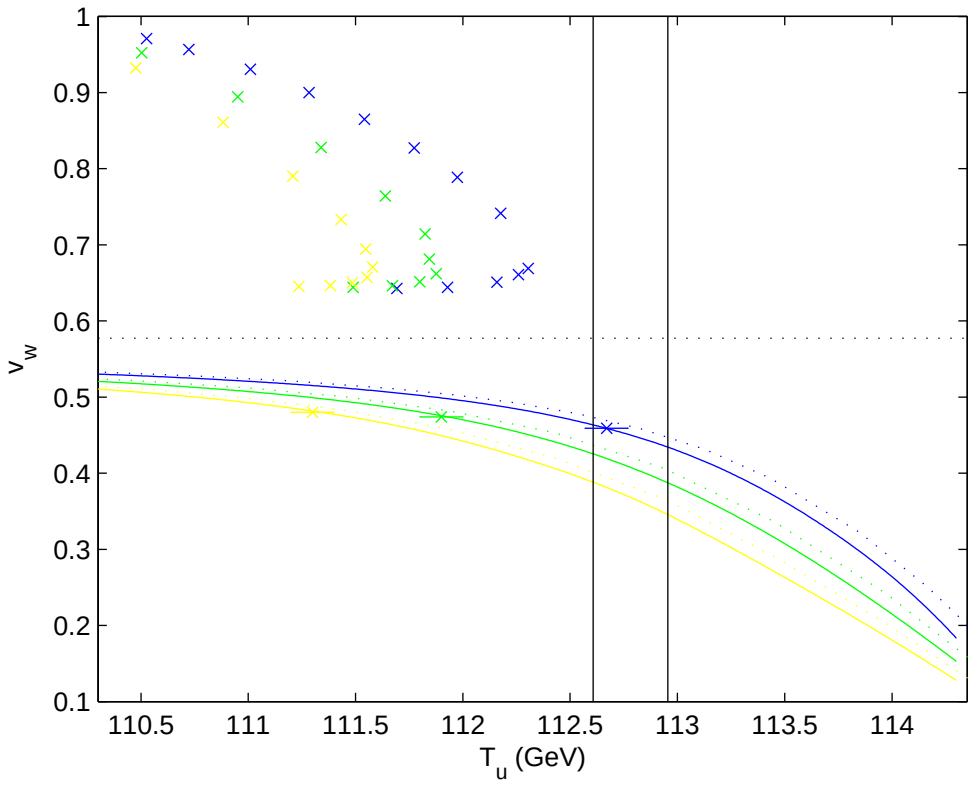

Figure 2.8: Steady-state bubble wall velocity vs temperature of the universe for three values of the friction coefficient η, 0.3 (blue, right), 0.4 (green) and 0.5 (yellow, left) for the dimension-6 model with $M = 800$ GeV, $m_h = 120$ GeV. The horizontal dotted line marks the speed of sound in the medium. The solid (dotted) lines below the speed of sound limit are subsonic solutions found through taking into account (neglecting) the sphericity of the bubble. At the horizontal error bars the stability criterion for subsonic solutions proposed in [31] changes sign (the stability region lies to the right of the mark). The crosses above the speed of sound show two branches of supersonic solutions (only the upper one is physical, see eg [60]). The two vertical lines mark the nucleation (right) and finalisation (left) temperatures for the phase transition for this choice of parameters. Note that for this example and for these values of η supersonic steady-state solutions would be excluded but (stable) subsonic ones allowed for the duration of the phase transition.

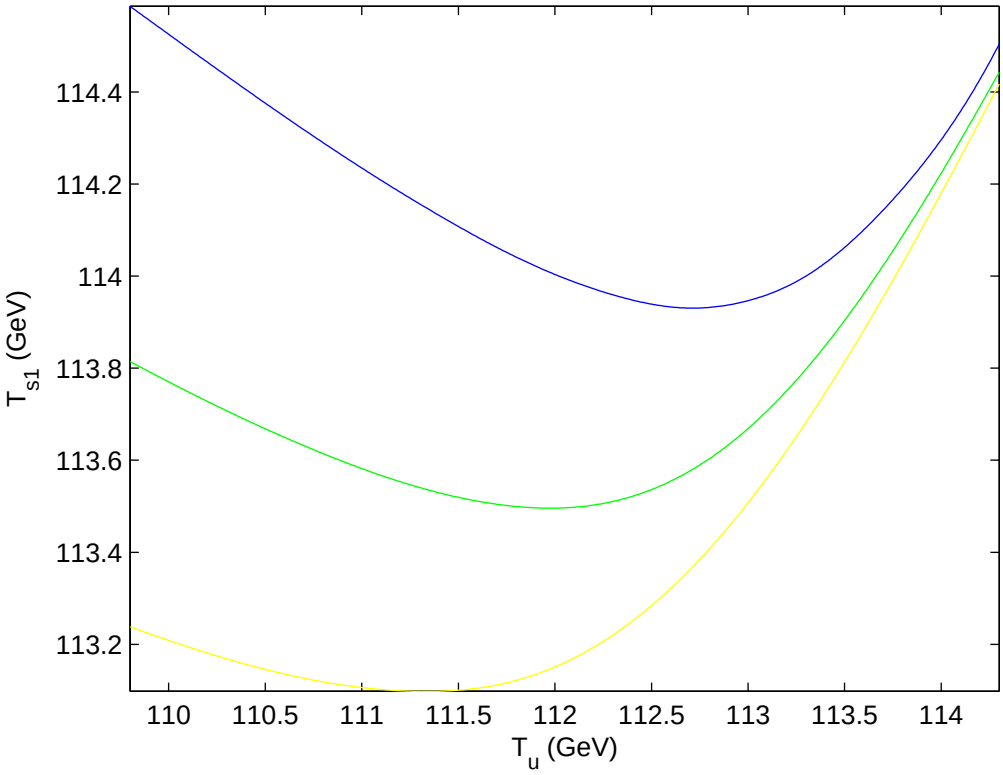

Figure 2.9: Temperatures in the symmetric phase just ahead of the bubble wall vs plasma temperature outside the bubble for the parameters of figure 2.8 and values of the friction parameter $\eta = 0.3, 0.4, 0.5$ (blue, green and yellow, from top down). Right of the minimum T_{s1} for each η is the stability region for subsonic solutions according to the criterion in [31].

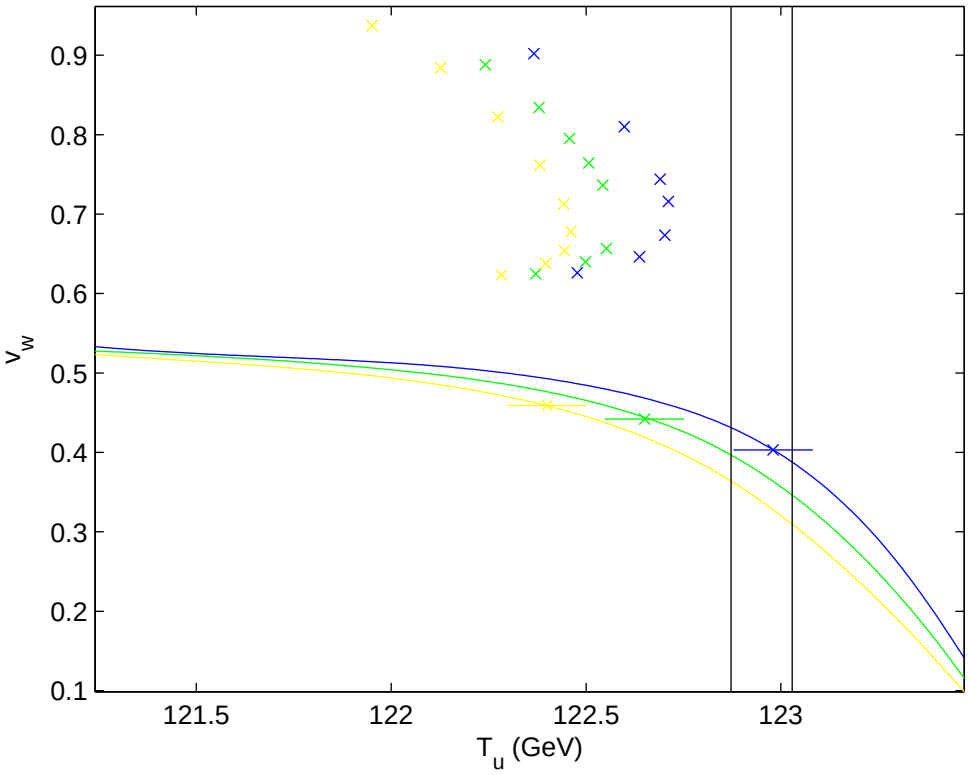

Figure 2.10: Steady-state bubble wall velocity vs temperature of the universe for three values of the friction coefficient η, 0.3 (blue, right), 0.4 (green) and 0.5 (yellow, left) for the dimension-6 model with $M = 900$ GeV, $m_h = 120$ GeV. The horizontal dotted line marks the speed of sound in the medium. The solid lines below the speed of sound limit are subsonic solutions. At the horizontal error bars the stability criterion for subsonic solutions proposed in [31] changes sign. The crosses above the speed of sound show two branches of supersonic solutions, only the upper one physical. The vertical lines mark the nucleation (right) and finalisation (left) temperatures for the phase transition for this choice of parameters.

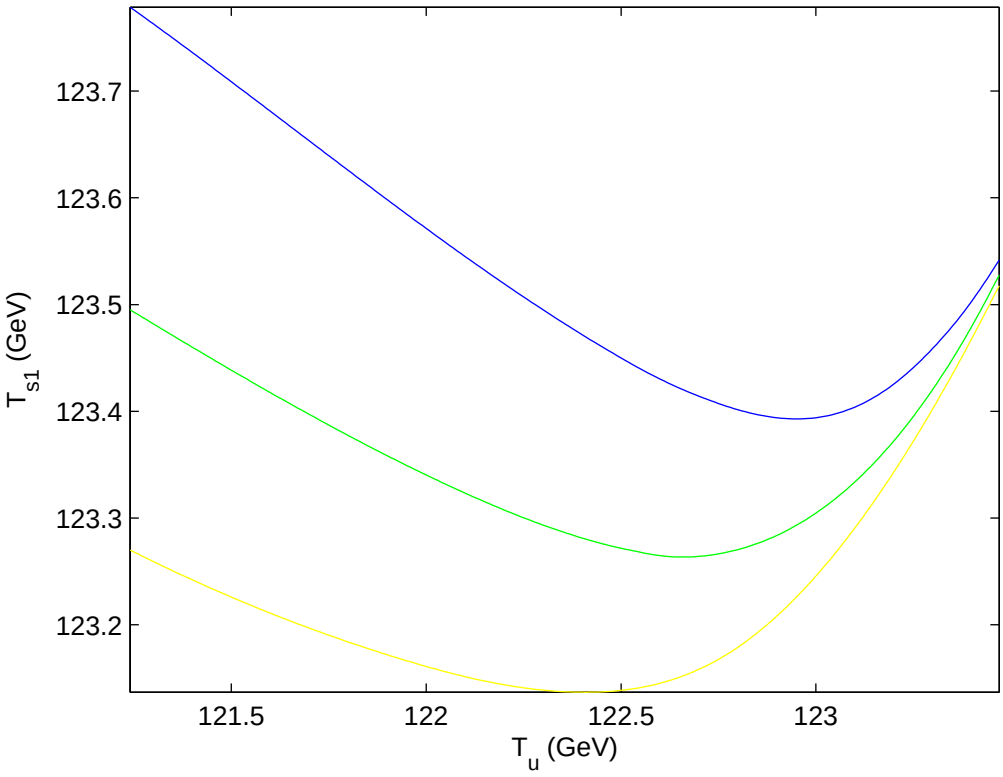

Figure 2.11: Temperatures in the symmetric phase just ahead of the bubble wall vs plasma temperature outside the bubble for the parameters of figure 2.10 and values of the friction parameter $\eta = 0.3, 0.4, 0.5$ (blue, green and yellow, from top down). Right of the minimum T_{s1} for each η is the stability region for subsonic solutions.

model.

Calibration of the friction parameter in a Standard Model-like situation as a function of the strength of the phase transition

To relate the existing SM calculation of the wall velocity to the dimension-6 model we recall (see 1.3.6) the form of the friction term for a 'slow' wall in the relaxation time approximation (eq 1.33) (for one degree of freedom and in the rest frame of the advancing wall),

$$\begin{aligned}\frac{dm^2}{d\phi}\int\frac{d^3p}{(2\pi)^3 2E}\delta f(p,x) = \\ \frac{dm^2}{d\phi}\int\frac{d^3p}{(2\pi)^3 2E}\tau\beta\gamma v\frac{(m^2)'}{2E}\frac{e^{\beta\gamma(E-vp_z)}}{(e^{\beta\gamma(E-vp_z)}\pm 1)^2} \sim \\ \phi^2\phi'\tau\beta\gamma v\int\frac{d^3p}{(2\pi)^3 4E^2}\frac{e^{\beta\gamma(E-vp_z)}}{(e^{\beta\gamma(E-vp_z)}\pm 1)^2},\end{aligned} \tag{2.1}$$

where (as mentioned in 1.4.3) we go from the second to the third line by substituting the appropriate (fermionic or bosonic) mass dependence on the Higgs VEV which we take to be of the general form $m = y\phi$. This form of the friction term is equivalent to that introduced in our formalism and dependent on our phenomenological parameter η (eq 1.56), $\frac{\eta}{T_{s1}}\phi^2\phi'\gamma v$.

As mentioned we may change integration variables from $p \to p' = \frac{p}{T}$. Since $E = \sqrt{m^2+p^2}$, and since we may consider the friction parameter as independent of velocity (see 1.4.3), the friction term in the relaxation time approximation becomes

$$\begin{aligned}\frac{dm^2}{d\phi}\int\frac{d^3p}{(2\pi)^3(2E)^2}\delta f(p,x) \sim \\ \phi^2\phi'\gamma v\frac{1}{T}\int\frac{p'^2dp'}{8\pi^2\left((\frac{m}{T})^2+p'^2\right)}\frac{e^{\gamma\sqrt{(\frac{m}{T})^2+p'^2}}}{(e^{\gamma\sqrt{(\frac{m}{T})^2+p'^2}}\pm 1)^2}.\end{aligned} \tag{2.2}$$

Given the general field dependence of the mass ($m = y\phi$), the integral now contains factors of $\frac{y\phi}{T}$. In order to relate the friction to the strength of the phase transition (commonly expressed in the literature by the parameter $\xi_c = \frac{v_c}{T_c}$, see 1.3.1) we could essentially approximate these factors by $\frac{\phi}{T} \longrightarrow \frac{v_c}{T_c}$ and then carry out the integration over momentum as a function of ξ_c. However, there are other choices as regards expressing the strength of

the phase transition, namely as a function of the nucleation ($\xi_n = \frac{v_n}{T_n}$) or broken symmetry phase ($\xi_b = \frac{v_b}{T_b}$) temperatures. Because, as mentioned, the difference between the three temperatures turns out to be small in most cases, we may assume that the choice of ξ does not make an enormous difference to the hydrodynamic calculation. Nevertheless, in order to be as precise as possible, we choose to do the momentum integral and calculate the friction parameter for each M, m_h as a function of ξ_n, as a more representative value of the strength of the phase transition than ξ_c. The *prefactors* to the integral (which we must fix in order to calculate the wall velocity) are determined by the specific form of the relaxation time τ and the relevant coupling constants. Recall that the contributions from all relevant degrees of freedom (bosonic and fermionic) must be summed over to obtain the total friction coefficient. We now turn to the results of the microscopic calculation of the Standard Model wall velocity carried out at 2-loop in [30]. Our strategy is as follows: We first reproduce those Standard Model results, as a function of the Higgs mass, employing the 2-loop Standard Model effective potential and seeking an appropriate value of the friction coefficient η_0 for each relevant case. The results of such a fit are given in table 2.1 [3]. The authors of [30] estimate 60% of the Standard Model friction to come from fermions, 40% from bosons. We call the values of the bosonic and fermionic integrals in eq (2.2) for each case in [30] (calculated as a function of ξ) $I_{0b}(\xi)$, $I_{0f}(\xi)$. We consider friction processes to be a function of the particle content of the model and the relevant particle interactions. Thus, because we remain within a Standard Model-like situation, we consider the prefactors to the momentum integrals (the relevant coupling constants and the chosen form for the relaxation time parameter) to hold for our dimension-6 extension. We therefore use the calibration from [30] to find the friction parameter for our calculation within the dimension-6 model (and for the corresponding value of the strength of the phase transition) as

$$\eta(\xi) = \eta_0 \left(0.6 \frac{I_f(\xi)}{I_{0f}(\xi_0)} + 0.4 \frac{I_b(\xi)}{I_{0b}(\xi_0)} \right) \tag{2.3}$$

[3] The full form of the Standard Model thermal effective theory, as well as the effective theory for our dimension-6 extension, are given in Appendix A. We spotted an apparent mismatch between the values of the quartic coupling λ_T in [30] and the corresponding Higgs masses, and corrected the latter on the basis of the corresponding λ_T in the effective theory. The authors of [30] were also concerned that perturbation theory might break down in the symmetric phase as the two-loop results were comparable to the 1-loop contributions, and that the value of $V(\phi, T)$ may be shifted away from zero for $\phi = 0$ as a consequence. To account for this they considered the case in which an additional term is added to the effective theory, and computed the wall velocity for that case. We set that term to zero in our calculation.

Table 2.1: Values of the quartic coupling λ, Higgs mass, strength of the phase transition ξ_n, nucleation temperature and fitted friction coefficient η for relevant cases in [30].

λ_T	m_h (corrected)	ξ_n	v_w (from [30])	T_n (GeV)	η_0 (fitted)
0.023	0	0.98	0.374	57.192	0.522
0.030	50	0.80	0.392	83.426	0.536
0.041	68	0.65	0.412	100.352	0.586
0.050	79	0.58	0.428	111.480	0.606
0.060	88	0.53	0.441	120.934	0.602

Thus, with this prediction for η, we may calculate v_w for each set of model parameters M, m_h within our model.

Results of the calculation of the wall velocity.

The results of calculating the friction parameter (as per (2.3)) and the wall velocity for the two slices $m_h = 115$, 150 GeV across parameter space are shown in table 2.2 and represented in figures 2.12, 2.15. Note that for $m_h = 115$ GeV physical solutions become supersonic for $M \approx 630$ GeV, the hydrodynamic equations becoming increasingly difficult to solve as the solution approaches the speed of sound in the medium [4].

To illustrate the difference between describing the strength of the phase transition as given by the effective theory at the critical ($\xi_c = \frac{v_c}{T_c}$), nucleation ($\xi_n = \frac{v_n}{T_n}$), or broken symmetry phase ($\xi_b = \frac{v_b}{T_b}$) temperatures we show the three ratios as a function of M for $m_h = 115$, 150 GeV in figures 2.13, 2.16. Note that for most cases (except for very strong transitions with $\xi_n \gtrsim$ 2.5 - 3.0) ξ_n and ξ_b can be taken as equivalent, but the difference with ξ_c is always appreciable. In addition, figures 2.14 and 2.17 show the wall velocity as a function of ξ_b, the strength of the phase transition at the temperature inside the bubble, immediately behind the bubble wall, where it is most relevant to the possible washout of the newly-created baryon asymmetry.

This is the first attempt to extend the existing (2-loop) microscopic calculation of the wall velocity from [30] to the dimension-6 extension to the Standard Model.

[4] As shown in figures 2.8 and 2.10, when supersonic solutions exist, subsonic solutions should also be present. However the argument regarding stability of deflagration solutions plus the increasing difficulty in solving the hydrodynamic equations as the wall velocity approaches the speed of sound from below incline us to prefer the supersonic solutions when they are present.

Table 2.2: Fitted ηs and wall velocities v_w for $m_h = 115, 150$ GeV in the dimension-6 model.

m_h	M	T_n	$\xi = v_n/T_n$	η	v_w
115	900	115.92	1.26	0.477	0.34
	800	105.49	1.74	0.398	0.38
	700	88.86	2.47	0.305	0.45
	650	75.10	3.14	0.240	0.53
	630	67.00	3.56	0.207	-
	610	54.70	4.44	0.153	0.74
	600	45.65	5.35	0.110	0.83
150	700	144.64	0.92	0.539	0.35
	650	136.62	1.19	0.490	0.36
	600	126.46	1.48	0.438	0.39
	550	112.71	1.87	0.380	0.43
	500	91.61	2.53	0.298	0.50

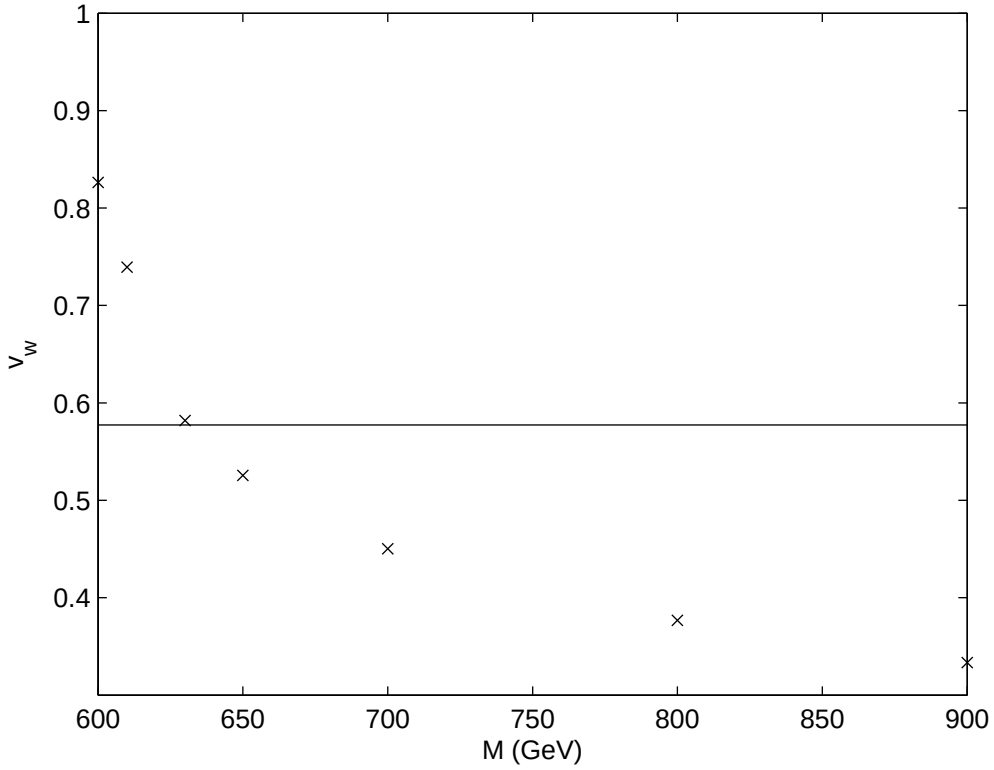

Figure 2.12: Wall velocity in the dimension-6 model for $m_h = 115$ GeV. The horizontal line marks the speed of sound in the medium.

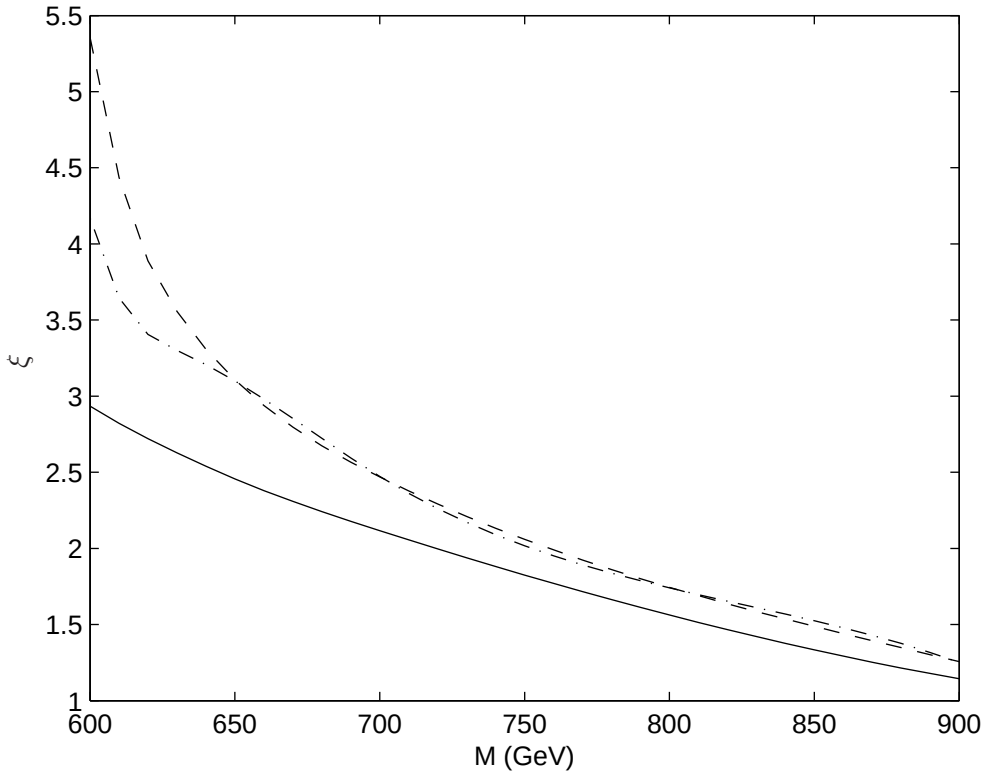

Figure 2.13: Strength of the phase transition as given by ξ_c (solid line), ξ_n (dashed) and ξ_b (dashed-dotted) vs M (in GeV) for $m_h = 115$ GeV.

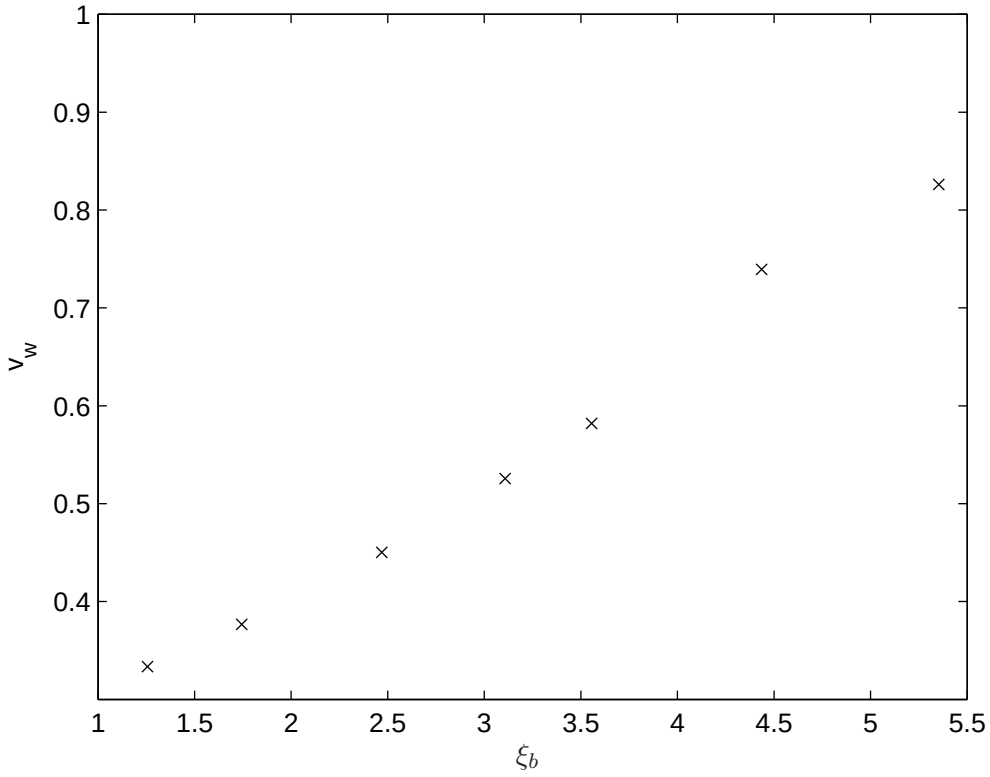

Figure 2.14: Wall velocity vs ξ_b for $m_h = 115$ GeV.

A note of caution on our calibration and possible runaway walls

We see from table 2.1 that the strength of the phase transition ξ_n stays below unity for all cases from [30] which we use as calibration for the friction in our dimension-6 model. It is clear, however (Fig 2.2) that in our parameter space we are dealing with much higher strengths of the phase transition. This calls for caution in accepting the values for the friction parameter produced by our calibration (eq (2.3)). In particular, applying the criterion for runaway walls described in 1.3.7 we find that for $\xi_n \gtrsim 2$ the wall would appear to run away (as opposed to reaching a steady state), even though the results from our calibration are consistent with propagation with steady (subsonic or supersonic) velocity. It appears that further investigation of this region in parameter space would be required before we can reach fully authoritative conclusions.

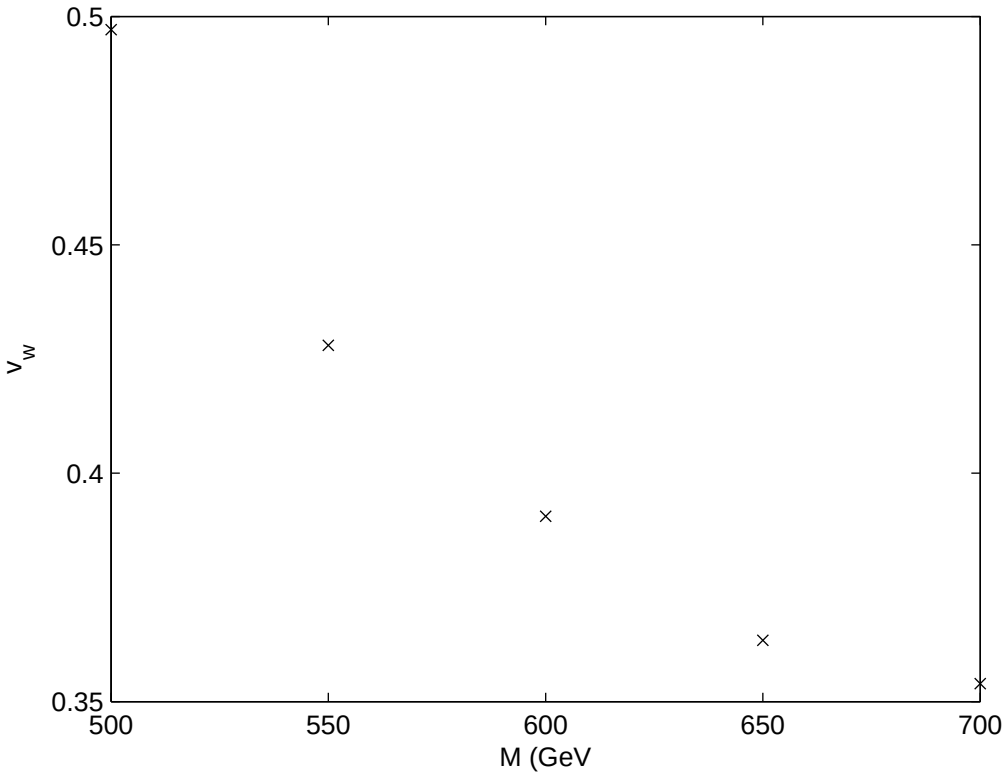

Figure 2.15: Wall velocity in the dimension-6 model for $m_h = 150$ GeV.

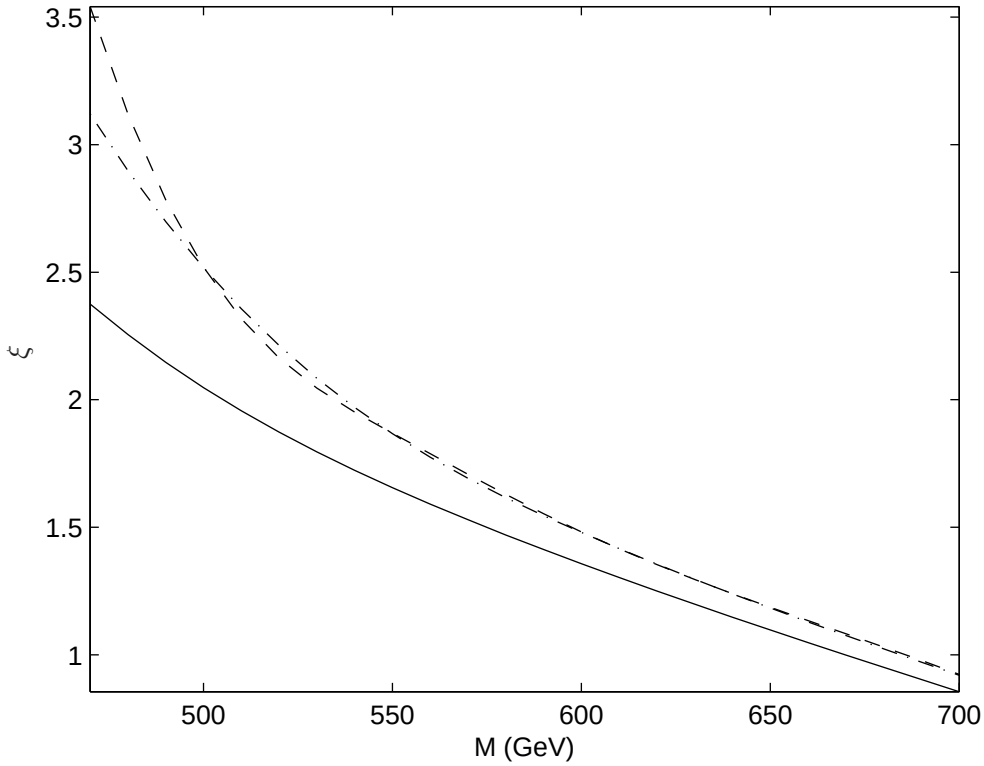

Figure 2.16: Strength of the phase transition as given by ξ_c (solid line), ξ_n (dashed) and ξ_b (dashed-dotted) vs M (in GeV) for $m_h = 150$ GeV.

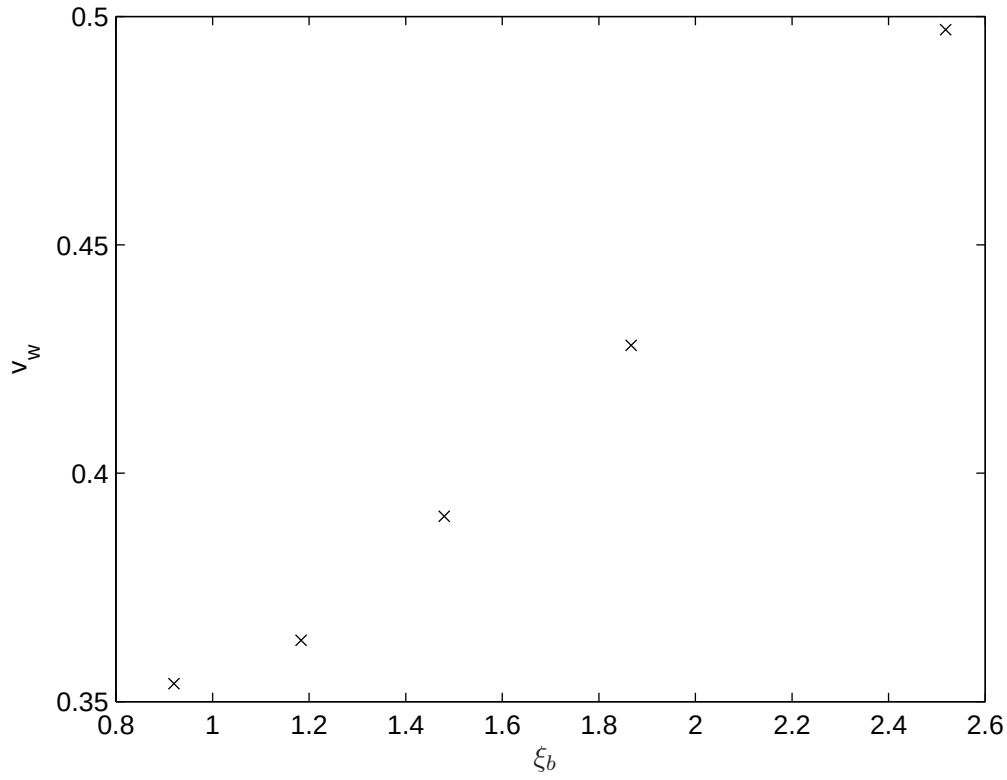

Figure 2.17: Wall velocity vs ξ_b for $m_h = 150$ GeV.

Chapter 3

The wall velocity in the Light Stop Scenario (LSS) of the Minimal Supersymmetric Standard Model

3.1 The LSS scenario of the MSSM

3.1.1 Supersymmetry and baryogenesis

The search for supersymmetric particles is one of the main goals of currently running experiments like the Large Hadron Collider. The Minimal Supersymmetric Standard Model (MSSM) solves the so-called 'hierarchy problem' (that is, the fact that in the Standard Model the mass of the Higgs boson receives large quantum corrections which would threaten the consistency of the theory in the absence of highly fine-tuned cancellations between independent contributions; Supersymmetry solves this issue because corrections to the Higgs mass from Standard Model particles and their supersymmetric partners exactly cancel each other out). In addition, supersymmetry leads to a natural unification of the gauge couplings consistent with precision electroweak data, and provides a natural candidate for the Dark Matter of the universe in the form of the lightest neutralino [26]. The possibility of a strong electroweak phase transition in a supersymmetric setting leading to the production of a baryon asymmetry consistent with observations has been studied extensively in the literature [61–64]. Electroweak baryogenesis has been shown to be feasible in a specific region in the supersymmetric mass parameter space. This setting is generally known as the Light Stop Scenario (LSS) [26, 27, 65–87]. It is important to point out that the LSS is not the only supersymmetric setting compatible with the observed

baryon asymmetry. An alternative possibility would be the out-of-equilibrium decay of superheavy squarks [88]; Another, the next-to-Minimal Supersymmetric Standard Model (nMSSM) with an added gauge singlet [89, 90]; Alternatively, adding an extra Z' gauge boson (for a total $SU(3)_C \times SU(2)_L \times U(1)_Y \times U(1)'$ symmetry) has been suggested [91]. This study focuses exclusively on the hydrodynamic analysis of bubble expansion within the LSS.

3.1.2 The Light Stop Scenario

The Light Stop Scenario of the MSSM is characterised by a (predominantly right-handed) light stop with a mass comparable to that of the top quark. All other (bosonic) squarks and sleptons are typically taken to be at a common, much higher mass scale $\tilde{m}$, in order to accommodate present bounds on the Higgs mass and avoid excessively large flavour and CP-violation and electric dipole moment effects [26, 92, 93]. Fermionic Higgsinos and gauginos are taken to be at the electroweak scale in order to provide both the CP-violating currents needed for baryogenesis [75] and a natural Dark Matter candidate [94,95]. Gluinos are generally considered heavy and thus decoupled from the thermal bath in order to suppress their potentially large contribution to the effective finite-T stop mass. Being one more light bosonic species (in addition to the weak gauge bosons) that couples to the Higgs, the light stop increases the upper bound on the Higgs mass compatible with a strong phase transition to about 127 GeV [27]. In turn, the predominantly left-handed stop must be heavy to agree with electroweak precision tests and with a sufficiently heavy Higgs boson. The CP-odd Higgs mass is large to avoid potentially large contributions to the electric dipole moments of the electron and the neutron. Therefore, at low energy, the light Higgs emulates the Standard Model Higgs sector.

This split in the LSS between light and heavy particles (in relation to the electroweak scale) makes it convenient to study the electroweak phase transition in this setting through the appropriate effective theory below the common mass scale $\tilde{m}$ assumed for squarks and sleptons other than the light stop [26, 27].

3.2 Calculating the wall velocity

3.2.1 Strategy and parameter space

We wish to produce a reliable hydrodynamical prediction for the wall velocity in the Light Stop Scenario of the MSSM. To this end we base ourselves in existing 2-loop calculations of

the LSS finite-temperature effective theory and start by identifying the region in parameter space compatible both with a sufficiently strong electroweak phase transition and presently acceptable values of the mass of the SM-like Higgs boson. We base ourselves on the 2-loop effective potential in [73] (see Appendix B for the full expression). On top of SM model parameters, the relevant additional supersymmetric parameters are as follows: In the absence of stop mass mixing (the most favourable situation as regards obtaining a strong enough phase transition [73]) the left- and right-handed stop masses depend respectively on the soft supersymmetry-breaking parameters m_Q, m_U. The other relevant supersymmetric parameter is $\tan\beta = \frac{v_2}{v_1}$, with v_1, v_2 the 1-loop, zero temperature expectation values of the real parts ϕ_1, ϕ_2 of the neutral components of the two supersymmetric Higgs doublets. We restrict ourselves to low values of $\tan\beta$ ($\lesssim 6$) as most adequate to produce a strong phase transition within presently acceptable Higgs mass bounds [32]. In figure 3.1 we show the region in m_U^2-m_Q space (for fixed $\tan\beta = 4$) chosen for our calculations, plotting the strength of the phase transition and the Higgs mass[1].

3.2.2 Calibration of the friction parameter

In order to produce a meaningful prediction for the wall velocity within our parameter space we need to estimate the friction. We do this as follows: A full, microscopic calculation of the wall velocity in the MSSM was carried out (at 1-loop) in [32], through a procedure similar to that followed in [30] for the Standard Model [2]. Similarly to how we proceeded in Chapter 2, we shall extrapolate the estimation of the friction implicit in [32] to the region in LSS parameter space of interest to us. As in Chapter 2, we start by finding the fitted set

[1]Note that the author of [73], when writing the 2-loop finite-temperature effective potential for the MSSM, envisaged only taking positive values of m_U^2. The need to assume negative values of m_U^2 in the context of the LSS was realised later (see eg [27]) because of the large finite-temperature corrections to the light stop mass. On choosing the region of parameter space for our study we ran into difficulties with values of the right-handed stop mass parameter $m_U^2 \lesssim -12000$ GeV^2 due to negative values of the stop mass $m_{\tilde{t}_R}$. In addition, it became extremely hard or impossible to calculate the nucleation temperature T_n in the lower left area of the region in fig 3.1 and beyond (for higher strengths of the phase transition), the indications being that the high-temperature expansion of the effective theory was breaking down and causing the free energy of the critical bubble divided by temperature, ($\frac{F_c}{T}$), to reach a minimum and rise again with decreasing temperature of the universe T_u. Note also that as this work was in progress there was no indication yet that the values of the Higgs mass in fig 3.1 may lie outside experimental bounds, as recent LHC results indicate. See below for an application of our results to Higgs masses as high as $m_h \sim 127$ GeV.

[2]Those authors also assumed a low $\tan\beta$ and comparatively low (if not as low as ours) values of m_U^2, see Fig 3.2.

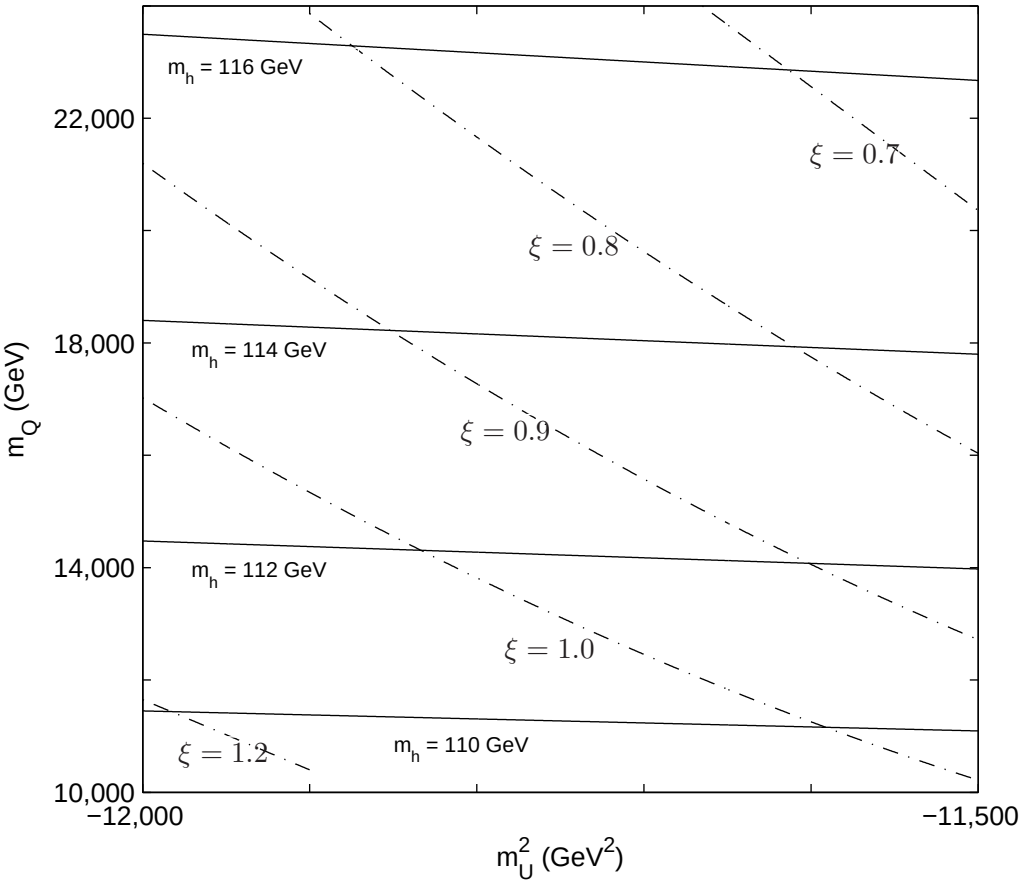

Figure 3.1: Values of the strength of the phase transition $\xi = \frac{v_c}{T_c}$ and the Higgs mass in the region of parameter space (with $\tan\beta = 4$) of interest for baryogenesis. For this value of $\tan\beta$ the right-handed stop mass (we assume no mixing) varies in this range from $m_{\tilde{t}_R} \sim 135.2$ to $m_{\tilde{t}_R} \sim 138.8$ GeV and the left-handed-stop mass is given by m_Q.

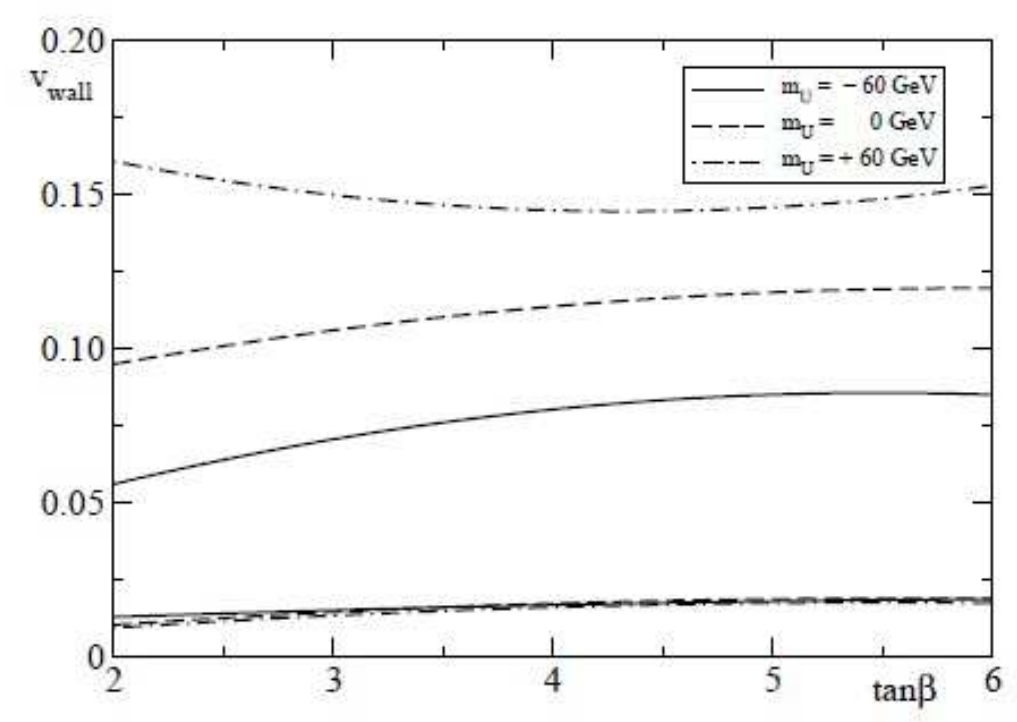

Figure 3.2: MSSM wall velocity calculated microscopically in [32] as a function of $\tan\beta$ for $m_Q = 2000$ GeV and $m_U^2 = -60^2$, 0, $+60^2$ GeV^2 (assuming no stop mixing). The lower bunch of graphs are obtained by neglecting the vector of the spatial derivatives of the perturbations to the temperature, velocity and chemical potential, $\delta T'$, $\delta v'$ and $\delta\mu'$ (Figure from [32]).

of ηs which allows us to reproduce with our hydrodynamical approach the wall velocities found in [32] (Figure 3.2). In order to extrapolate our findings to LSS parameter space we recall that the friction parameter is fundamentally a function of the particle content of the model (and the interactions between particles). Thus, and since we consider the left-handed stop to be heavy and decoupled, it is safe to consider η as independent of the mass parameter m_Q, and therefore an exclusive function of $\tan\beta$ and m_U (and essentially unaffected by the addition of 2-loop corrections to the effective potential). Consequently, for each value of $\tan\beta$, we can carry out an extrapolation to our parameter space as a function of only one variable, m_U (or m_U^2). With the extrapolated values of η we are in a position to produce a (2-loop) estimation of the wall velocity in the LSS.

Table 3.1: Phenomenological friction coefficient η fitted to the 1-loop MSSM wall velocity in [32] for $m_Q = 2000$ GeV and different values of $\tan\beta$, m_U (see fig 3.2).

$\tan\beta$	m_U^2	v_w (John and Schmidt)	Fitted η
2	-60^2	0.060	4.58
	0	0.090	3.36
	$+60^2$	0.160	1.92
4	-60^2	0.080	4.35
	0	0.115	3.16
	$+60^2$	0.140	2.72
6	-60^2	0.085	4.65
	0	0.120	3.06
	$+60^2$	0.155	2.55

3.3 Results

3.3.1 Fitting a friction parameter to existing results

Table 3.1 shows the results of reproducing the wall velocities in [32] through our hydrodynamical method with a phenomenological parameter, for $\tan\beta = 2$, 4, 6 and $m_U^2 = -60^2$, 0, $+60^2$ GeV^2. This has been done with the 1-loop version of our effective theory (see Appendix B). The calibration points thus produced are plotted in figure 3.3.

3.3.2 Calculating the wall velocity in LSS parameter space

Extrapolating the friction linearly

Given the approximately linear disposition of the fitted ηs as a function of m_U^2 for a given $\tan\beta$, it seems to make sense to extrapolate linearly to the low m_U^2 region in parameter space of interest to us. The results for $\tan\beta = 4$, 6 can be seen in figure 3.3. We see that, in comparison with the Standard Model, the friction parameter η is enhanced roughly by 4-7, reflecting the increase in friction provided by the light stops. To estimate the error implicit in our extrapolation we calculate the highest possible η variation found by taking only two calibration points from [32] for the case $\tan\beta = 4$. We show the result of this two-point calibration also in figure 3.3. The results suggest an uncertainty $\Delta\eta \sim \pm$1-1.5.

Testing our extrapolation further through the relaxation time approximation

To further elucidate whether a linear extrapolation to low m_U^2 regions makes sense we turn to our functional model for the friction, the 'slow wall' form of the relaxation time approximation (1.33). Our argument here is an extension of the calculation carried out in

Table 3.2: Fitted constants to the bosonic momentum integral in the relaxation time approximation model for η across the bubble wall (see fig 1.10) for the 1-loop data points in [32] with $\tan\beta = 4$ ($m_Q = 2000$ GeV).

m_U^2 (GeV^2)	T_c (GeV)	ϕ_0 (GeV)	Fit (bosons)
-60^2	126.44	39.60	0.59
0	129.21	33.85	0.48
+60^2	131.41	30.90	0.41

1.4.3 to make sure that it made sense to represent friction *across the bubble wall* as a single number. We saw then (Fig 1.10) that the (position-dependent) momentum integral in the expression for η supplied by the relaxation time approximation can generally be fitted by a constant which reproduces the shape of the friction term. Back then we simply assumed a general mass dependence with the Higgs VEV $m = y\phi$. We now repeat the calculation through the bosonic form of the integral with the specific mass dependence of the light stop, the species which dominates friction in the LSS of the MSSM. We do this for each of the three calibration points available from [32] for the choice $\tan\beta = 4$. Assuming a fixed τ dependence our fitted constant will be proportional to the friction parameter η predicted by our model. The results of such a calculation are shown in table 3.2. We see that the fitted constants show an approximately linear dependence with m_U^2, mirroring that of the fitted ηs in table 3.1. The relaxation time approximation model therefore encourages us to stick to our linear extrapolation to the region of lower m_U^2 in parameter space.

To further test that we are on the right track, we carry out a last check based on the relaxation time approximation through the same procedure we employed to extrapolate fitted ηs within the Standard Model to cases of interest within the dimension-6 extension to the SM (2.2.3). Following the reasoning that led to equation (2.3), we may calculate η for a point of interest through the expression

$$\eta(\xi) = \eta_0 \frac{I_b}{I_{ob}} \tag{3.1}$$

where, for the LSS, we require only one integral over momentum, that for the light stops, which dominate friction in this case. The momentum integral is a function of the relevant ratio $(\frac{m}{T})$, which we take to be the light stop's finite-temperature mass in the broken symmetry phase divided by T_b. If we extrapolate thus to one of the points of interest in our parameter space (see table 3.3 below) with $\xi_c = 1$, $m_h = 112$ GeV, we find $\eta = 5.12$, consistent with our results so far and compatible with an uncertainty $\Delta\eta \sim \pm 1$.

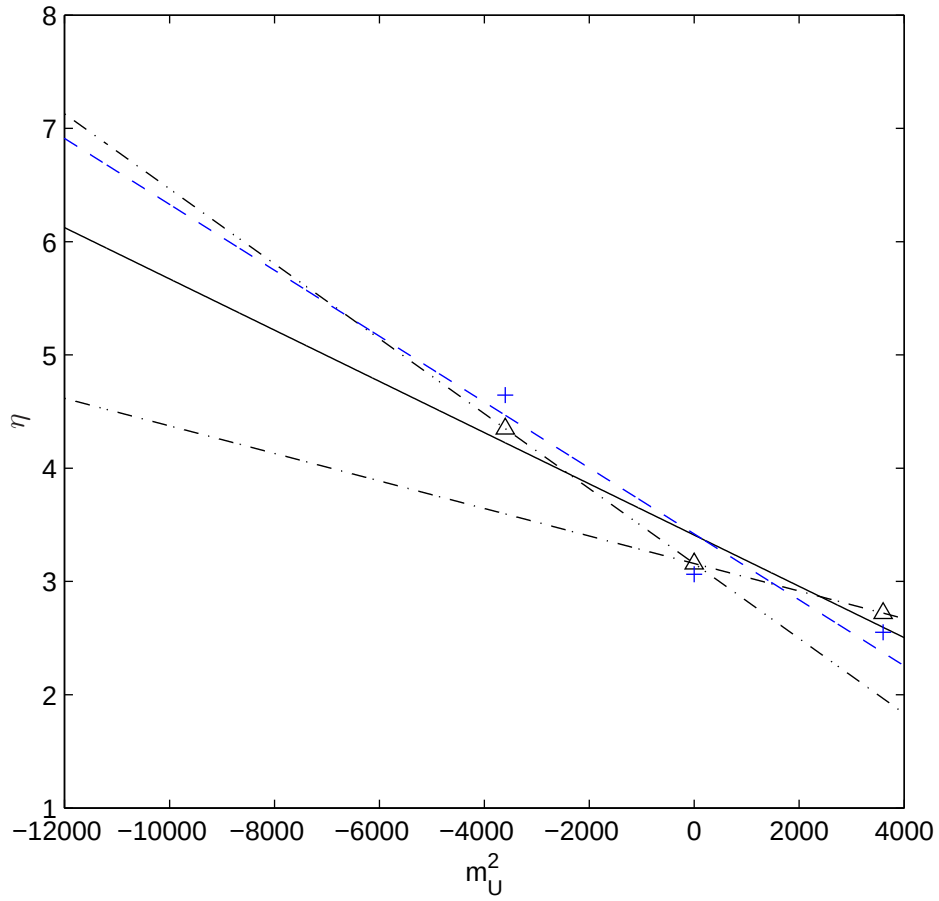

Figure 3.3: Linear extrapolation of η values to m_U^2 region of interest for $\tan\beta = 4$ (solid line, calibration values from [32] as triangles), $\tan\beta = 6$ (dashed line, calibration values as crosses). $m_{\tilde{t}_R} \in [135.2, 184.1]$ GeV (no dependence on β). Dot/dash lines mark the extreme 2-point calibration lines for $\tan\beta = 4$.

We shall therefore adopt our original linear extrapolation with m_U^2 as our preferred method to find η in our chosen parameter space.

The wall velocity in the LSS

With the extrapolated values of the friction parameter the coupled hydrodynamic equations can be solved at 2-loop. The results of the 2-loop calculation are shown in table 3.3 in two representative cases for $\tan\beta = 4$, 6. The alternative wall velocities found with the 2-point calibration for the case $m_h = 112$ GeV, $\xi_c = \frac{v_c}{T_c} = 1$, $\tan\beta = 4$ are also shown in table 3.3. As can be seen, the influence of the choice of calibration on the wall velocity is considerable. It is interesting to note that growing bubbles in this regime are *stable* according to the criterion in [31] which we described in 1.3.1 and 2.2.2.

Table 3.3: Results of wall velocity calculation at 2 loop for Higgs mass $m_h = 112$ GeV, $\tan\beta = 4$,6 and strength of the phase transition $\frac{v_c}{T_c}$ close to 1. The values of $\xi_b = \frac{v_b}{T_b}$ in the broken symmetry phase behind the bubble wall are given for comparison.

$\tan\beta$	$\xi_c = \frac{v_c}{T_c}$	$\xi_{bs} = \frac{v_b}{T_b}$	Fitted η	v_w
4	0.9	1.01	5.94	0.044
	1.0	1.14	6.05	0.043
		1.14	4.58 (2-point)	0.057
		1.14	7.02 (2-point)	0.037
6	0.9	1.00	6.66	0.039
	1.0	1.14	6.79	0.038

Keeping our original (3-point) calibration and sampling the most promising (as regards baryogenesis and the Higgs mass) areas of parameter space we find that the wall velocity varies less than 10% across the region in figure 3.1. Our results confirm previous values of $v_w \sim 0.05$ used in calculations of the baryon asymmetry, eg in [86]. Notably, from table 3.3 we also find a near-perfect inverse proportionality between η and the wall velocity, with $\eta \cdot v_w \sim 0.26$. This makes it straightforward to produce an estimation of v_w from η in this regime. As an application we turn to the results in [27]. That study, working in a separate region in parameter space within the LSS, found that a strong phase transition may occur for a Higgs mass $m_h \sim 125$ GeV (with a light stop mass $m_{\tilde{t}_R} \sim 100$ GeV). In that setting our extrapolation produces an estimation of the friction parameter $\eta \sim 8.2$, and a wall velocity $v_w \sim 0.03$.

It is worth pointing out briefly that the relaxation time approximation may be employed to estimate the wall velocity in other supersymmetric settings. For example, making a rough assumption for the nucleation temperature ($T_n \sim 100$ GeV) for the Next-to-Minimum Supersymmetric Standard Model (NMSSM), we obtain, for a much higher value of the light stop mass $m_{\tilde{t}_R} \sim 350$ GeV, a Standard Model-like $\eta \sim 0.2$, which would correspond to a wall velocity $v_w \sim 0.3$-0.4.

In addition to showing the ratio $\xi = \frac{v}{T}$ (the strength of the phase transition) at the critical temperature T_c, table 3.3 shows this parameter also at $T_b < T_c$, the temperature in the broken symmetry phase immediately behind the advancing bubble wall. As mentioned, the ξ parameter is quoted in most studies as $\xi_c = \frac{v_c}{T_c}$, which corresponds to the critical temperature. As noted in Chapter 2, for each temperature of the universe, the value of $\frac{v}{T}$ is different in the broken symmetry phase inside the bubble, at the critical temperature, and at the nucleation temperature. We show these three ξs (ξ_c, ξ_n, and ξ_b) in figure 3.4 as a function of m_U^2 for the slice $\tan\beta = 4$, $m_Q = 14,000$ (note that in this particular case

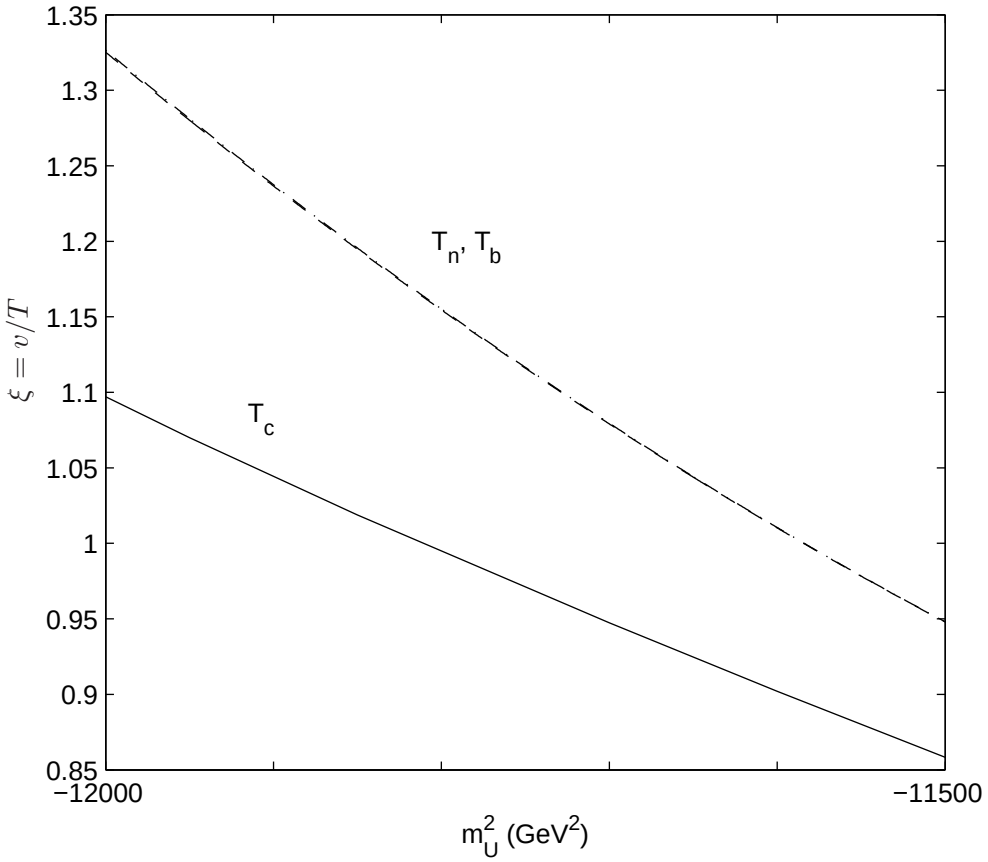

Figure 3.4: Values of $\xi = v/T$ for the slice $\tan\beta = 4$, $m_Q = 14,000$ GeV ($m_h \sim 112$ GeV) at the critical (solid line) and nucleation (dashed line) temperatures and in the broken symmetry phase (where reverse sphalerons must be suppressed to avoid washing out the newly-generated baryon asymmetry) (dashed-dot line). Note that for this example T_n and T_b turn out to be nearly identical.

the nucleation temperature and the temperature inside the bubbles happen to be nearly identical). We see that the value of ξ is significantly higher (by $\sim 10\%$) in the new phase inside the bubble, where it is relevant to the possible wipeout of the newly-created baryon asymmetry.

Another issue raised by the low values of the wall velocity found for the MSSM is whether they contradict some of the assumptions made at the start of our hydrodynamic calculation. Note that the relatively slow expansion speed of the bubbles makes for a broader gap between the nucleation temperature and the so-called *finalisation temperature* T_f, at which the proportion of space occupied by the growing bubbles reaches unity and the phase transition ends. As an approximation it is usually assumed in the calculation

Table 3.4: Wall velocity for the case $m_h = 116$ GeV, $m_U^2 = -11900$ choosing as the temperature of the universe: 1) The nucleation temperature, T_n; 2) The finalisation temperature calculated on the assumption $v_w = 1$, T_f; 3) Same with $v_w = 0.05$, $T_f^{'}$

$\tan\beta$	T	$\xi = \frac{v}{T}$	Fitted η	v_w
4	T_n	0.92	6.10	0.044
	T_f	0.94		0.051
	$T_f^{'}$	0.94		0.054
6	T_n	0.95	6.88	0.039
	T_f	0.96		0.045
	$T_f^{'}$	0.96		0.047

of T_f (eg [14]) that the bubbles expand at the speed of light, and that has also been our assumption so far (recall that, in our original analysis of bubble nucleation and the start and completion of the phase transition, see 1.2.2, we referred to the wall expansion velocity as β and equated $\beta \equiv 1$). It seems reasonable in this case to question this assumption. We start by proposing an alternative initial choice of eg $v_w = 0.05$, which results in a different finalisation temperature $T_f^{'}$. We then calculate the wall velocity by taking as the temperature of the undisturbed universe outside the bubble a) The nucleation temperature, T_n; b) The finalisation temperature calculated in the usual way, T_f; and c) The finalisation temperature found assuming a slow wall velocity, $T_f^{\prime}$. The results are shown in table 3.4 for the case $m_h = 116$ GeV, $m_U^2 = -11900$ GeV^2 [3] with $\tan\beta = 4$, 6. As we can see, the choice of finalisation temperature does *not* introduce a huge variation in v_w but taking the temperature of the undisturbed universe as T_n or T_f *does* make a significant difference.

We finish by recalling that our hydrodynamic treatment assumes bubble expansion at a steady-state velocity. Therefore, in itself it cannot account for bubble wall acceleration, due to the variation in temperature between the beginning and the end of the phase transition or for any other reason (like, for instance, in the context of a runaway regime in which friction fails to stabilise the wall velocity).

[3] Low values of m_U^2 are most favourable for baryogenesis.

Conclusions

Out of the several mechanisms proposed to explain the baryon asymmetry of the Universe, electroweak baryogenesys has lately received renewed attention. This mechanism relies on the creation of the matter-antimatter asymmetry in the context of the electroweak phase transition, understood to be first-order and thus to proceed through the nucleation of regions ('bubbles') of the broken symmetry phase. Such a transition would explicitly satisfy Sakharov's conditions for the creation of a baryon asymmetry (departure from thermodynamic equilibrium, violation of baryon number, and the presence of CP-violating processes). All necessary ingredients for generating a baryon asymmetry are already present in the Standard Model, but the observed asymmetry cannot be replicated in the context of the unaugmented SM. Consequently, for baryogenesys to be viable in the context of the EWPT, new Physics must exist which couple significantly to the Standard Model and is sufficiently thermally abundant at the electroweak scale. If so, we should be able to probe this BSM Physics through an array of presently running and upcoming experiments, including the Large Hadron Collider. This explains the recent theoretical and phenomenological efforts to elucidate further the features of baryogenesis in the context of the EWPT.

In Chapter 1 of this work we explain the concepts of cosmological phase transition and symmetry breaking at finite temperature, and in particular the breaking of electroweak symmetry through the Higgs mechanism. We describe the electroweak phase transition as first-order. The main features of such a transition are: (a) The critical temperature T_c and the nucleation temperature T_n at which the transition actually occurs; (b) the sphaleron transition rate which determines the B-number generation rate; and (c) The rate of nucleation of bubbles of the broken symmetry phase. These quantities can be studied through a variety of methods, the most reliable being non-perturbative Monte Carlo computations which, because of their complexity, have only been applied to a few specific settings. The alternative is to resort to perturbative methods as we do here. To this effect we introduce the concept of effective potential, from which T_c, T_n, and the bubble nucleation rate may

be calculated. The generation of the baryon asymmetry is very sensitive to the profile and propagation speed of the walls of the expanding bubbles, because as the advancing walls induce a chiral asymmetry on both sides of the interface the generation of a net B number through sphaleron transitions depends in turn on the interplay of the relevant processes which affect the creation of the chiral asymmetry and diffuse it into the symmetric phase, where sphalerons are active. Therefore, the determination of the wall velocity and profile are the main goals of this study. To this effect we describe the propagation of the bubble walls formally, starting from the conservation of the energy-momentum tensor of the system and the equations of motion for the background Higgs field, whose vacuum expectation value (VEV) is taken as the order parameter for the phase transition. We describe the friction term in the hydrodynamical equations, which stems from the deviation from equilibrium of the populations of the particles present in the plasma and which couple strongly to the Higgs. In order to account for this deviation from equilibrium we introduce the Boltzmann evolution equations, dependent on the term known as the collision integral, $C[f]$. We introduce the full form of this term as well as the relevant simplified forms and, in particular, the so-called relaxation time approximation, which assumes $C[f] \equiv \frac{\delta f}{\tau}$. We reexpress the equations of motion and calculate the pressure on the advancing bubble wall according to these approximations for the friction term. We note that the relaxation time approximation in the form we have adopted breaks down for values of the wall velocity close to 1, wrongly predicting a diverging pressure difference when, in fact, the pressure difference approaches a constant value for $v_w \longrightarrow 1$, which we show by introducing an alternative description based on the exchange of kinetic momentum between the wall and the particles in the plasma. This conclusion makes a 'runaway regime' (in which the wall accelerates without bound) possible in principle, as opposed to the usual assumption that friction effects equilibrate with the pressure difference to produce a 'steady-state' wall propagation at a fixed velocity $v_w < 1$. We then introduce the mathematical formalism we employ in our calculations of the wall velocity and profile. We start from the conservation of the energy-momentum tensor of the Higgs-plasma system (written in covariant form) and introduce a friction term dependent on a dimensionless friction parameter η. We develop and apply our formalism to the whole bubble profile in the subsonic (deflagration) and supersonic (detonation) cases, relating the temperature and fluid velocity profiles to the variation of the Higgs VEV and to the temperature in the undisturbed universe outside the bubble, which we take to be the nucleation temperature T_n (at which, as determined by the shape of the effective potential, bubble nucleation starts). We finish

by investigating the accuracy of modelling friction across the bubble profile by a single numerical parameter, concluding that it is indeed an adequate description.

In Chapter 2 we apply our formalism to an extension of the Standard Model with dimension-6 operators. Ours is the first explicit calculation of the velocity of electroweak bubble walls in this setting. We first investigate the general shape of the solutions to the hydrodynamic equations as a function of the model parameters and friction, obtaining results consistent with previous studies. We then look for realistic values for η basing ourselves on the best existing perturbative calculations of the wall velocity for the Standard Model. We first calculate the values of η which would reproduce the existing results for the wall velocity, then use the relaxation time approximation to the collision integral as a model for friction that allows us to produce new values of η for the parameter space of the dimension-6 model, on the assumption that friction is determined by the particle content of the model. We find subsonic wall velocities $v_w \approx 0.4$ for strengths of the phase transition $\xi \approx 1$ and supersonic solutions for larger ξs, including the possibility of runaway walls.

It is interesting to reflect on the consequences of our findings for the broader aspects of the electroweak phase transition. The first issue is whether our results may affect the suitability of this model as regards replicating the observed baryon asymmetry of the Universe. Existing studies [25] calculate the baryon asymmetry in this setting by solving the relevant system of transport equations (as outlined above, detailing how the relevant reactions affecting the chiral asymmetry induced by the advancing wall diffuse into the symmetric phase) near the bubble wall, but they do not carry out, as we do, a detailed calculation of the wall velocity. Those studies conclude that the model can replicate the observed baryon asymmetry for a broad and natural range of the model parameters including the recently determined mass of the Higgs boson $m_h \approx 125$ GeV, and with only a very mild dependence on the wall velocity. However, along with most existing studies of electroweak baryogenesis, they assume relatively low, subsonic values of the wall velocity and make the corresponding simplifying assumptions in the treatment of transport mechanisms. Strictly speaking it would therefore be necessary (and beyond the scope of this work) to explore the implications of large, even supersonic, wall velocities in the baryon asymmetry predicted by the Standard Model with dimension-6 interactions. More broadly, the study of supersonic wall velocities (or indeed runaway walls) and their larger impact on electroweak baryogenesis is generally accepted as in need of further development, including, for example, the possible appearance of turbulence in the plasma.

Another field of particular interest which may be probed by upcoming experiments is the possible production of gravitational waves (GW) in the context of a first-order EWPT. A stochastic background of gravitational waves may be produced as soon as expanding bubbles collide and their spherical symmetry is broken. There are two contributions to the GW background: the collisions between bubble walls, and the turbulent motions of the plasma. Methodological differences in the treatment of the problem persist to this day but researchers agree on the validity of the so-called *envelope approximation*, that is, the principle that the energy spectrum of gravitational wave production depends not on the detailed history of colliding bubbles but on the overall features of the problem, namely the energy available in the form of latent heat and the typical size of bubbles at the time of collision. It is also accepted that subsonic bubble propagation strongly suppresses GW production, and therefore supersonic wall velocities are usually assumed and taken as an upper bound on the predicted GW spectrum. Predictions of the GW background usually study the peak frequency and the behaviour of the energy spectrum on either side of the peak. In any given setting, stronger phase transitions with higher latent heats result in larger bubbles at the time of collision and larger energy spectra, but lower peak frequencies. This compromises possible GW detection because the peak sensitivity of the proposed space-based experiments LISA and BBO occurs at higher frequencies than the peaks predicted for EWPT GW production in most relevant settings. In any case, of these two experiments only BBO is predicted to have a chance of picking up the high frequency tail of an EWPT-generated GW spectrum. Given these complications (and given the discrepancies among different research approaches) it is outside the scope of this work to try to outline precise consequences of our wall velocity results for the Standard Model with dimension-6 operators on the chances of detecting a GW background from a first-order EWPT, even though the consensus seems to be that a strong phase transition with a relatively flat high frequency tail might indeed produce a GW spectrum detectable by BBO as long as the relevant backgrounds (eg from inflation or astrophysical sources like white dwarf binaries) are properly understood.

With regard to the issue of gravitational wave production it is also worth noting that there is no clear correlation between large GW production and the creation of a sufficiently high baryon asymmetry in the context of a first-order EWPT. For example, highly supersonic wall velocities, as mentioned, favour in principle the production of gravitational waves but may compromise the generation of a sufficiently large B-asymmetry through suppression of the relevant diffusion processes into the symmetric phase. Conversely set-

tings in which the baryon asymmetry of the Universe may be replicated might lead to comparatively low (perhaps undetectable) GW production.

Chapter 3 of this work applies our formalism to the Light Stop Scenario (LSS) of the Minimal Supersymmetric Standard Model (MSSM). We start again from existing supersymmetric calculations of the wall velocity from first principles and find the values of the friction parameter η which reproduce those results. Proceeding on the assumption that friction is determined by particle content and particle interactions, and since we know that the light right-handed stops dominate the friction in this case, we make a linear extrapolation for the friction from the values of the friction parameter just calculated to LSS parameter space based on the value of the light stop mass parameter m_U^2. We test this extrapolation with the help of the relaxation time approximation and find it to be robust. With the values of the friction parameter we thus found we calculate the wall parameter at 2-loop for the LSS, the first time such a calculation has been carried out. We extend our extrapolation to estimate the wall velocity in a few other supersymmetric scenarios, including for values of the Higgs mass ≈ 125 GeV, the value recently confirmed by LHC results. Our findings for the wall velocity in the Light Stop Scenario are in accordance with previous studies for the MSSM and therefore do not, in themselves, compromise the capacity of the LSS to reproduce the observed baryon asymmetry of the Universe (whether the LSS is still a valid setting for electroweak baryogenesis given recent LHC data is the object of ongoing debate). Likewise, as regards the production of gravitational waves, our results for the wall velocity are in accordance with previous assumptions which resulted in the conclusion that a gravitational wave background from an EWPT in the MSSM would in any case be too weak to be picked up by LISA, and would be suppressed even further by very subsonic wall velocities.

Appendix A: The Standard Model effective potential with dimension-6 operators

The high-temperature expansion of the Standard Model 2-loop, finite-T effective potential is given in [30] as

$$V_{eff}(\phi, T) = D(T^2 - T_0^2)\phi^2 - CT^2\phi^2 \ln(\frac{\phi}{T}) - ET\phi^3 + \frac{\lambda}{4}\phi^4 \tag{3.2}$$

with

$$\lambda = \frac{m_h^2}{2v_0^2} - \frac{3}{16\pi v_0^4}[2m_w^4 \ln(\frac{m_w^2}{a_b T^2}) + m_z^4 \ln(\frac{m_z^2}{a_b T^2}) - 4m_t^4 \ln(\frac{m_t^2}{a_f T^2})]$$

$$D = \frac{1}{8v_0^2}(2m_w^2 + m_z^2 + 2m_t^2)$$

$$C = \frac{1}{16\pi^2}(1.42g_w^4 + 4.8g_w^2\lambda - 6\lambda^2)$$

$$E = \frac{1}{12\pi}[4(\frac{m_w}{v_0})^3 + 2(\frac{m_z}{v_0})^3 + (3 + 3^{1.5})\lambda^{1.5}]$$

$$B = \frac{3}{64\pi^2 v_0^4}(2m_w^4 + m_z^4 - 4m_t^4)$$

$$T_0 = \sqrt{\frac{1}{4D}(m_h^2 - 8Bv_0^2)}$$

and

$$g_w = \frac{2m_w}{v_0}$$

$$m_w = 80.4 \text{ GeV}$$

$$m_z = 91.2 \text{ GeV}$$

$$m_t = 174.0 \text{ GeV}$$

$$
\begin{aligned}
v_0 &= 246.0 \text{ GeV} \\
a_b &= 49.78019250 \\
a_f &= 3.111262032
\end{aligned}
\tag{3.3}
$$

As dimension-6 effective potential we adopt [25]

$$
\begin{aligned}
V_{eff}(\phi, T) = \frac{1}{2}(-\mu^2 + (\frac{1}{2}\lambda + \frac{3}{16}g_2^2 + \frac{1}{16}g_1^2 + \frac{1}{4}y_t^2)T^2)\phi^2 \\
-\frac{g_2^3}{16\pi}T\phi^3 + \frac{\lambda}{4}\phi^4 + \frac{3}{64\pi^2}y_t^4\phi^4 \ln(\frac{Q^2}{c_F T^2}) \\
+\frac{1}{8M^2}(\phi^6 + 2\phi^4 T^2 + \phi^2 T^4)
\end{aligned}
\tag{3.4}
$$

where $Q \equiv m_{top} = 178$ GeV[4] and $c_F \approx 13.94$. M and m_h are the free parameters of the model. μ and λ are found through the conditions for the zero-temperature potential ($v_0 = 246$ GeV)

$$
V_{eff}(\phi, 0) = -\frac{\mu^2}{2}\phi^2 + \frac{\lambda}{4}\phi^4 + \frac{1}{8M^2}\phi^6 - \frac{3}{64\pi^2}y_t^4\phi^4 \ln(\frac{y_t^2\phi^2}{2Q^2}) \tag{3.5}
$$

$$
\frac{\partial V_{eff}(\phi,0)}{\partial\phi}_{\phi=v_0} = 0, \qquad \frac{\partial^2 V_{eff}(\phi,0)}{\partial\phi^2}_{\phi=v_0} = m_h^2 \tag{3.6}
$$

[4]Note the slightly different value of the top mass as opposed to that from [30]. We decided to respect the respective conventions to help us reproduce existing results, as described.

Appendix B: The effective theory of the Light Stop Scenario

The existing 2-loop MSSM effective theory at the electroweak scale with one light Higgs doublet can be expressed, as in the Standard Model, as a function of only one background field. Only third-generation squarks are considered to be at the electroweak scale.

1-loop potential

The 1-loop portion of the effective potential is [73]

$$V_{tree}(\varphi) = -\frac{1}{2}\mu^2\varphi^2 + \frac{1}{32}\varphi^4 g^2 \cos^2 2\beta$$
$$V_{1-loop,0-T}(\varphi) = \sum \frac{n_i}{64\pi^2} m_i^4(\varphi)[\log \frac{m_i^2(\varphi)}{Q^2} - C_i]$$
$$V_{1-loop,thermal}(\varphi, T) = \frac{T^4}{2\pi^2} \sum n_i J_i[\frac{\bar{m}_i^2(\varphi, T)}{T^2}]$$

Note that we take $g' = 0$. Since 1-loop contributions to the potential are comparable to the tree-level portion, the parameter μ^2 in the tree-level part is chosen so that the minimum of the total 1-loop, non-thermal potential lies at $\varphi_0 = 245.7497$ GeV.

Sums run over all species that contribute significantly. For the 1-loop part this includes stops, tops and W and Z bosons, minus the contribution from the heavy and decoupled left-handed stop in the thermal piece. The number of degrees of freedom for each species, n_i, is

$$n_t = -12,\ n_{\tilde{t}_R} = n_{\tilde{t}_L} = 6,\ n_W = 6,\ n_Z = 3 \tag{3.7}$$

We take $Q = m_Z$ and $C_i = \frac{5}{6}$ for vector bosons, $\frac{3}{2}$ for scalars and fermions. The relevant expansion of the J functions in the 1-loop, thermal bit is of the form

$$J_{bosons}\left(\frac{\bar{m}_i^2}{T^2}\right) \equiv \int_0^\infty dx\, x^2 \log\left(1-\exp\left(-\sqrt{x^2+(\frac{\bar{m}_i^2}{T^2})}\right)\right) =$$
$$= (2\pi^2)\left(\frac{2}{48}\left(\frac{\bar{m}_i}{T}\right)^2 - \frac{1}{12\pi}\left(\frac{\bar{m}_i}{T}\right)^3 - \frac{1}{64\pi^2}\left(\frac{\bar{m}_i}{T}\right)^4 \log\left(\left(\frac{\bar{m}_i}{T}\right)^2 - 5.408\right)\right)$$
$$J_{fermions}\left(\frac{m_i^2}{T^2}\right) \equiv \int_0^\infty dx\, x^2 \log\left(1+\exp\left(-\sqrt{x^2+(\frac{m_i^2}{T^2})}\right)\right) =$$
$$= -(2\pi^2)\left(\frac{1}{48}\left(\frac{m_i}{T}\right)^2 + \frac{1}{64\pi^2}\left(\frac{m_i}{T}\right)^4 \log\left(\left(\frac{m_i}{T}\right)^2 - 2.635\right)\right)$$

The notation $\bar{m}_i$ (for bosons) in the 1-loop, thermal piece indicates resummed masses. $\bar{m}_i^2$ are obtained from m_i^2 by adding the leading temperature-dependent self-energy contributions (see below). An effect of the 2-loop calculation is to resum all masses in the thermal piece of the 1-loop potential[5].

The expressions for the particle masses are:

$$m_{top}^2(\varphi) = \frac{1}{2}h_t^2\varphi^2\sin^2\beta,$$
$$m_{\tilde{t}_L}^2(\varphi) = m_Q^2 + m_t^2(\varphi) + D_{\tilde{t}_L}^2(\varphi),$$
$$m_{\tilde{t}_R}^2(\varphi) = m_U^2 + m_t^2(\varphi) + D_{\tilde{t}_R}^2(\varphi)$$

assuming no mixing between left- and right-handed stops and taking

$$D_{\tilde{t}_L}^2(\varphi) = \frac{1}{4}\left(\frac{1}{2} - \frac{2}{3}\sin^2\theta_W\right)g^2\varphi^2\cos 2\beta,$$
$$D_{\tilde{t}_R}^2(\varphi) = \frac{1}{4}\left(\frac{2}{3}\sin^2\theta_W\right)g^2\varphi^2\cos 2\beta$$

Note that with the choice $g' = 0$ $D_{\tilde{t}_R}^2 \equiv 0$ for all φ.

As field-dependent mass for the W and Z gause bosons we take

$$m_W^2(\varphi) = m_Z^2(\varphi) = \frac{1}{4}g^2\varphi^2 \tag{3.8}$$

[5]In the 1-loop version of our potential (which we use to reproduce the results of [32]) the masses in the 1-loop, T-dependent piece are not resummed. Following [73] we do resum the bosonic masses (only the longitudinal degrees of freedom for the gauge bosons, photons included) in the term cubic in m in the expansion, through the addition of the piece $\Delta V(\varphi,T) = -\frac{T}{12\pi}\Sigma n_i[\bar{m}_i^3(\phi,T) - m_i^3(\varphi,T)]$ running over the relevant species with $n_{W_L} = 2$, $n_{Z_L} = n_{\gamma_L} = 1$.

2-loop contributions

Following the notation in [73] the relevant Standard Model 2-loop contribution to the potential can be written as

$$V_{SM}^{(2)} = \frac{g^2}{16\pi^2}T^2\left[M^2\left(\frac{3}{4}\log\frac{M_L}{T} - \frac{51}{8}\log\frac{M}{T}\right) + \frac{3}{2}\left(M^2 - 4M_L^2\right)\log\frac{M+2M_L}{3T} + 3MM_L\right] + \\ + \frac{m_t^2(\varphi)T^2}{64\pi^2}\left[16g_s^2\left(\frac{8}{3}\log 2 - \frac{1}{2} - c_B\right) + 9h_t^2\sin^2\beta\left(\frac{4}{3}\log 2 - c_B\right)\right]$$

where $c_B = \log(4\pi) - \gamma_E$, $\gamma_E \approx 0.577215665$ being Euler's constant. We take the strong coupling and top Yukawa coupling respectively as $g_S \approx 1.228$ and $h_t \equiv \frac{\sqrt{2}M_t}{\varphi_0 \sin\beta}$ with the top mass $M_t \equiv 150$ GeV[6]. Here $M^2 = \frac{1}{4}g^2\varphi^2$ is the weak gauge boson mass and $M_L^2 = M^2 + \frac{7}{3}g^2T^2$ the longitudinal resummed mass (corrected by the self-energy).

We have retained the supersymmetric contributions which relate to non-decoupled species in the plasma. The relevant diagrams are shown in [73]. We take as the total supersymmetric, 2-loop part of the potential for our calculation

$$V_{2-loop,\,MSSM} = -\frac{g_s^2(N_c^2-1)\,T^2}{16\pi^2}\left(\bar{m}_{\tilde{t}_R}^2\log\frac{2\bar{m}_{\tilde{t}_R}}{3T}\right) + \\ + \frac{N_c\varphi^2T^2}{32\pi^2}\left(h_t^2\sin^2\beta\right)^2\log\frac{\bar{m}_h + 2\bar{m}_{\tilde{t}_R}}{3T} - \\ - \frac{g_s^2T^2}{64\pi^2}(N_c^2-1)(c_2-1)\bar{m}_{\tilde{t}_R}^2 + \\ + \frac{3N_c}{128\pi^2}T^2h_t^4\sin^4\beta c_2\phi^2 + \\ + \frac{N_cT^2}{16\pi^2}\left[\frac{g_S^2}{6}(N_c+1)\bar{m}_{\tilde{t}_R}^2 + \frac{1}{2}h_t^2\sin^2\beta\left(\bar{m}_h\bar{m}_{\tilde{t}_R} + 3\bar{m}_\chi\bar{m}_{\tilde{t}_R}\right)\right]$$

We take the number of colours N_c as 3, and $c_2 \approx 3.3025$.

Note that, given the large 1-loop corrections to the Higgs mass, $\bar{m}_h$ and $\bar{m}_\chi$ are expressed on the basis on taking $m_h^2 = \frac{\partial^2 V_{1-loop}}{\partial\varphi^2}$ at the minimum of the 1-loop potential.

[6] Note again the different convention as regards the top quark mass, which we respected.

Bibliography

[1] P. A. M. Dirac, Proc. Roy. Soc. Lond. **A133** (1931) 60-72.

[2] A. G. Cohen, A. De Rujula and S. L. Glashow, Astrophys. J. **495** (1998) 539 [arXiv:astro-ph/9707087].

[3] D. N. Spergel *et al.* [WMAP Collaboration], "First year Wilkinson Microwave Anisotropy Probe (WMAP) observations: Determination of cosmological parameters", Astrophys. J. Suppl. **148** (2003) 175 [astro-ph/0302209].

[4] M. Tegmark *et al.* [SDSS Collaboration], "Cosmological parameters from SDSS and WMAP", Phys. Rev. D **69** (2004) 103501 [astro-ph/0310723].

[5] E. W. Kolb, M. S. Turner, "The Early universe", Front. Phys. **69** (1990) 1-547.

[6] R. H. Cyburt, Phys. Rev. D **70** (2004) 023505 [arXiv:astro-ph/0401091].

[7] A. D. Sakharov, Pisma Zh. Eksp. Teor. Fiz. **5** (1967) 32-35.

[8] J. M. Cline, [hep-ph/0609145].

[9] D. V. Nanopoulos, S. Weinberg, Phys. Rev. **D20** (1979) 2484.

[10] G. 't Hooft, Phys. Rev. Lett. **37** (1976) 8.

[11] M. Fukugita and T. Yanagida, Phys. Lett. B **174** (1986) 45.

[12] M. C. Gonzalez-Garcia, Y. Nir, Rev. Mod. Phys. **75** (2003) 345-402. [hep-ph/0202058].

[13] I. Affleck, M. Dine, Nucl. Phys. **B249** (1985) 361.

[14] G. W. Anderson, L. J. Hall, Phys. Rev. **D45** (1992) 2685-2698.

[15] K. Kajantie, M. Laine, K. Rummukainen and M. E. Shaposhnikov, Phys. Rev. Lett. **77** (1996) 2887 [arXiv:hep-ph/9605288].

[16] M. Trodden, Rev. Mod. Phys. **71** (1999) 1463-1500. [hep-ph/9803479].

[17] G. Aad *et al.* [ATLAS Collaboration], Phys. Lett. B **716** (2012) 1 [arXiv:1207.7214 [hep-ex]].

[18] S. Chatrchyan *et al.* [CMS Collaboration], Phys. Lett. B **716** (2012) 30 [arXiv:1207.7235 [hep-ex]].

[19] S. Y. Khlebnikov, M. E. Shaposhnikov, Nucl. Phys. **B308** (1988) 885-912.

[20] D. Bodeker, G. D. Moore, K. Rummukainen, Phys. Rev. **D61** (2000) 056003. [arXiv:hep-ph/9907545 [hep-ph]].

[21] M. B. Gavela, P. Hernandez, J. Orloff and O. Pene, In *Vladimir 1994, Quarks '94* 96-111

[22] M. E. Shaposhnikov, JETP Lett. **44** (1986) 465-468.

[23] L. D. McLerran, Phys. Rev. Lett. **62** (1989) 1075.

[24] L. Fromme, S. J. Huber, M. Seniuch, JHEP **0611** (2006) 038. [hep-ph/0605242].

[25] D. Bodeker, L. Fromme, S. J. Huber, M. Seniuch, JHEP **0502** (2005) 026. [hep-ph/0412366].

[26] M. Carena, G. Nardini, M. Quiros, C. E. M. Wagner, JHEP **0810** (2008) 062. [arXiv:0806.4297 [hep-ph]].

[27] M. Carena, G. Nardini, M. Quiros, C. E. M. Wagner, Nucl. Phys. **B812** (2009) 243-263. [arXiv:0809.3760 [hep-ph]].

[28] A. Megevand, A. D. Sanchez, Nucl. Phys. **B825** (2010) 151-176. [arXiv:0908.3663 [hep-ph]].

[29] J. Ignatius, K. Kajantie, H. Kurki-Suonio, M. Laine, Phys. Rev. **D49** (1994) 3854-3868. [astro-ph/9309059].

[30] G. D. Moore, T. Prokopec, Phys. Rev. **D52** (1995) 7182-7204. [hep-ph/9506475].

[31] P. Y. Huet, K. Kajantie, R. G. Leigh, B. -H. Liu, L. D. McLerran, Phys. Rev. **D48** (1993) 2477-2492. [hep-ph/9212224].

[32] P. John, M. G. Schmidt, *Nucl. Phys.* **B598** (2001) 291-305. [hep-ph/0002050].

[33] D. Bodeker, G. D. Moore, JCAP **0905** (2009) 009. [arXiv:0903.4099 [hep-ph]].

[34] D. Grasso, H. R. Rubinstein, Phys. Rept. **348** (2001) 163-266. [astro-ph/0009061].

[35] A. Vilenkin, in *Kyoto 1985, Proceedings, Quantum Gravity and Cosmology*, 269-302.

[36] A. Megevand, F. Astorga, Phys. Rev. **D71** (2005) 023502. [hep-ph/0409321].

[37] C. Grojean, G. Servant, Phys. Rev. **D75** (2007) 043507. [hep-ph/0607107].

[38] S. J. Huber, T. Konstandin, JCAP **0809** (2008) 022. [arXiv:0806.1828 [hep-ph]].

[39] P. W. Higgs, Phys. Rev. Lett. **13** (1964) 508-509.

[40] W. N. Cottingham, D. A. Greenwood, "An introduction to the standard model of particle physics", Cambridge, UK: Univ. Pr. (2007) 272 p.

[41] J. S. Langer, Annals Phys. **41** (1967) 108 [Annals Phys. **281** (2000) 941].

[42] J. S. Langer, Annals Phys. **54** (1969) 258.

[43] J. R. Espinosa, T. Konstandin, J. M. No, G. Servant, JCAP **1006** (2010) 028. [arXiv:1004.4187 [hep-ph]].

[44] M. Dine, R. G. Leigh, P. Y. Huet, A. D. Linde, D. A. Linde, Phys. Rev. **D46** (1992) 550-571. [hep-ph/9203203].

[45] B. -H. Liu, L. D. McLerran, N. Turok, Phys. Rev. **D46** (1992) 2668-2688

[46] S. Y. Khlebnikov, Phys. Lett. **B282** (1992) 459-465.

[47] P. B. Arnold, Phys. Rev. **D48** (1993) 1539-1545. [hep-ph/9302258].

[48] G. D. Moore, N. Turok, Phys. Rev. **D55** (1997) 6538-6560. [hep-ph/9608350].

[49] K. Enqvist, J. Ignatius, K. Kajantie, K. Rummukainen, Phys. Rev. **D45** (1992) 3415-3428.

[50] H. Kurki-Suonio, M. Laine, Phys. Rev. **D51** (1995) 5431-5437. [hep-ph/9501216].

[51] P. J. Steinhardt, Phys. Rev. **D25** (1982) 2074.

[52] M. Laine, Phys. Rev. **D49** (1994) 3847-3853. [hep-ph/9309242].

[53] M. Kamionkowski, K. Freese, Phys. Rev. Lett. **69** (1992) 2743-2746. [hep-ph/9208202].

[54] S. M. Carroll, "Spacetime and geometry: An introduction to general relativity", San Francisco, USA: Addison-Wesley (2004) 513 p.

[55] X. m. Zhang, Phys. Rev. D **47** (1993) 3065 [arXiv:hep-ph/9301277].

[56] M. Dine, P. Huet, R. L. Singleton and L. Susskind, Phys. Lett. B **257** (1991) 351.

[57] X. Zhang, S. K. Lee, K. Whisnant and B. L. Young, Phys. Rev. D **50** (1994) 7042 [arXiv:hep-ph/9407259].

[58] C. Grojean, G. Servant and J. D. Wells, Phys. Rev. D **71** (2005) 036001 [arXiv:hep-ph/0407019].

[59] S. W. Ham and S. K. Oh, Phys. Rev. D **70** (2004) 093007 [arXiv:hep-ph/0408324].

[60] Megevand A and Sanchez AD 2009 *Nucl. Phys. B* **820** 47 [arXiv:0904.1753 [hep-ph]].

[61] M. S. Carena, M. Quiros, C. E. M. Wagner, Phys. Lett. **B380** (1996) 81-91. [hep-ph/9603420].

[62] S. Myint, Phys. Lett. **B287** (1992) 325-330. [hep-ph/9206266].

[63] J. R. Espinosa, M. Quiros, F. Zwirner, Phys. Lett. **B307** (1993) 106-115. [hep-ph/9303317].

[64] A. Brignole, J. R. Espinosa, M. Quiros, F. Zwirner, Phys. Lett. **B324** (1994) 181-191. [hep-ph/9312296].

[65] D. Delepine, J. M. Gerard, R. Gonzalez Felipe, J. Weyers, Phys. Lett. **B386** (1996) 183-188. [hep-ph/9604440].

[66] J. M. Cline, K. Kainulainen, Nucl. Phys. **B482** (1996) 73-91. [hep-ph/9605235].

[67] J. M. Cline, K. Kainulainen, Nucl. Phys. **B510** (1998) 88-102. [hep-ph/9705201].

[68] M. Laine, K. Rummukainen, Nucl. Phys. **B535** (1998) 423-457. [hep-lat/9804019].

[69] M. Laine, K. Rummukainen, Phys. Rev. Lett. **80** (1998) 5259-5262. [arXiv:hep-ph/9804255 [hep-ph]].

[70] M. Laine, Nucl. Phys. **B481** (1996) 43-84. [hep-ph/9605283].

[71] M. Losada, Phys. Rev. **D56** (1997) 2893-2913. [arXiv:hep-ph/9605266 [hep-ph]].

[72] G. R. Farrar, M. Losada, Phys. Lett. **B406** (1997) 60-65. [hep-ph/9612346].

[73] J. R. Espinosa, Nucl. Phys. **B475** (1996) 273-292. [hep-ph/9604320].

[74] B. de Carlos, J. R. Espinosa, Nucl. Phys. **B503** (1997) 24-54. [hep-ph/9703212].

[75] M. S. Carena, M. Quiros, A. Riotto, I. Vilja, C. E. M. Wagner, Nucl. Phys. **B503** (1997) 387-404. [hep-ph/9702409].

[76] M. S. Carena, M. Quiros, C. E. M. Wagner, Nucl. Phys. **B524** (1998) 3-22. [hep-ph/9710401].

[77] J. M. Cline, M. Joyce, K. Kainulainen, Phys. Lett. **B417** (1998) 79-86. [hep-ph/9708393].

[78] T. Multamaki, I. Vilja, Phys. Lett. **B411** (1997) 301-305. [hep-ph/9705469].

[79] A. Riotto, [hep-ph/9807454].

[80] M. P. Worah, Phys. Rev. **D56** (1997) 2010-2018. [hep-ph/9702423].

[81] D. Bodeker, P. John, M. Laine, M. G. Schmidt, Nucl. Phys. **B497** (1997) 387-414. [hep-ph/9612364].

[82] J. M. Cline, K. Kainulainen, Phys. Rev. Lett. **85** (2000) 5519-5522. [hep-ph/0002272].

[83] J. M. Cline, M. Joyce, K. Kainulainen, JHEP **0007** (2000) 018. [hep-ph/0006119].

[84] M. S. Carena, J. M. Moreno, M. Quiros, M. Seco, C. E. M. Wagner, Nucl. Phys. **B599** (2001) 158-184. [hep-ph/0011055].

[85] M. S. Carena, M. Quiros, M. Seco, C. E. M. Wagner, Nucl. Phys. **B650** (2003) 24-42. [hep-ph/0208043].

[86] T. Konstandin, T. Prokopec, M. G. Schmidt, M. Seco, Nucl. Phys. **B738** (2006) 1-22. [hep-ph/0505103].

[87] V. Cirigliano, S. Profumo, M. J. Ramsey-Musolf, JHEP **0607** (2006) 002. [hep-ph/0603246].

[88] S. J. Huber, JCAP **0602** (2006) 008 [hep-ph/0508208].

[89] S. J. Huber and M. G. Schmidt, Nucl. Phys. B **606** (2001) 183 [hep-ph/0003122].

[90] M. Pietroni, Nucl. Phys. B **402** (1993) 27 [hep-ph/9207227].

[91] J. Kang, P. Langacker, T. -j. Li and T. Liu, Phys. Rev. Lett. **94** (2005) 061801 [hep-ph/0402086].

[92] D. Chang, W. -Y. Keung and A. Pilaftsis, Phys. Rev. Lett. **82** (1999) 900 [Erratum-ibid. **83** (1999) 3972] [hep-ph/9811202].

[93] B. C. Regan, E. D. Commins, C. J. Schmidt and D. DeMille, Phys. Rev. Lett. **88** (2002) 071805.

[94] C. Balazs, M. S. Carena and C. E. M. Wagner, Phys. Rev. D **70** (2004) 015007 [hep-ph/0403224].

[95] C. Balazs, M. S. Carena, A. Menon, D. E. Morrissey and C. E. M. Wagner, Phys. Rev. D **71** (2005) 075002 [hep-ph/0412264].